iScience

CellPress

Article

A Gallium-based Chiral Solvating Agent Enables the Use of ^{1}H NMR Spectroscopy to Differentiate Chiral Alcohols

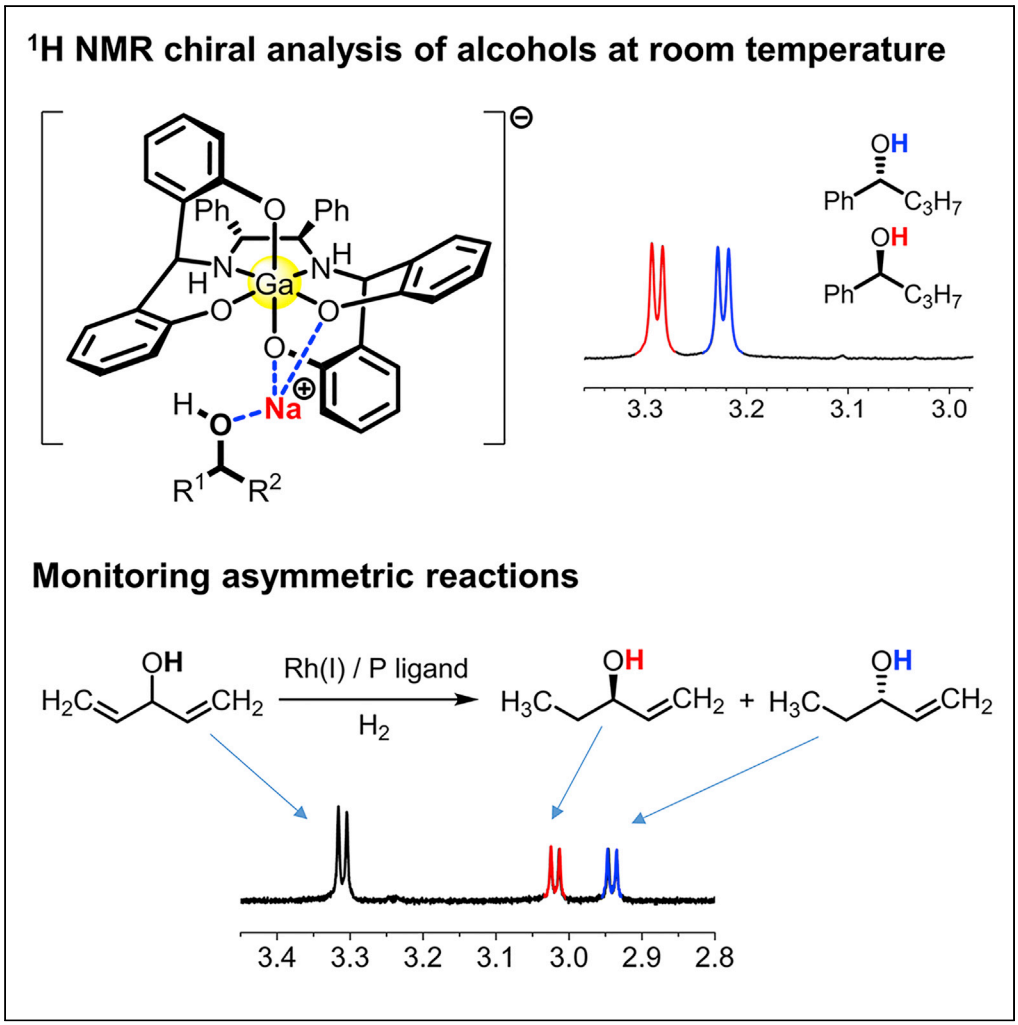

Sumin Jang, Hyunwoo Kim

hwkim@kaist.edu

HIGHLIGHTS

In situ, direct ^{1}H NMR chiral analysis of alcohols by a chiral solvating agent

Rapid determination of enantiomeric excess and conversion

Monitoring asymmetric reactions by ^{1}H NMR spectroscopy

Jang & Kim, iScience *19*, 425–435
September 27, 2019
https://doi.org/10.1016/j.isci.2019.07.051

iScience

CellPress

Article

A Gallium-based Chiral Solvating Agent Enables the Use of ^{1}H NMR Spectroscopy to Differentiate Chiral Alcohols

Sumin Jang[1] and Hyunwoo Kim[1,2,*]

SUMMARY

***In situ*, direct ^{1}H NMR chiral analysis by using chiral solvating agents is a convenient and efficient analytical technique. Here we developed a Ga-based chiral anionic metal complex for ^{1}H NMR chiral analysis of alcohols. Utilizing the optimal pK_a value, the Ga complex was able to differentiate ^{1}H NMR signals of each (*R*)- and (*S*)-enantiomer of alcohols, measured at room temperature. This direct ^{1}H NMR chiral analysis of alcohols was used to rapidly determine enantiomeric excess and conversion in a kinetic resolution and an asymmetric synthesis.**

INTRODUCTION

The chirality of molecules is an exceptionally important property, and a large community in organic chemistry is dedicated to preparing and characterizing chiral molecules for a variety of applications (Chen et al., 2015; You et al., 2015; Leung et al., 2012; Hembury et al., 2008). Among the standard methods of analysis, nuclear magnetic resonance (NMR) spectroscopy enjoys a special status, as it is convenient, versatile, and routinely available. Unfortunately, the NMR signatures of enantiomers are by definition identical and it is therefore not possible to use standard NMR techniques to differentiate enantiomers from each other. Thus, chromatographic techniques, such as high-performance liquid chromatography (HPLC) or gas chromatography (GC), that can separate enantiomers are commonly used for characterization and reaction monitoring (Han, 1997; Schurig and Nowotny, 1990). One possible way of enabling NMR to differentiate enantiomers is to employ chiral solvating agents that form diastereomeric adducts with the substrate in question and deliver distinctive NMR signatures for each diastereomer (Figure 1) (Wenzel, 2007, 2017; Lacour and Moraleda, 2009; Seco et al., 2004; Schneider et al., 1998; Parker, 1991).

This useful technique was successfully demonstrated for a variety of substrates with chiral amines and carboxylic acids being the most commonly targeted substrates (Benedict et al., 2018; Chen et al., 2018; Ema et al., 2018; Khanvilkar and Bedekar, 2018; Merino et al., 2018; Liu et al., 2011; Chinchilla et al., 1995). The emphasis on these species is not surprising, because the majority of chiral solvating agents employ non-covalent interactions such as hydrogen bonds and electrostatic attractions for structural recognition (Benedict et al., 2018; Chen et al., 2018; Ema et al., 2018; Khanvilkar and Bedekar, 2018; Merino et al., 2018; Liu et al., 2011; Chinchilla et al., 1995). Substrates that form relatively weak hydrogen bonds and are less strongly coordinating such as alcohols are more challenging to study. Nonetheless, several reagents have been shown to be effective at stereospecifically binding to chiral alcohols and allowing for separation of the NMR signals of the enantiomeric alcohols.

To overcome the intrinsic difficulty of relatively weak non-covalent interactions that are common for alcohols, several multifunctional analytes such as β-hydroxy esters (Uccello-Barretta et al., 1995), 1,2-diols (Pal et al., 2014; Ema et al., 2007; Wilen and Qi, 1991; Sweeting, 1987), cyanohydrins (Moon et al., 2009, 2010), and α-hydroxy carboxylic acids (Bai et al., 2019; Pal et al., 2015) or amides (Wolf et al., 2014) have been used to enhance interactions with chiral solvating agents, as shown in Figure 1A. For alcohols without any other polar functional groups, bis(seleno)urea (Bian et al., 2016) and cobalt(III) trication (Luu et al., 2018) were reported to be effective, but the scope of the substrates tested was relatively narrow. In 2018, we demonstrated that the sodium salt of a negatively charged aluminum complex (CASA-Na) can be used for the solvation and resolution of chiral alcohols (Figure 2) (Seo et al., 2018). Various substrates were successfully analyzed including primary, secondary, and tertiary alcohols with alkyl and aryl substituents. Unfortunately, low temperatures in a range of 0°C to −40°C were required owing to the small binding constants. Thus, one desirable enhancement strategy is to strengthen the intermolecular interactions between the anionic metal complex and the analyte. We discovered that significant improvement can

[1]Department of Chemistry, Korea Advanced Institute of Science and Technology, 291 Daehak-ro, Yuseong-gu, Daejeon 34141, Republic of Korea

[2]Lead Contact

*Correspondence: hwkim@kaist.edu

https://doi.org/10.1016/j.isci.2019.07.051

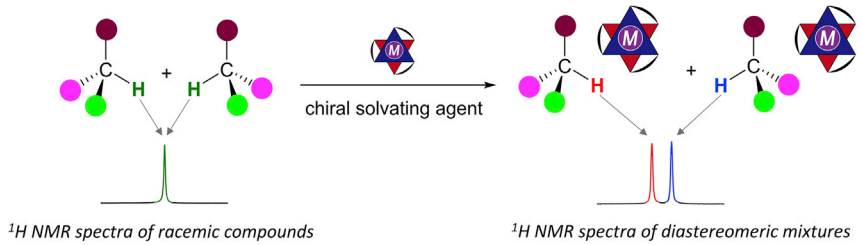

Figure 1. ^{1}H NMR Chiral Analysis by Using a Chiral Solvating Agent

be achieved by replacing aluminum with gallium, which is not only environmentally benign, non-toxic, and inexpensive, but also allows for differentiating the chiral alcohols with standard NMR methods at room temperature. In addition, *in situ* chiral analysis of an alcohol was practically demonstrated in a chiral resolution and an asymmetric synthesis.

RESULTS AND DISCUSSION

Preparation and Physical Properties of Charged Metal Complexes

Our chiral aluminum complex (CASA) is a unique class of ^{1}H NMR chiral solvating agent based on a negatively charged "ate" complex with metal-centered chirality. Experimental data such as crystal structures

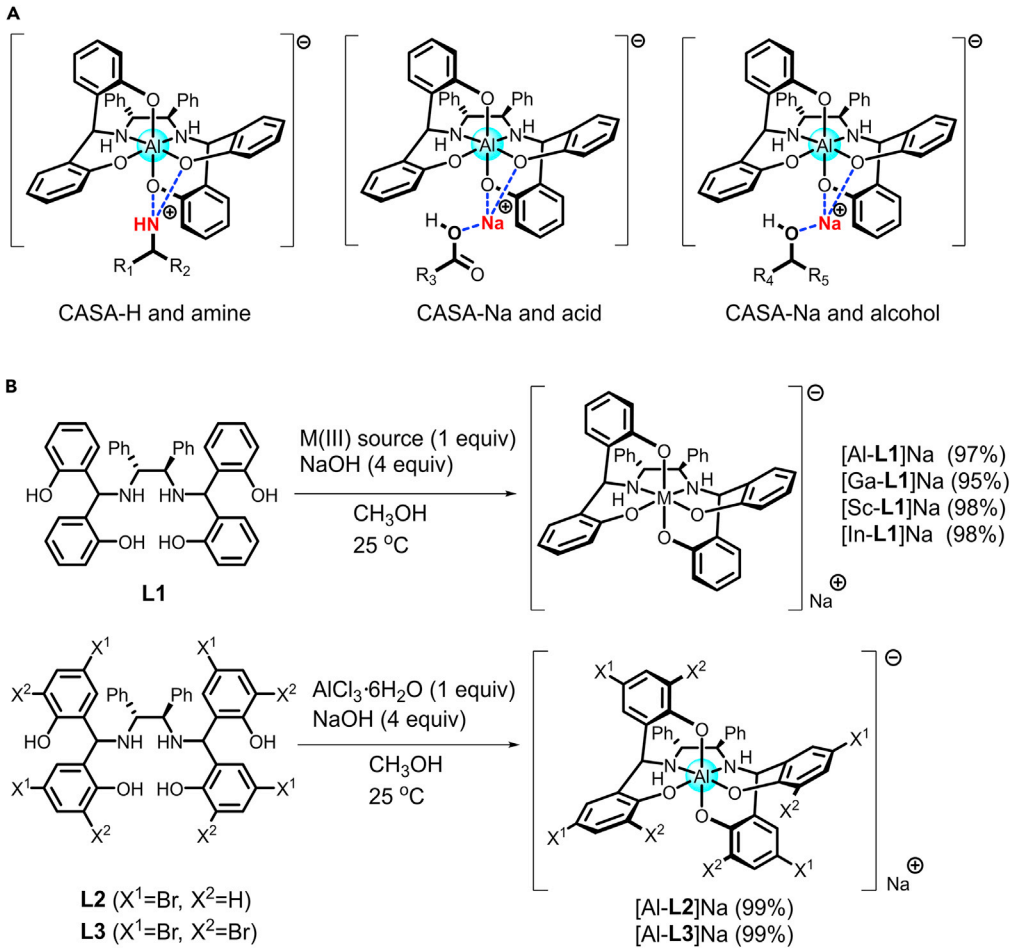

Figure 2. Binding Models and Synthetic Procedure

(A) Binding models of CASA.

(B) Synthetic procedure of metal complexes with L1-L3. See also Figures S1–S7 for ^{1}H & ^{13}C NMR spectra.

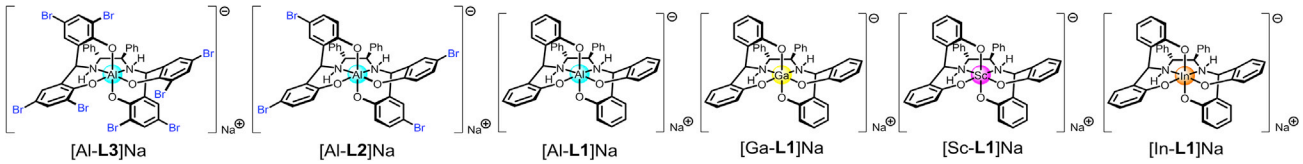

Figure 3. Anionic Octahedral Metal Complexes of Al, Ga, Sc, and In

and job plots supported 1:1 binding models between CASA and analytes, as shown in Figure 2A. Accordingly, two stable ionic salts with H^+ and Na^+, CASA-H and CASA-Na, were demonstrated to be effective for ^1H NMR chiral solvation of amines and carboxylic acids, respectively (Figure 2A) (Seo and Kim, 2015). CASA was shown to be an excellent chiral solvating agent working for all types of amines and carboxylic acids with a general analyte scope and a solvent compatibility. The utility of CASA-Na was recently expanded to cover chiral alcohols (Seo et al., 2018). Although the analyte scope of CASA-Na for chiral alcohols was sufficiently wide, low temperature measurement (0°C ~ −40°C) was required for baseline peak separation owing to weak intermolecular interaction between CASA-Na and an alcohol, which may limit the practical applications. According to our experiments, the binding constants for an alcohol are about 80–90 times weaker than those for the corresponding carboxylic acid (Seo et al., 2018). To achieve chiral solvation of alcohols at room temperature, we intended to further modulate the anionic octahedral metal complex. Our synthetic strategy is (1) to modulate the ligand's electronic property or (2) to change the metal(III) center. Although an increase of intermolecular interaction is desirable for better chiral solvation ability, the synthetic direction and the resulting physical properties are not simply predicted in the anionic octahedral complex.

In this study, six chiral metal complexes were prepared, as shown in Figure 2B (see also Transparent Methods). A base-mediated coupling between **L1** and M(III) precursors such as $AlCl_3$, $Ga(acac)_3$, $Sc(OTf)_3$, and $In(acac)_3$ gave [Al-**L1**]Na, [Ga-**L1**]Na, [Sc-**L1**]Na, and [In-**L1**]Na with excellent yield (95%–98%) and stereoselectivity (>99%) (Figure 2B and see also Figures S1–S7). In addition, bromo-substituted ligands **L2** and **L3** prepared by bromination of 2,2′-dihydroxybenzophenone with *N*-bromosuccinimide were used to form [Al-**L2**]Na and [Al-**L3**]Na, respectively, with 99% yields (Figure 2B and see also Transparent Methods). In all cases, the metal-centered chirality was completely controlled to provide a single diastereomeric metal complex.

We then evaluated the physical properties of six metal complexes by measuring pK_a values in dimethyl sulfoxide (DMSO) (Figure 3 and Table 1, see also Transparent Methods) (Christ et al., 2011). [Al-**L1**]H was previously measured to show a pK_a value of 5.02 (Seo and Kim, 2015). To develop better chiral solvating agents for alcohols than [Al-**L1**]Na, a more basic metal complex with a higher pK_a value may be necessary to establish stronger intermolecular interactions. Complexes with brominated ligands, [Al-**L2**]H and [Al-**L3**]H, were found to be more acidic, with pK_a values of 4.48 and 3.33, respectively. The inductive effect by electronegative Br atoms can stabilize the conjugate bases [Al-**L2**]Na and [Al-**L3**]Na, resulting in increased acidity of [Al-**L2**]H and [Al-**L3**]H. On the other hand, complexes with different central metals, [Ga-**L1**]H, [Sc-**L1**]H, and [In-**L1**]H, were found to be more basic, with pK_a values of 5.73, 6.35, and 6.77, respectively. These pK_a values are in a linear relationship with the effective ionic radii of Al^{3+}, Ga^{3+}, Sc^{3+}, and In^{3+}, which are 53.5, 62, 74.5, and 80 pm, respectively.

To understand the linear correlation between the ionic radii and pK_a values of the metal complexes, DFT computation was performed to optimize the complex geometries and to calculate M-O bond lengths (see also Tables S1–S6). For Al, Ga, Sc, and In complexes with **L1**, there is a good linear relationship

	Al-L3	Al-L2	Al-L1	Ga-L1	Sc-L1	In-L1
Average M-O (Å)	1.87	1.87	1.88	1.91	2.04	2.05
pK_a (DMSO)	3.33	4.48	5.02	5.73	6.32	6.77

Table 1. Measured pK_a Values and Metal to Oxygen Bond Lengths Obtained from Density Functional Theory Calculation

See also Tables S1–S11 for Cartesian coordinates.

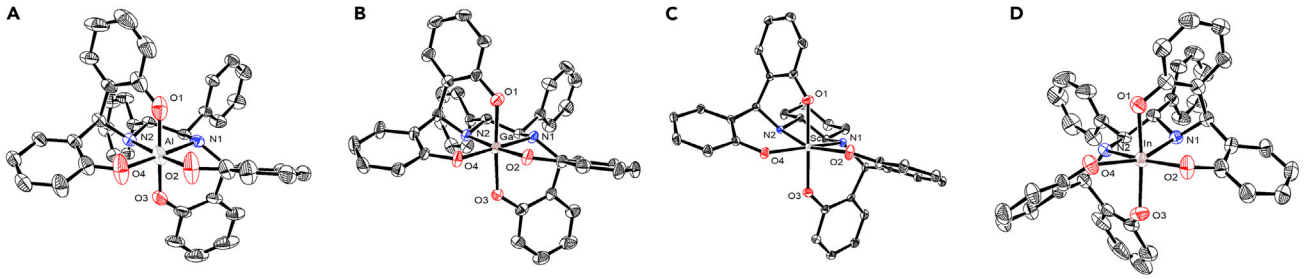

Figure 4. Crystal Structures (Thermal Ellipsoids at 50% Probability: All Hydrogens and Sodium Cations Are Omitted for Clarity)
(A) [Al-**L1**]Na.
(B) [Ga-**L1**]Na.
(C) [Sc-**L4**]Na.
(D) [In-**L1**]Na.
See also Figures S8–S10.

between the calculated average M-O bond lengths and the measured pK_a values with R_2 = 0.896 (Table 1). As the M-O bond increases in the anionic octahedral metal complex, the complex becomes more basic. A linear correlation between gas phase bond lengths and experimental pK_a values was well demonstrated in organic compounds, such as carboxylic acids and phenols (Caine et al., 2018; Harding and Popelier, 2011), and is applicable to anionic octahedral metal complexes. However, for Al complexes with **L1**-**L3**, almost the same M-O bond lengths of 1.87–1.88 were obtained despite the large difference in pK_a values (ΔpK_a = 1.7). It appears that the relationship between M-O bond length and pK_a value is not applicable to the inductive effect.

A linear relationship between bond length and pK_a value was then confirmed by solid-state crystal structures of Al, Ga, Sc, and In complexes. As shown in Figure 4, crystal structures of [Al-**L1**], [Ga-**L1**], [Sc-**L4**] (Seo and Kim, 2015), and [In-**L1**] were obtained (**L4** was prepared from diaminocyclohexane instead of diphenylethylenediamine) (see also Figures S8–S10). Interestingly, the average M-O bond lengths of 1.86, 1.94, 2.04, and 2.12 Å for Al, Ga, Sc, and In complexes, respectively, are in an excellent linear relationship with the measured pK_a values (R_2 = 0.988) (Table 2). Thus, both the computed and solid-state structures can be used to correlate the basicity of the negatively charged octahedral metal complexes. Accordingly, we prepared chiral anionic metal complexes with a pK_a range of 3.33–6.77.

Chiral Solvation of Alcohols with [Ga-L1]Na at Room Temperature

The chiral solvation ability of six anionic metal complexes was investigated. In CD_3CN (0.5 mL), an equimolecular amount of the metal complex (0.01 mmol) and *rac*-1-phenyl-1-butanol (**1**, 0.01 mmol) was mixed and ^{1}H NMR spectra were then recorded at room temperature. As found in the proposed binding model in Figure 2A, the hydroxyl group of the alcohol directly interacts with the metal complex mediated by the sodium cation and the peak separation of the hydroxyl group is mainly observed in this system. Compared with a default complex [Al-**L1**]Na providing $\Delta\Delta\delta$ of 0.020 ppm, [Al-**L2**]Na and [Al-**L3**]Na showed poor peak resolution owing to the decreased basicity with the bromo substituents (Figures 5, see also Figures S11 and S12). When a more basic metal complex [Ga-**L1**]Na was tested, a significant enhancement of the peak resolution ($\Delta\Delta\delta$ = 0.065 ppm) was observed with [Ga-**L1**]Na. However, when two more basic metal complexes

	Al-L1	Ga-L1	Sc-L4	In-L1
M-O1 (Å)	1.83	1.89	2.03	2.09
M-O2 (Å)	1.83	1.90	2.04	2.11
M-O3 (Å)	1.89	1.96	2.04	2.11
M-O4 (Å)	1.89	2.00	2.06	2.21
Average M-O (Å)	**1.86**	**1.94**	**2.04**	**2.12**

Table 2. Metal to Oxygen Bond Distances Obtained from the Crystal Structures

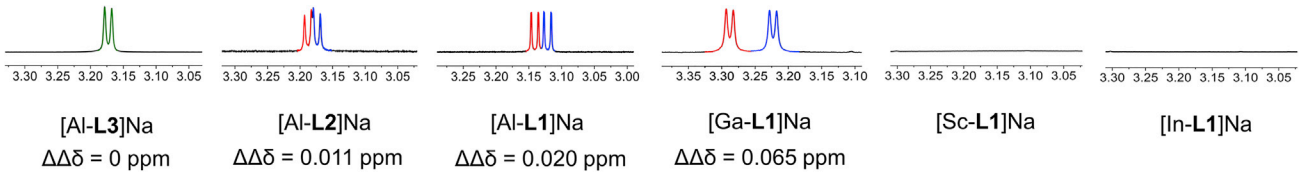

Figure 5. Partial ^{1}H NMR Spectra of Hydroxyl Peaks of *rac*-1 with the Anionic Metal Complexes in CD_3CN
See also Figures S11–S13 for full ^{1}H NMR spectra

[Sc-**L1**]Na and [In-**L1**]Na were used, the hydroxyl signal of the alcohol disappeared and merged with the water peak (Figure 5). Because of the observed intermolecular proton transfer between the hydroxyl analyte and the residual water, [Sc-**L1**]Na and [In-**L1**]Na are found to be too basic to observe the analyte's hydroxyl signals. Accordingly, [Ga-**L1**]Na exhibits an optimal basicity in terms of being used for chiral solvation of *rac*-1-phenyl-1-butanol (**1**).

To verify the assumption that a more basic anionic metal complex can strongly bind to an alcohol analyte, the binding constants of [Al-**L1**]Na and [Ga-**L1**]Na were compared. (*R*)- and (*S*)-1-phenylethanol (**2**) were used as an analyte, and the binding constants were measured by a ^{1}H NMR titration experiment (see also Transparent Methods). The binding constants of [Al-**L1**]Na with (*R*)-**2** and (*S*)-**2** were measured to be 0.382 and 0.136 M^{-1}, respectively, whereas those of [Ga-**L1**]Na with (*R*)-**2** and (*S*)-**2** were measured to be 1.01 and 0.493 M^{-1}, respectively (Figure 6). These data indicate that the more basic [Ga-**L1**]Na binds about 2.5–3.5 times stronger to the chiral alcohol **2** than [Al-**L1**]Na, consistent with our idea to enhance the intermolecular interactions with more basic anionic complexes. We also found that the binding constants of both Al and Ga complexes for (*R*)-**2** are about two times greater than those for (*S*)-**2**. The energy difference for the formation of diastereomeric mixtures may be further utilized in the separation of racemic analytes (Mittal et al., 2015; Fogassy et al., 2006). Indeed, the increased binding constants of [Ga-**L1**]Na resulted in a better peak resolution, as shown in Figure 6. Although [Al-**L1**]Na gave only partial peak separation of *rac*-**2** in CD_3CN at room temperature, [Ga-**L1**]Na provided cleanly separated ^{1}H NMR signals with a ΔΔδ value of 0.041 ppm.

In addition, the effect of counter cation was investigated. Among [Ga-**L1**] complexes with counter cations Li^+, Na^+, K^+, or Cs^+, [Ga-**L1**]Na was found to be the most efficient chiral solvating agent for **2** (see also Figure S13). Because the crystal structures showed various intermolecular interactions between the sodium cation and solvent molecules, we proposed a binding model as shown in Figure 2A, where the sodium cation plays a critical role to mediate the anionic complex and the alcohol analyte.

The analytical scope of [Ga-**L1**]Na is summarized in Figure 7 (see also Figures S14–S17). When various chiral alcohols **1**-**12** were mixed with a stoichiometric amount of [Ga-**L1**]Na at room temperature in CD_3CN

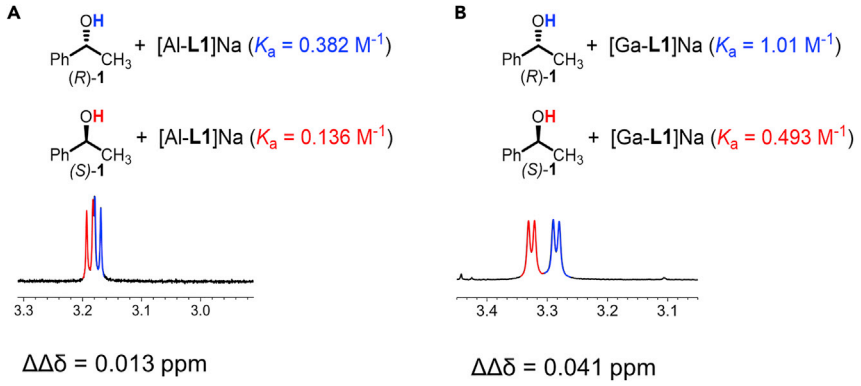

Figure 6. Binding Constants with 1-Phenylethanol (1)
(A) [Al-**L1**]Na.
(B) [Ga-**L1**]Na.

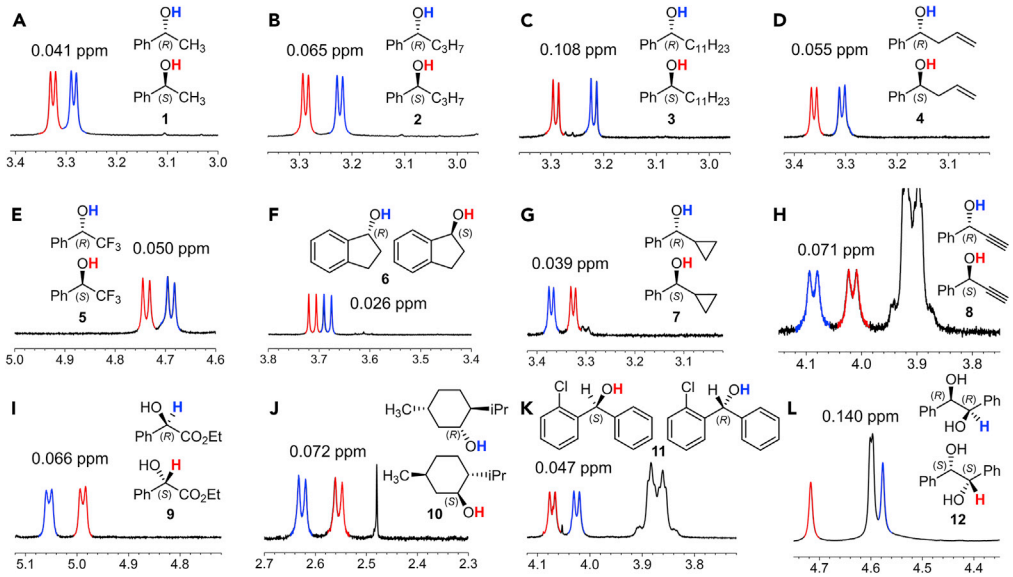

Figure 7. Partial ^{1}H NMR Spectra of Chiral Alcohols with [Ga-L1]Na at Room Temperature in CD_3CN. ^{1}H NMR Signals of Best Peak Separation Are Shown

(A) 1-Phenyl-1-ethanol.
(B) 1-Phenyl-1-butanol.
(C) 1-Phenyl-1-dodecanol.
(D) 1-Phenyl-4-buten-1-ol.
(E) α-(Trifluoromethyl)benzyl alcohol.
(F) 1-Indanol.
(G) α-Cyclopropylbenzyl alcohol.
(H) 1-Phenyl-2-propyn-1-ol.
(I) Ethyl mandelate.
(J) Menthol.
(K) 1-(2-Chlorophenyl)-1-phenylmethanol.
(L) 1,2-Diphenylethane-1,2-diol.
See also Figures S14–S17 for full ^{1}H NMR spectra and Figures S18–S20 for comparison with reported chiral solvating agents.

(20 mM), the ^{1}H NMR spectra showed full baseline peak separation for efficient and reliable chiral analysis. In many cases, the hydroxyl proton signals were split upon the addition of [Ga-**L1**]Na, supporting our proposed intermolecular interactions among [Ga-**L1**]$^{-}$, Na^{+}, and the analyte alcohol (Figure 2A). Secondary chiral alcohols **1**-**6** with phenyl substituents showed the same peak pattern where (*S*)-enantiomer is more downfield shifted. This splitting pattern can be used to determine the absolute chirality of secondary alcohols, but the opposite splitting pattern was found for phenyl-substituted alcohols **7**, **8**, and **9** with cyclopropyl, acetyl, and ester groups, respectively. Thus, statistical analysis as well as theoretical investigation is further required to use this chiral solvating agent for the determination of absolute chirality.

In addition, other secondary alcohols including dialkyl or diaryl-substituted alcohols (**10** or **11**) and diol **12** were successfully used for ^{1}H NMR baseline peak separation of enantiomers with [Ga-**L1**]Na. However, 2-butanol (**13**) and mevalonolactone (**14**) gave poor peak resolution when a stoichiometric amount of [Ga-**L1**]Na was used at room temperature. Instead of low temperature measurement, we sought other convenient operational protocols. We found that an increased amount of [Ga-**L1**]Na improved the peak separation of enantiomers and six equivalents of [Ga-**L1**]Na gave a full baseline peak separation for **13** and **14** (Figure 8, see also Figures S21–S23). Given the general analyte scope shown in Figures 6 and 7, ^{1}H NMR chiral analysis of alcohols by using [Ga-**L1**]Na can be an efficient and convenient procedure at room temperature. To compare the chiral solvation ability of [Ga-**L1**]Na with other chiral solvating agents, we tested ^{1}H NMR chiral analysis of four alcohols **1**, **4**, **10**, and **15** with previously reported chiral solvating agents, including Pirkle's alcohol (Wenzel, 2017; Wenzel and Chisholm, 2011), chiral crown

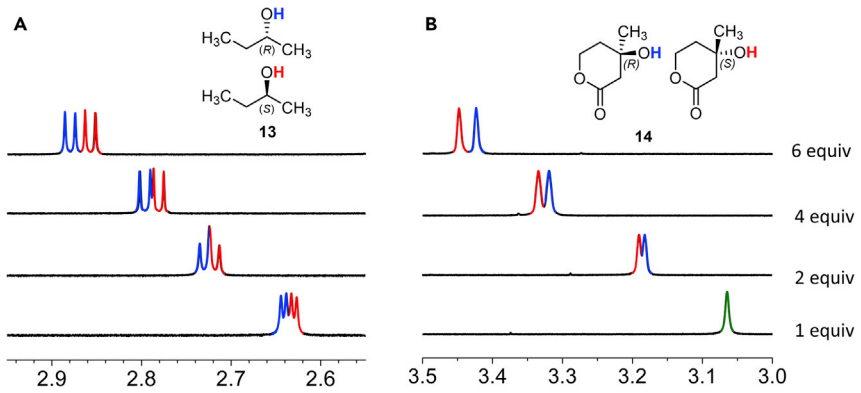

Figure 8. Partial ^{1}H NMR Spectra of Chiral Alcohols with Different Equivalents of [Ga-L1]Na Complex in CD_3CN

(A) 2-Butanol.

(B) Mevalonolactone.

See also Figures S21–S23 for full ^{1}H NMR spectra.

ether (Lacour and Moraleda, 2009), β-cyclodextrin (Schneider et al., 1998), and europium shift agent (Sweeting, 1987), in CD_3CN (see also Figures S18–S20). Among 14 chiral solvating agents, [Ga-**L1**]Na was the only one to give the full baseline peak separation of the four analytes, whereas other chiral solvating agents showed no or partial peak separation. Moreover, ligand **L1** was not effective for the chiral analysis of alcohols, supporting the importance of chiral octahedral anionic metal complex for chiral solvation of alcohols.

Direct ^{1}H NMR Analysis of Chiral Alcohol with [Ga-L1]Na in Kinetic Resolution and Asymmetric Synthesis

Chiral alcohols can be synthesized via (1) multistep transformations from a chiral pool such as terpenes, amino acids, and carbohydrates (Fan et al., 2019; Hung et al., 2019; Brill et al., 2017) or (2) kinetic resolution of racemic alcohols or their derivatives (Liu et al., 2019; Selier et al., 2019; Zhang and Ma, 2018). In addition, asymmetric synthesis such as reduction or nucleophilic addition of prochiral carbonyls recently has been developed (Neves-Garcia et al., 2018; Tsai et al., 2018; Bieszczad and Gilheany, 2017; Nakamura et al., 2017). Although HPLC and GC with chiral stationary phases are commonly used for chiral analysis of alcohols as a reliable direct analytical technique, derivatization of alcohols such as introducing chromophores, polar functional groups, or hydrophobic units is often necessary for the desirable analytical results. However, the chiral analysis of alcohols by ^{1}H NMR spectroscopy can be a direct, efficient, and convenient analytical technique that is practically applicable for the synthesis of chiral alcohols by resolution or asymmetric synthesis.

To demonstrate the utility of ^{1}H NMR chiral analysis of alcohols with [Ga-**L1**]Na, a challenging analyte, 1-penten-3-ol (**15**), was selected in this study. In the previous reports, the direct chiral analysis of 1-penten-3-ol (**15**) was not achieved by HPLC or GC analysis, likely due to the lack of aryl chromophores or minor structural differences between ethyl and ethylene groups (Fernandez-Perez et al., 2016; Ryan and Jaimison, 2006; Paquette and Sweeney, 1990). Accordingly, further synthetic efforts such as benzoylation are required for the HPLC analysis, which takes an additional 18 h together with purification by silica gel column chromatography (Fernandez-Perez et al., 2016). In contrast, we demonstrated that [Ga-**L1**]Na can be used for a direct chiral analysis of 1-penten-3-ol within minutes by ^{1}H NMR spectroscopy.

Kinetic resolution is a protocol to separate enantiomers by a kinetically controlled reaction. Because the reaction theoretically is quenched at 50% conversion, direct reaction monitoring is highly desirable to achieve high yields and enantiopurities. The Sharpless epoxidation of 1-penten-3-ol (**15**) was reported for kinetic resolution of 1-penten-3-ol (**15**), but the enantiopurity of the product was determined only by measuring optical rotation and the detailed conditions were not provided (Ryan and Jaimison, 2006; Paquette and Sweeney, 1990). As we can directly analyze the enantiopurity of 1-penten-3-ol (**15**), the Sharpless epoxidation was monitored by ^{1}H NMR spectroscopy. As shown in Figure 9, the enantiomeric excess was found to be 66% after 7 h and >99% *ee* after 14 h (see also Figure S24). Thus, the kinetic resolution process can be readily optimized and this protocol can be used for other kinetic resolutions of alcohols.

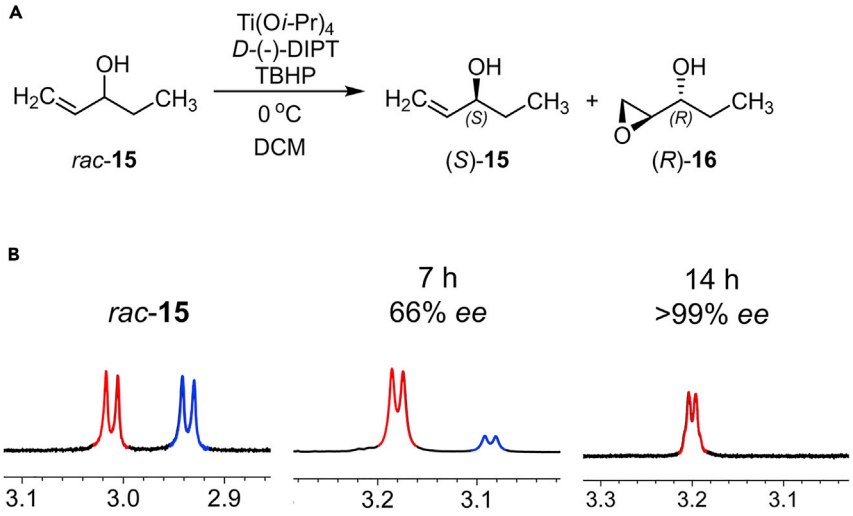

Figure 9. Kinetic Resolution by Sharpless Asymmetric Epoxidation of 1-peten-3-ol (15)

(A) Reaction scheme.

(B) Partial ^{1}H NMR spectra of 1-penten-3-ol (**15**) with [Ga-**L1**]Na during kinetic resolution.

See also Figure S24.

The second practical example of using [Ga-**L1**]Na is a rapid chiral analysis of 1-penten-3-ol (**15**) in Rh-catalyzed hydrogenative desymmetrization of 1,4-pentadien-3-ol (**17**) (Figure 10) (Fernandez-Perez et al., 2016). This reaction was reported by Vidal-Ferran and co-workers and a chiral phosphite ligand was found to be efficient (>99% yield and 84% *ee*). To demonstrate the direct assessment of %*ee* by ^{1}H NMR, a mixture of 1,4-pentadien-3-ol (**17**) and *rac*-1-penten-3-ol (**15**) was mixed with [Ga-**L1**]Na in CD_3CN. ^{1}H NMR spectra showed clean baseline separation of all hydroxyl peaks, allowing us to calculate conversion and enantiomeric excess together by a single measurement (Figure 10A, see also Figures S25 and S26). Using this rapid analytical protocol within minutes employing ^{1}H NMR spectroscopy, we tested 14 commercially available chiral phosphorus ligands and the resulting %conversion and %*ee* are summarized in Figure 10C (see also Figures S27 and S28). In general reaction conditions, a solution of $[Rh(nbd)_2]BF_4$, phosphine ligand, and 1,4-pentadien-3-ol (**17**) in CD_2Cl_2 (0.2 mmol) was stirred for 23 h at −40°C with a H_2 balloon. For the determination of %*ee* and %conversion, 50 μL of crude mixture was mixed with 0.04 mmol of [Ga-**L1**]Na in 450 μL of CD_3CN. The enantiomeric excess ranging from 3% to 88% was successfully measured, even when the yield was as low as 11%. As the enantiomeric excess can be measured at low conversion, the ^{1}H NMR chiral analysis by using [Ga-**L1**]Na can be used to monitor asymmetric reactions.

Conclusion

In summary, we have developed a Ga-based chiral metal complex as a general, efficient, and practical ^{1}H NMR chiral solvating agent for various alcohols. ^{1}H NMR chiral analysis of chiral alcohols without any other functional groups has been challenging owing to weak binding interactions with chiral solvating agents. In this study, several anionic chiral metal complexes were synthesized and we found that the pK_a values are in a good linear relationship with M-O bonds in the octahedral geometries. The Ga-based chiral metal complex had an optimal pK_a value of 5.7 in DMSO, providing sufficient baseline peak separations of chiral alcohols when [Ga-**L1**]Na was simply added to CD_3CN. Various chiral alcohols, including primary, secondary, and tertiary alcohols, with alkyl and aryl substituents were tested, and all enantiomers were cleanly resolved in ^{1}H NMR spectra measured at room temperature with [Ga-**L1**]Na. To develop a practical direct technique for chiral analysis of alcohols, we demonstrated that ^{1}H NMR chiral analysis of 1-penten-3-ol can be efficiently used for a kinetic resolution by the Sharpless epoxidation and Rh-catalyzed hydrogenative desymmetrization of 1,4-pentadien-3-ol, where both %*ee* and %conversion were determined by a single measurement. As a complementary analytical technique, ^{1}H NMR spectroscopy will be useful for rapid and reliable chiral analysis of alcohols under operationally simpler and more practical conditions with a general chiral solvating agent.

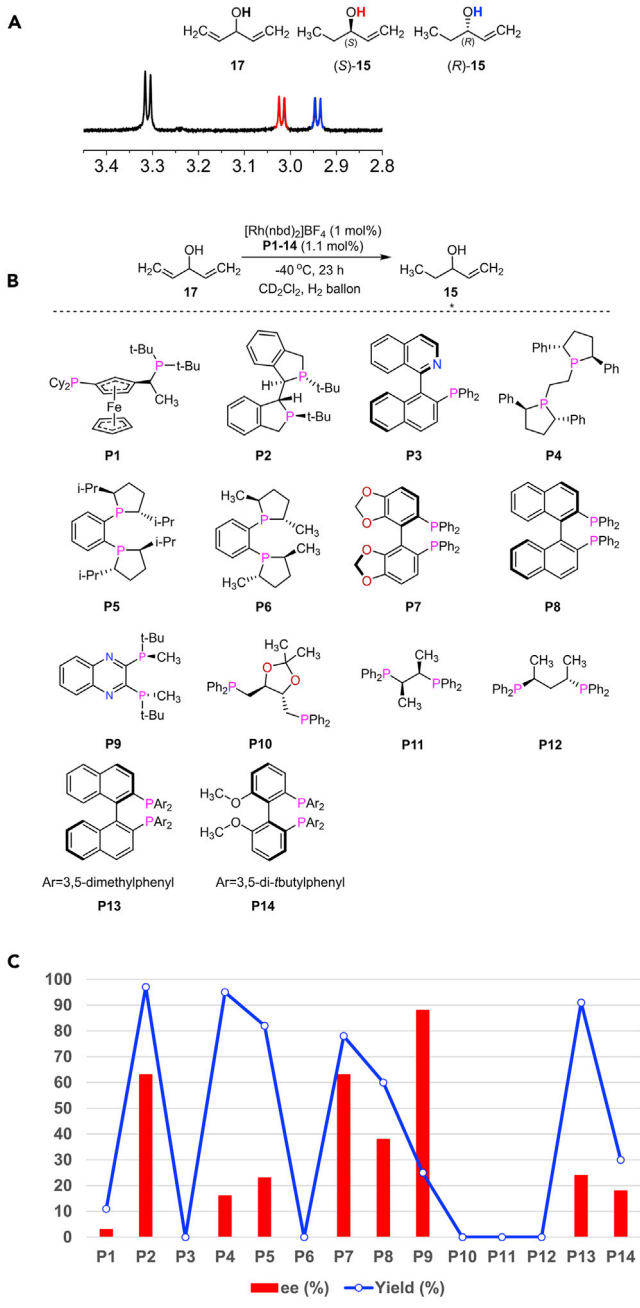

Figure 10. Rh-Catalyzed Hydrogenative Desymmetrization of 1,4-Pentadiene-3-ol

(A) Partial ^{1}H NMR spectrum of 1:1:2 mixture of 1,4-pentadiene-3-ol (17) and 1-penten-3-ol (15) with [Ga-L1]Na. See also Figures S25–S27.

(B) Reaction scheme and structures of ligand P1-14.

(C) Direct analysis of %conversion and %enantiomeric excess with various phosphorus ligands P1-P14 using [Ga-L1]Na. See also Figure S28.

EXPERIMENTAL PROCEDURES

General Procedure for ^{1}H NMR Chiral Analysis of Alcohols

In a 5-mm NMR tube, 1.5 μL of *rac*-1-phenyl-1-butanol was dissolved in 0.5 mL of CD_3CN. ^{1}H NMR spectra (400 MHz) was taken of the solution (**data-1**). To the solution, 7.0 mg of [Ga-**L1**]Na was added and shaken until the solution became clear. ^{1}H NMR spectra (400 MHz) was taken of the solution (**data-2**). By

comparing two spectra of **data-1** and **data-2**, resolved peaks of the hydroxy group at 3.20–3.35 ppm were analyzed. For the determination of *R*/*S* configuration, enantiopure or enantioriched samples can be analyzed.

Limitations of the Study

^{1}H NMR chiral analysis of alcohols with [Ga-**L1**]Na could not be achieved in polar solvents such as DMSO-d_6, Acetone-d_6, and methanol-d_4. Moreover, anhydrous CD_3CN dried over 4Å molecular sieves is necessary because residual water in the NMR solvent decreases the amount of peak separation and increases line broadening of hydroxyl proton signals.

METHODS

All methods can be found in the accompanying Transparent Methods supplemental file.

DATA AND CODE AVAILABILITY

The data for the X-ray crystallographic structures of [Al-**L1**]Na, [Ga-**L1**]Na, and [In-**L1**]Na are available free of charge from the Cambridge Crystallographic Data Center under accession numbers CCDC: 1913315, 1913316, and 1913317, respectively.

SUPPLEMENTAL INFORMATION

Supplemental Information can be found online at https://doi.org/10.1016/j.isci.2019.07.051.

ACKNOWLEDGMENTS

The authors are grateful for the financial support provided by Samsung Science and Technology Foundation (SSTF-BA1601-10). Ha Jin Lee (Korea Basic Science Institute) and Jongho So (KAIST) are acknowledged for X-ray crystallographic analysis. We thank Prof. Mu-Hyun Baik for valuable advice on the preparation of this manuscript.

AUTHOR CONTRIBUTIONS

Conceptualization, S.J. and H.K.; Investigation, S.J.; Writing-Original Draft, S.J. and H.K.; Writing-Review and Editing, S.J. and H.K.; Supervision, H.K.; Funding Acquisition, H.K.

DECLARATION OF INTERESTS

The authors declare no competing interests.

Received: May 16, 2019
Revised: July 9, 2019
Accepted: July 30, 2019
Published: September 27, 2019

REFERENCES

Bai, L., Chen, P., Xiang, J., Sun, J., and Lei, X. (2019). Enantiomeric NMR discrimination of carboxylic acids using actinomycin D as a chiral solvating agent. Org. Biomol. Chem. *17*, 1466–1477.

Benedict, B., Lietz, C.E., and Wenzel, T.J. (2018). Comparison of chiral NMR solvating agents for the enantiodifferentiation of amines. Tetrahedron *74*, 4846–4856.

Bian, G., Yang, S., Huang, H., Zong, H., Song, L., Fan, H., and Sun, X. (2016). Chirality sensing of tertiary alcohols by a novel strong hydrogen-bonding donor – Selenourea. Chem. Sci. *7*, 932–938.

Bieszczad, B., and Gilheany, D.G. (2017). Asymmetric Grignard synthesis of tertiary alcohols through rational ligand design. Angew. Chem. Int. Ed. *56*, 4272–4276.

Brill, Z.G., Condakes, M.L., Ting, C.P., and Maimone, T.J. (2017). Navigating the chiral pool in the total synthesis of complex terpene natural products. Chem. Rev. *117*, 11753–11795.

Caine, B.A., Dardonville, C., and Popelier, P.L.A. (2018). Prediction of aqueous pK_a values of guanidine-containing compounds using ab initio gas-phase equilibrium bond lengths. ACS Omega *3*, 3835–3850.

Chen, Z., Fan, H., Yang, S., Bian, G., and Song, L. (2018). Chiral sensors for determining the absolute configurations of α-amino acid derivatives. Org. Biomol. Chem. *16*, 8311–8317.

Chen, Z., Wang, Q., Wu, X., Li, Z., and Jiang, Y.-B. (2015). Optical chirality sensing using macrocycles, synthetic and supramolecular oligomers/polymers, and nanoparticle based sensors. Chem. Rev. *44*, 4249–4263.

Chinchilla, R., Foubelo, F., Najera, C., and Yus, M. (1995). (R)-O-Aryllactic acids: convenient chiral solvating agents for direct ^{1}H NMR determination of the enantiomeric composition of amines and amino alcohols. Tetrahedron Asymmetry *6*, 1877–1880.

Christ, P., Lindsay, A., Vormittag, S., Neudörfl, J.-M., Berkessel, A., and O'Donoghue, A. (2011). pK_a values of chiral Brønsted acid catalysts: phosphoric acids/amides, sulfonyl/sulfuryl imides, and perfluorinated TADDOLs (TEFDDOLs). Chem. Eur. J. *17*, 8524–8528.

Ema, T., Tanida, D., and Sakai, T. (2007). Versatile and practical macrocyclic reagent with multiple hydrogen-bonding sites for chiral discrimination in NMR. J. Am. Chem. Soc. *129*, 10591–10596.

Ema, T., Yamasaki, T., Watanabe, S., Hiyoshi, M., and Takaish, K. (2018). Cross-coupling approach to an array of macrocyclic receptors functioning as chiral solvating agents. J. Org. Chem. *83*, 10762–10769.

Fan, J.-H., Hu, Y.-J., Guo, Q., Li, S., Zhao, J., and Li, C.-C. (2019). Asymmetric synthesis of the tetracyclic core of bufogargarizin C by an intramolecular [5 + 2] cycloaddition. Org. Chem. Front. *6*, 22–26.

Fernandez-Perez, H., Lao, J.R., and Vidal-feran, A. (2016). Stereoselective Rh-catalyzed hydrogenative desymmetrization of achiral substituted 1,4-dienes. Org. Lett. *18*, 2836–2839.

Fogassy, E., Nógrádi, M., Kozma, D., Egri, G., Pálovics, E., and Kiss, V. (2006). Optical resolution methods. Org. Biomol. Chem. *4*, 3011–3030.

Han, S. (1997). Direct enantiomeric separations by high performance liquid chromatography using cyclodextrins. Biomed. Chromatogr. *11*, 259–271.

Harding, A.P., and Popelier, P.L.A. (2011). pK_a prediction from an *ab initio* bond length: part 2—phenols. Phys. Chem. Chem. Phys. *13*, 11264–11282.

Hembury, G.A., Borovkov, V.V., and Inoue, Y. (2008). Chirality-sensing supramolecular systems. Chem. Rev. *108*, 1–73.

Hung, K., Condakes, M.L., Novaes, L.F.T., Harwood, S.J., Morikawa, T., Yang, Z., and Maimone, T.J. (2019). Development of a terpene feedstock-based oxidative synthetic approach to the *Illicium* sesquiterpenes. J. Am. Chem. Soc. *141*, 3083–3099.

Khanvilkar, A., and Bedekar, A. (2018). Optically pure 2-(quinolin-8-yloxy)cyclohexan-1-ol as a practical agent for molecular recognition by NMR and fluorescence spectroscopy. Chem. Commun. (Camb.) *54*, 11037–11040.

Lacour, J., and Moraleda, D. (2009). Chiral anion-mediated asymmetric ion paring chemistry. Chem. Commun. (Camb.) *14*, 7073–7089.

Leung, D., Kang, S.O., and Anslyn, E.V. (2012). Rapid determination of enantiomeric excess: a focus on optical approaches. Chem. Soc. Rev. *41*, 448–479.

Liu, L., Ye, M., Hu, X., Yu, X., Zhang, L., and Lei, X. (2011). Chiral solvating agents for carboxylic acids based on the salen moiety. Tetrahedron Asymmetry *22*, 1667–1671.

Liu, Y., Liu, S., Li, D., Zhang, N., Peng, L., Ao, J., Song, C.E., Lan, Y., and Yan, H. (2019). Kinetic resolution of allylic alcohol with Chiral BINOL-based alkoxides: a combination of experimental and theoretical studies. J. Am. Chem. Soc. *141*, 1150–1159.

Luu, Q.H., Lewis, K.G., Banerjee, A., Bhuvanesh, N., and Gladysz, J.A. (2018). The robust, readily available Cobalt(III) trication $[Co(NH_2CHPhCHPhNH_2)]^{3+}$ is a progenitor of broadly applicable chirality and prochirality sensing agents. Chem. Sci. *41*, 5087–5099.

Merino, J., Keppler, A., and Silva, M. (2018). (+)-BIONOL and pure shift experiment: a bidirectional approach for NMR chiral discrimination of overcrowded spectra of primary amines. J. Braz. Chem. Soc. *8*, 1638–1644.

Mittal, N., Lippert, K.M., De, C.K., Klauber, E.G., Emge, T.J., Schreiner, P.R., and Seidel, D. (2015). A dual-catalysis anion-binding approach to the kinetic resolution of amines: insights into the mechanism via a combined experimental and computational study. J. Am. Chem. Soc. *137*, 5748–5758.

Moon, L.S., Jolly, R.S., Kasetti, Y., and Bharatam, P.V. (2009). A new chiral shift reagent for the determination of enantiomeric excess and absolute configuration in cyanohydrins. Chem. Commun. (Camb.), 1067–1069, https://doi.org/10.1039/b817800c.

Moon, L.S., Pal, M., Kasetti, Y., Bharatam, P.V., and Jolly, R.S. (2010). Chiral solvating agents for cycanohydrins and carboxylic acids. J. Org. Chem. *75*, 5487–5498.

Nakamura, S., Hara, Y., Furukawa, T., and Hirashita, T. (2017). Enantioselective barbier-type allylation of ketones using allyl halide and indium in water. RSC Adv. *7*, 15582–15585.

Neves-Garcia, T., Vélez, A., Martínez-llarduya, M., and Espinet, P. (2018). Highly enantioselective addition of dimethylzinc to fluorinated alkyl ketones, and the mechanism behind it. Chem. Commun. (Camb.) *54*, 11809–11812.

Pal, I., Chaudhari, S.R., and Suryaprakash, N. (2014). A versatile ternary ionic complex for chiral discrimination of molecules with diverse functionalities using ^{1}H NMR. New J. Chem. *38*, 4908–4912.

Pal, I., Chaudhari, R., and Suryaprakash, N.R. (2015). Chiral discrimination of secondary alcohols and carboxylic acids by NMR spectroscopy. Magn. Reson. Chem. *53*, 142–146.

Paquette, L.A., and Sweeney, T.J. (1990). Stereospecific approach to 3-Oxocen-7-ones via aliphatic claisen rearrangement. Synthesis of (+)-(2*R*,8*S*)- and (+)-(2*R*,8*R*)-lauthisan. Tetrahedron *46*, 4487–4502.

Parker, D. (1991). NMR determination of enantiomeric purity. Chem. Rev. *91*, 1441–1457.

Ryan, M.M., and Jaimison, T.F. (2006). Mechanistic implications of nickel-catalyzed reductive coupling of aldehydes and chiral 1,6-enynes. Org. Lett. *8*, 455–458.

Schneider, H.-J., Hacket, F., Rüdiger, V., and Ikeda, H. (1998). NMR studies of cyclodextrins and cyclodextrin complexes. Chem. Rev. *98*, 1755–1785.

Schurig, V., and Nowotny, H.-P. (1990). Gas chromatographic separation of enantiomers on cyclodextrin derivatives. Angew. Chem. Int. Ed. *29*, 939–1076.

Seco, J.M., Quiñoá, E., and Riguera, R. (2004). The assignment of absolute configuration by NMR. Chem. Rev. *104*, 17–117.

Selier, J., Dong, X., and Oestreich, M. (2019). Kinetic resolution of tertiary propargylic alcohols by enantioselective Cu-H-catalyzed Si-O coupling. Angew. Chem. Int. Ed. *58*, 1970–1974.

Seo, M.-S., Jang, S., and Kim, H. (2018). A chiral aluminum solvating agent (CASA) for ^{1}H NMR chiral analysis of alcohols at low temperature. Chem. Commun. (Camb.) *54*, 6804–6807.

Seo, M.-S., and Kim, H. (2015). ^{1}H NMR chiral analysis of charged molecules via ion pairing with aluminum complexes. J. Am. Chem. Soc. *137*, 14190–14195.

Sweeting, L.M. (1987). Determination of enantiomeric purity of polar substrates with chiral lanthanide NMR shift reagents in polar solvents. J. Org. Chem. *52*, 2273–2276.

Tsai, E.Y., Liu, R.Y., Yang, Y., and Buchwald, S.L.A. (2018). Regio- and enantioselective CuH-catalyzed ketone allylation with terminal allenes. J. Am. Chem. Soc. *140*, 2007–2011.

Uccello-Barretta, G., Pini, D., Mastantuono, A., and Salvadori, P. (1995). Direct NMR assay of the enantiomeric purity of chiral β-Hydroxy esters by using quinine as chiral solvating agent. Tetrahedron Asymmetry *6*, 1965–1972.

Wenzel, T.J. (2017). Strategies for using NMR spectroscopy to determine absolute configuration. Tetrahedron Asymmetry *28*, 1212–1219.

Wenzel, T.J. (2007). Discrimination of Chiral Compounds Using NMR Spectroscopy (Wiley-VCH).

Wenzel, T.J., and Chisholm, C.D. (2011). Assignment of absolute configuration using chiral reagents and NMR spectroscopy. Chirality *23*, 190–214.

Wilen, S.H., and Qi, J.Z. (1991). Resolution, asymmetric transformation, and configuration of Tröger's Base. application of Tröger's base as a chiral solvating agent. J. Org. Chem. *56*, 485–487.

Wolf, C., Cook, A.M., and Dannat, J.E. (2014). Enantiodifferentiation of multiple tertiary alcohols by NMR spectroscopy with a Whelk-O type chiral solvating agent. Tetrahedron Asymmetry *25*, 163–169.

You, L., Zha, D., and Anslyn, E.V. (2015). Recent advances in supramolecular analytical chemistry using optical sensing. Chem. Rev. *115*, 7840–7892.

Zhang, W., and Ma, S. (2018). Palladium/H^+-cocatalyzed kinetic resolution of tertiary propagylic alcohols. Chem. Commun. (Camb.) *54*, 6064–6067.

ISCI, Volume *19*

Supplemental Information

A Gallium-based Chiral Solvating Agent Enables the Use of ^{1}H NMR Spectroscopy to Differentiate Chiral Alcohols

Sumin Jang and Hyunwoo Kim

Supplemental Figures

Figure S1. ^{1}H and ^{13}C NMR spectrum of [Ga-**L1**]Na. Related to Figure 2.

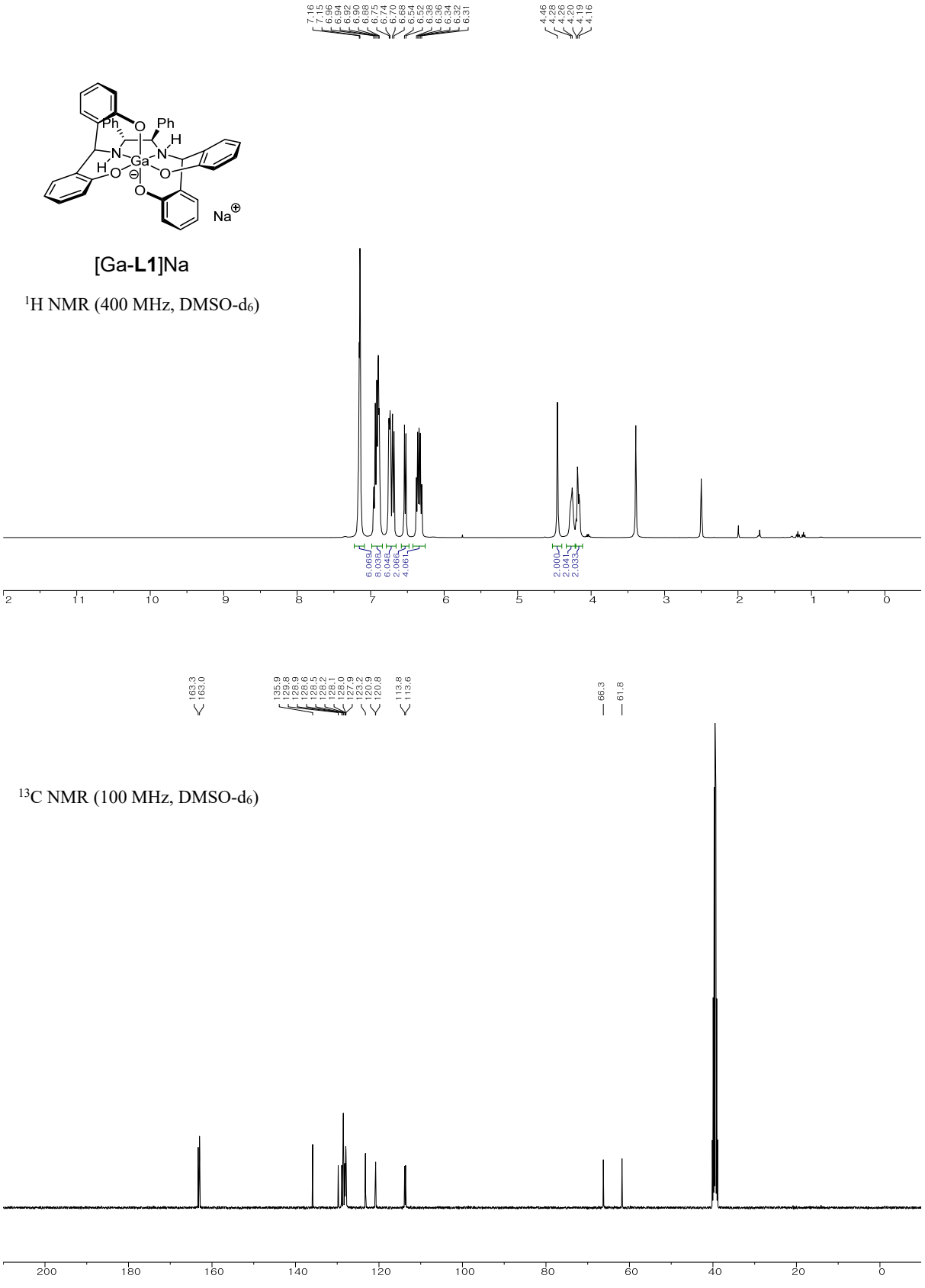

Figure S2. ^{1}H and ^{13}C NMR spectrum of [Sc-**L1**]Na. Related to Figure 2.

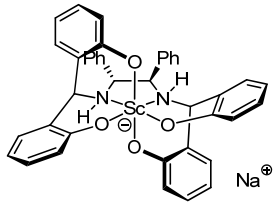

[Sc-**L1**]Na

^{1}H NMR (400 MHz, DMSO-d_6)

^{13}C NMR (100 MHz, DMSO-d_6)

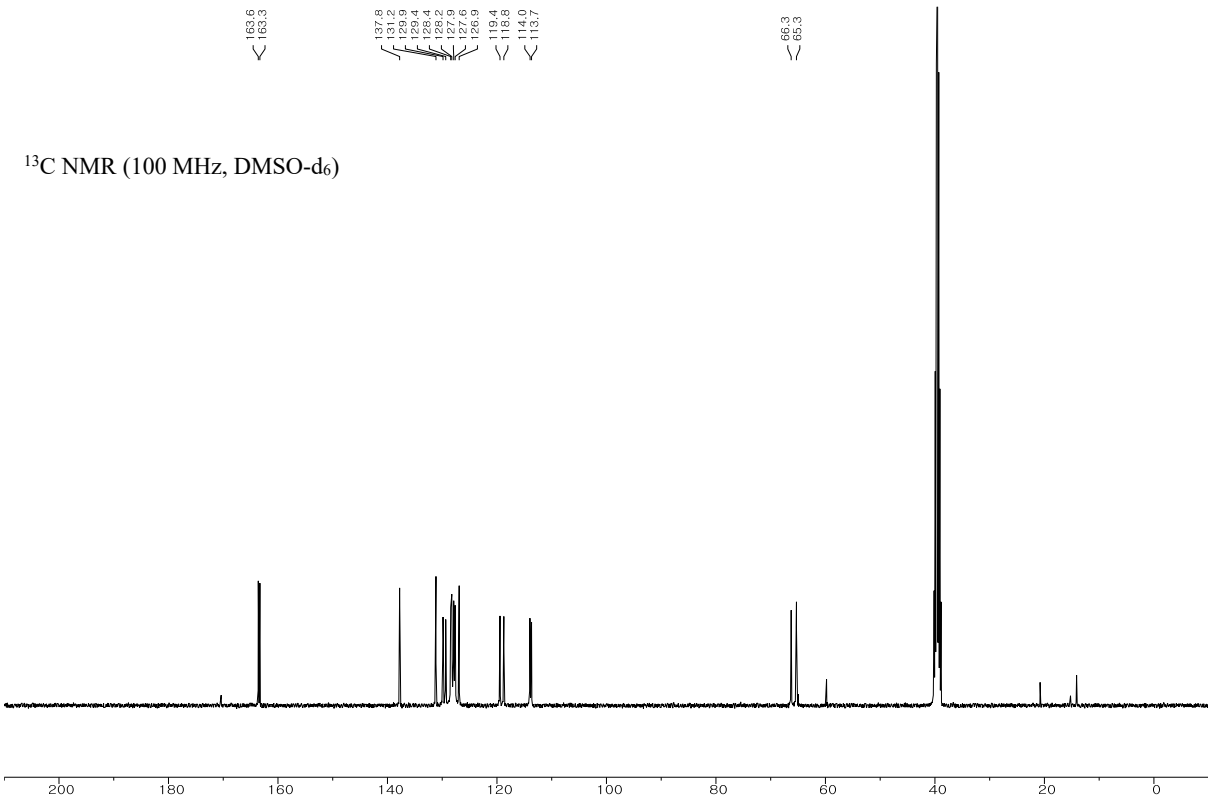

Figure S3. ^{1}H and ^{13}C NMR spectrum of [In-**L1**]Na. Related to Figure 2.

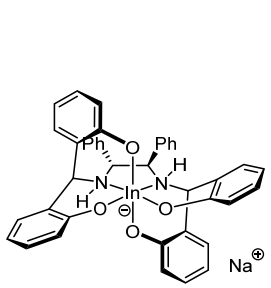

[In-**L1**]Na

^{1}H NMR (400 MHz, DMSO-d_6)

^{13}C NMR (100 MHz, DMSO-d_6)

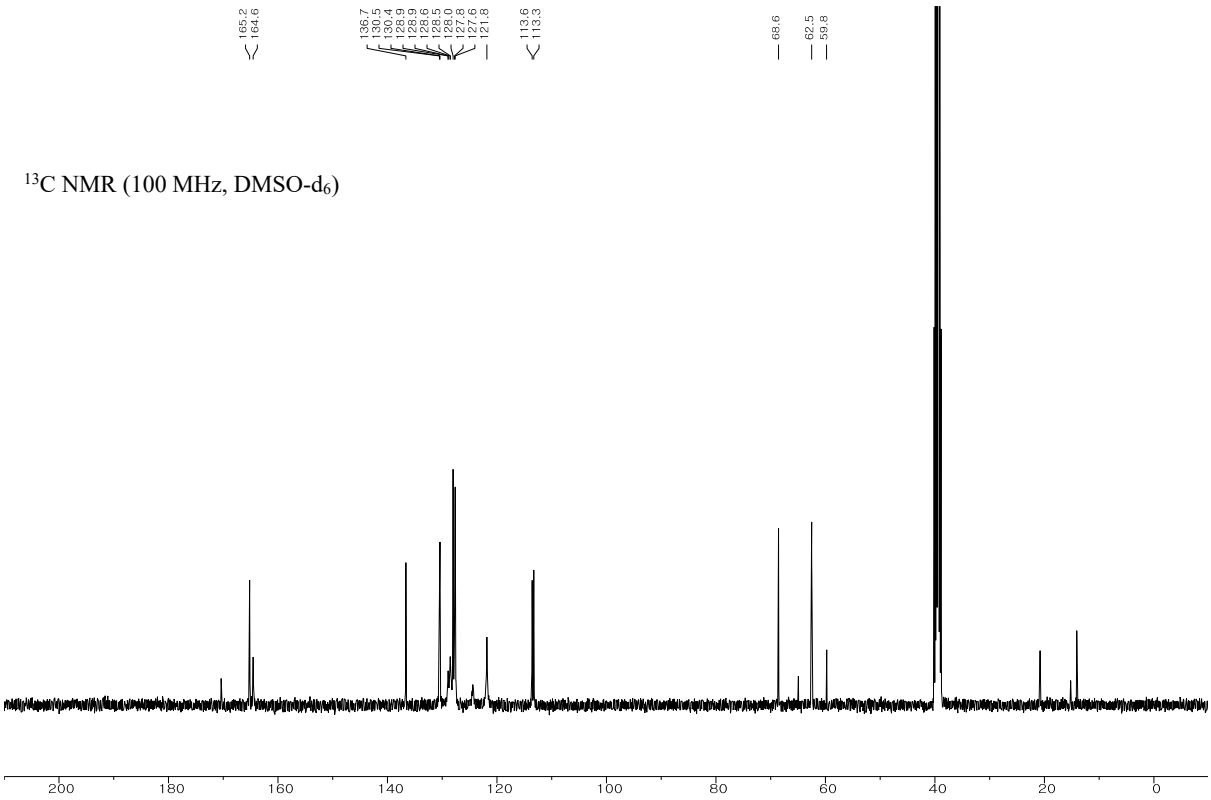

Figure S4. ^{1}H and ^{13}C NMR spectrum of **L2.** Related to Figure 2.

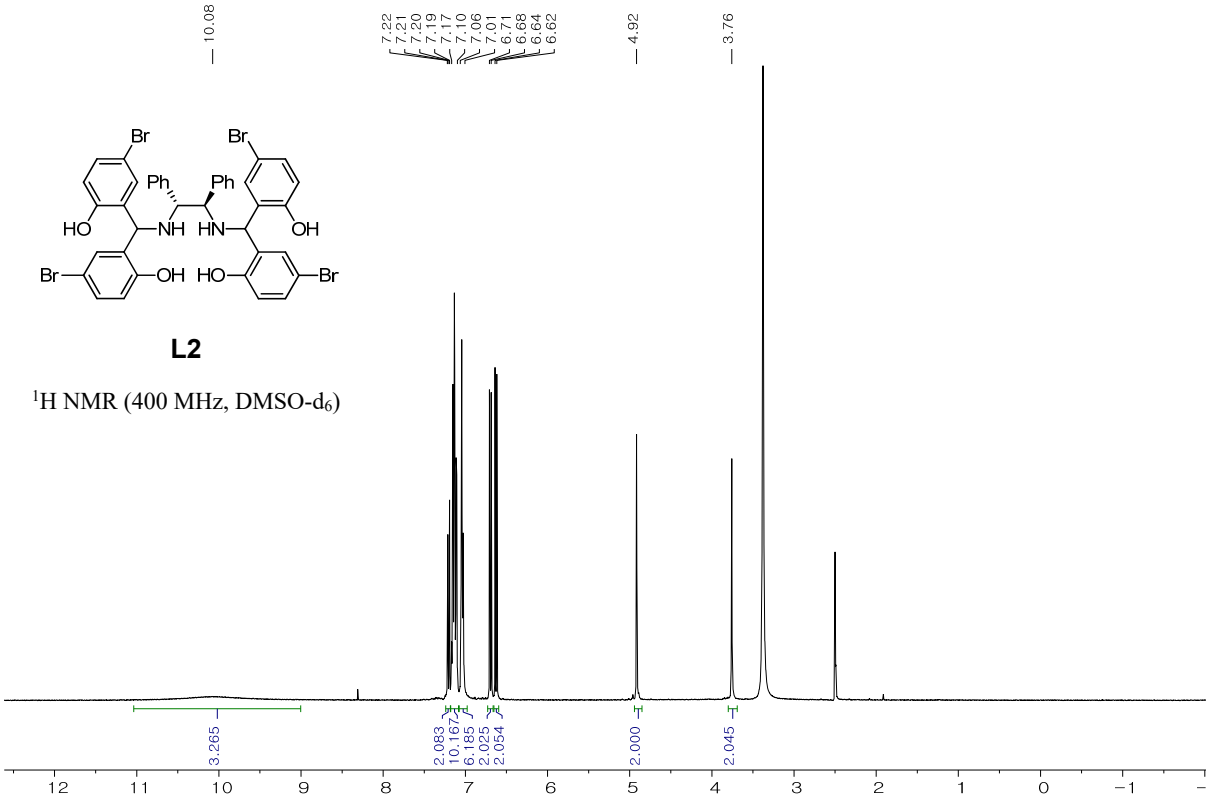

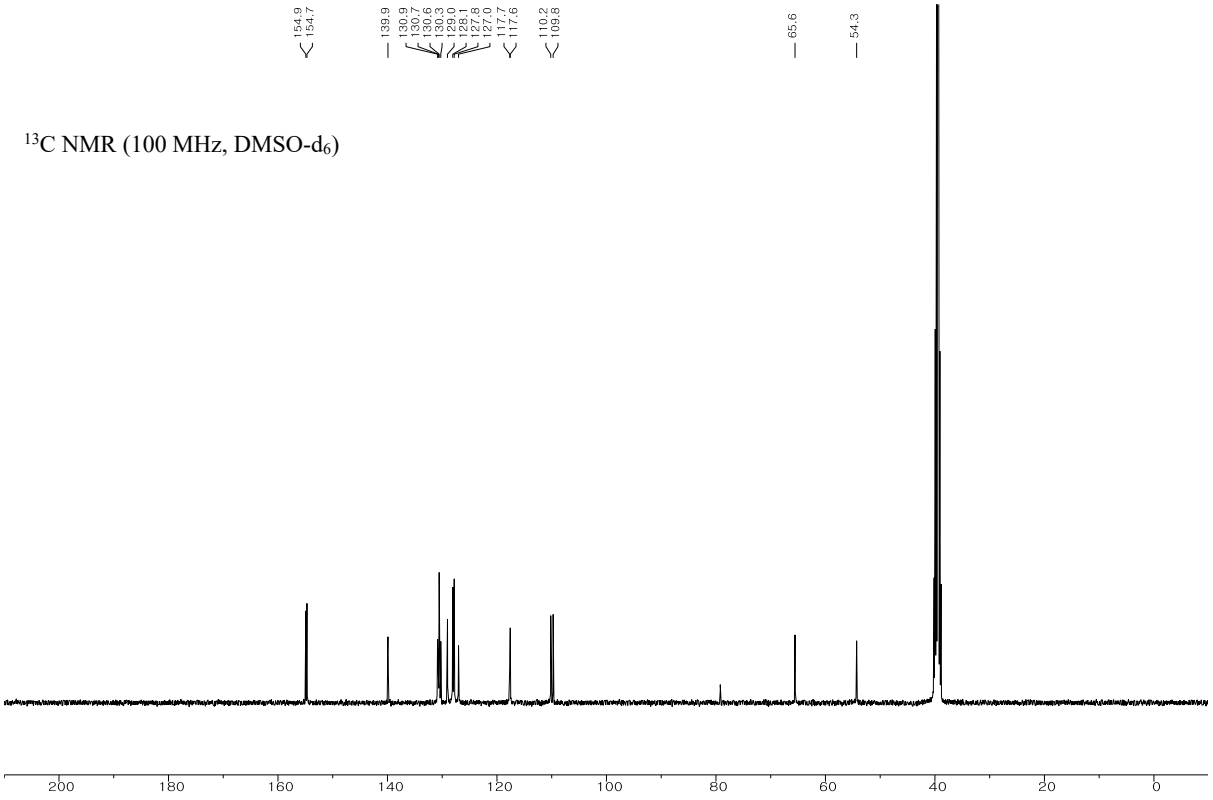

Figure S5. ^{1}H and ^{13}C NMR spectrum of [Al-**L2**]Na. Related to Figure 2.

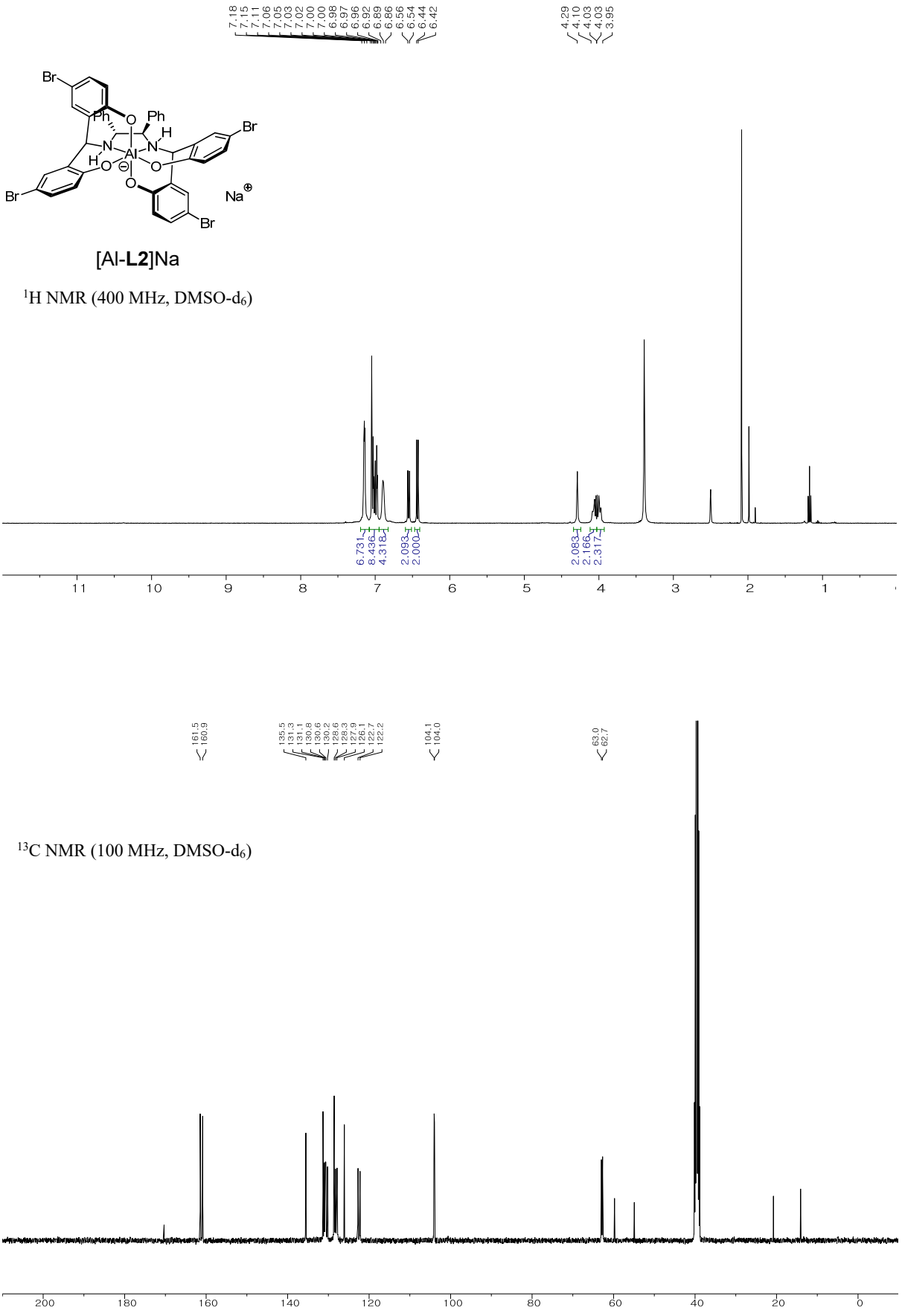

Figure S6. ^{1}H and ^{13}C NMR spectrum of **L3.** Related to Figure 2.

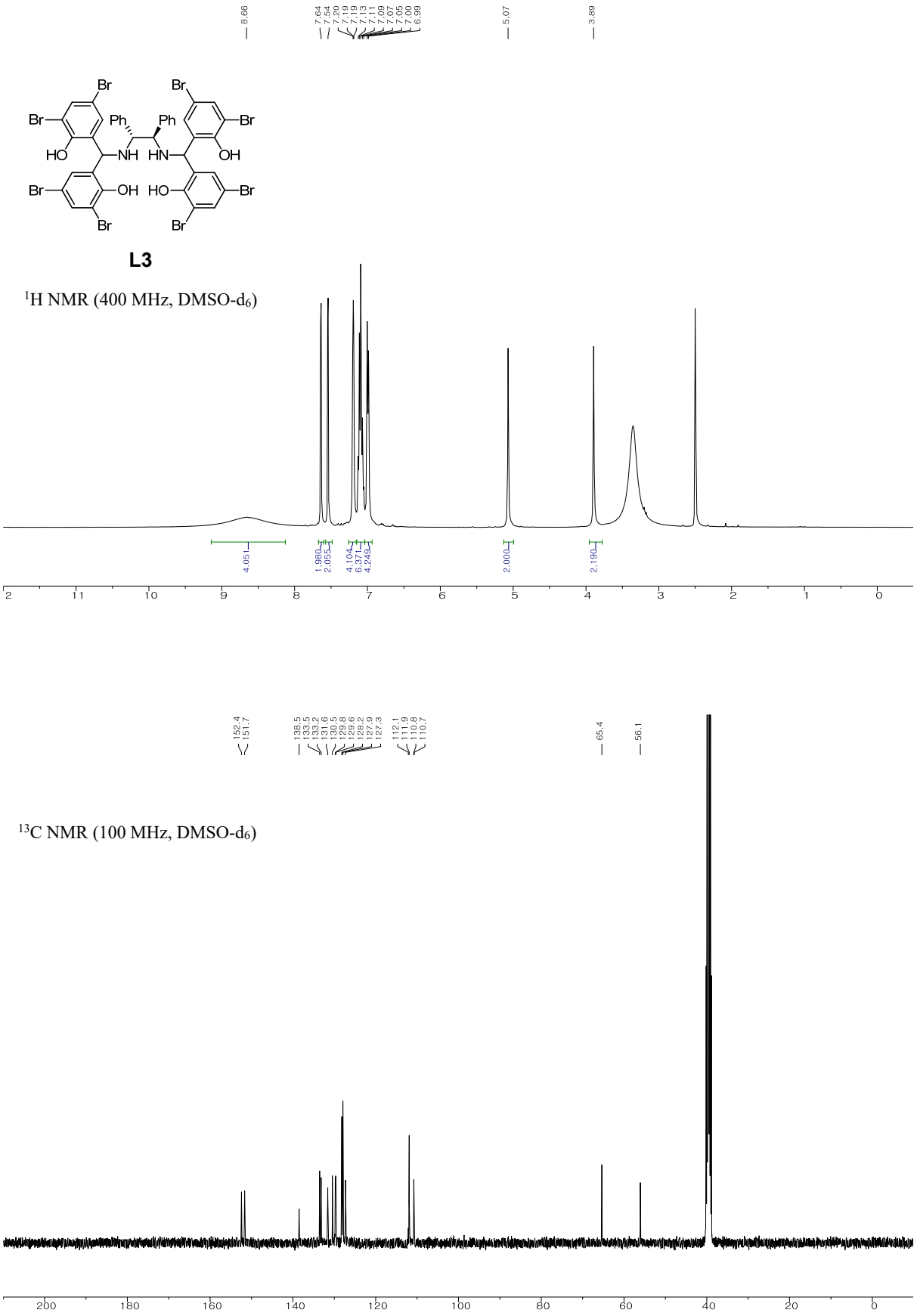

Figure S7. ^{1}H and ^{13}C NMR spectrum of [Al-**L3**]Na. Related to Figure 2.

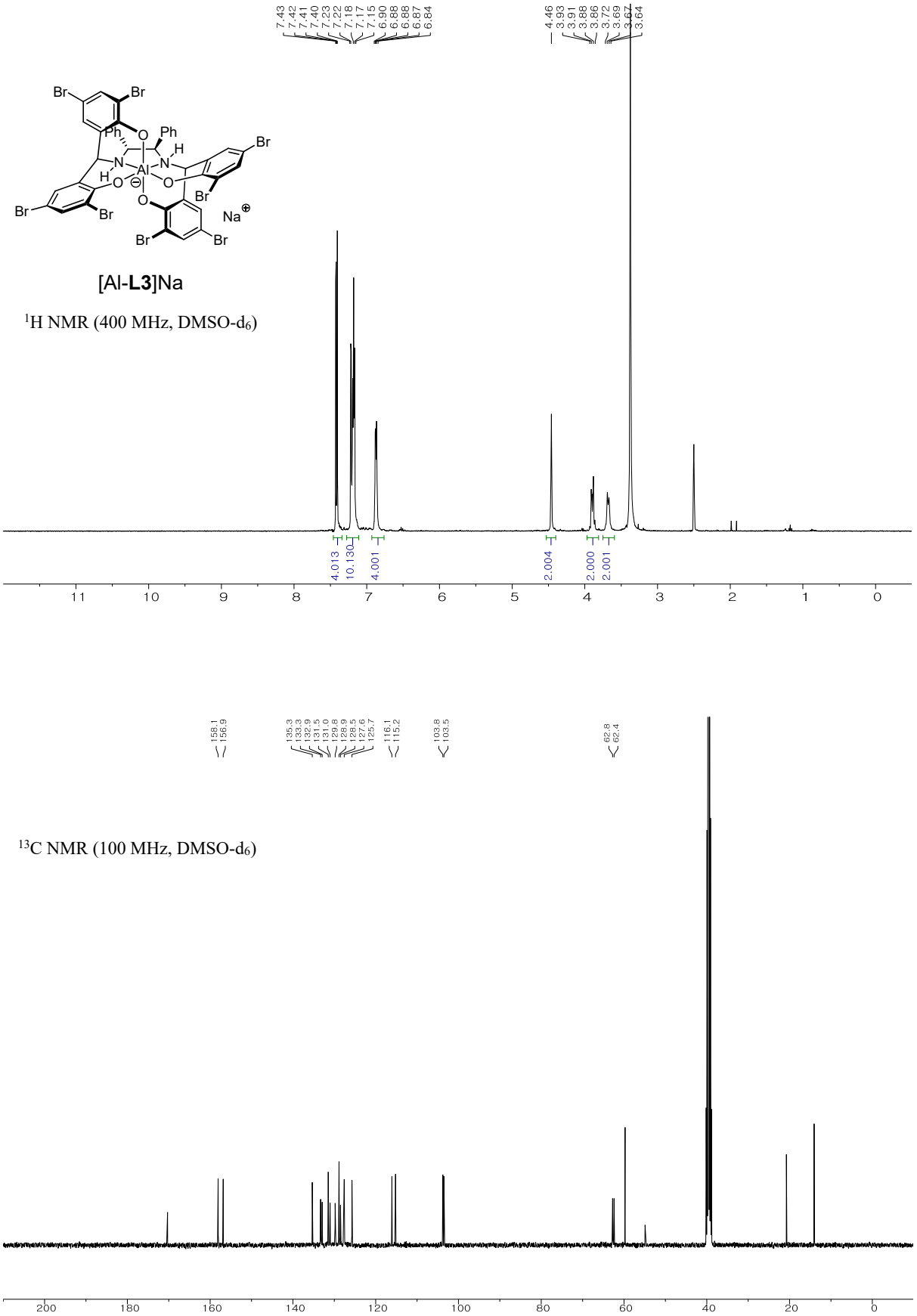

Figure S8. ORTEP representation (50% probability) of the crystal structure of [Al-**L1**]Na. All hydrogens are omitted for clarity. Related to Figure 4.

X-ray quality crystals for [Al-L1]Na were obtained by slow evaporation of its saturated solution in EtOH at RT.

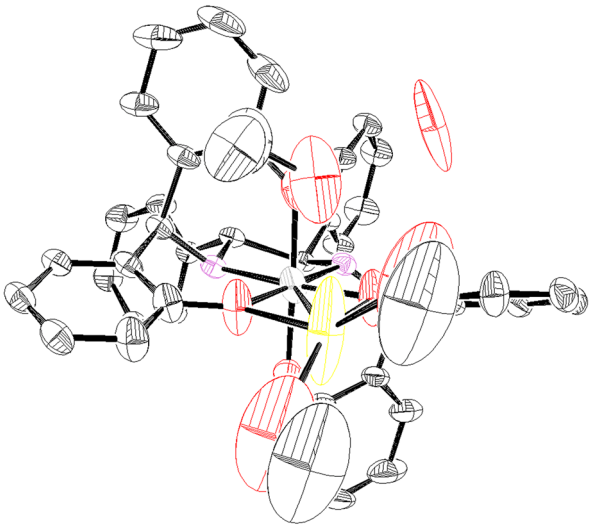

Empirical formula	C46 H52 Al N2 Na O8	
Formula weight	810.86	
Temperature	120(2) K	
Wavelength	0.71073 Å	
Crystal system	Monoclinic	
Space group	C2	
Unit cell dimensions	a = 16.8015(7) Å	a= 90°.
	b = 15.3768(7) Å	b= 94.624(2)°.
	c = 8.5410(4) Å	g = 90°.
Volume	2199.41(17) $Å^3$	
Z	2	
Density (calculated)	1.224 Mg/m^3	
Absorption coefficient	0.110 mm^{-1}	
F(000)	860	
Crystal size	0.25 x 0.2 x 0.2 mm^3	
Theta range for data collection	1.798 to 30.526°.	
Index ranges	-23<=h<=24, -21<=k<=21, -12<=l<=12	
Reflections collected	24971	
Independent reflections	6686 [R(int) = 0.0264]	
Completeness to theta = 25.242°	100.0 %	
Refinement method	Full-matrix least-squares on F^2	
Data / restraints / parameters	6686 / 18 / 272	
Goodness-of-fit on F^2	1.047	
Final R indices [I>2sigma(I)]	R1 = 0.0747, wR2 = 0.2159	
R indices (all data)	R1 = 0.0843, wR2 = 0.2284	
Absolute structure parameter	0.00(5)	
Extinction coefficient	n/a	
Largest diff. peak and hole	0.845 and -0.572 $e.Å^{-3}$	

Figure S9. ORTEP representation (50% probability) of the crystal structure of [Ga-**L1**]Na. All hydrogens are omitted for clarity. Related to Figure 4.

X-ray quality crystals for [Ga-**L1**]Na were obtained by slow diffusion of its DMSO solution in ether at RT.

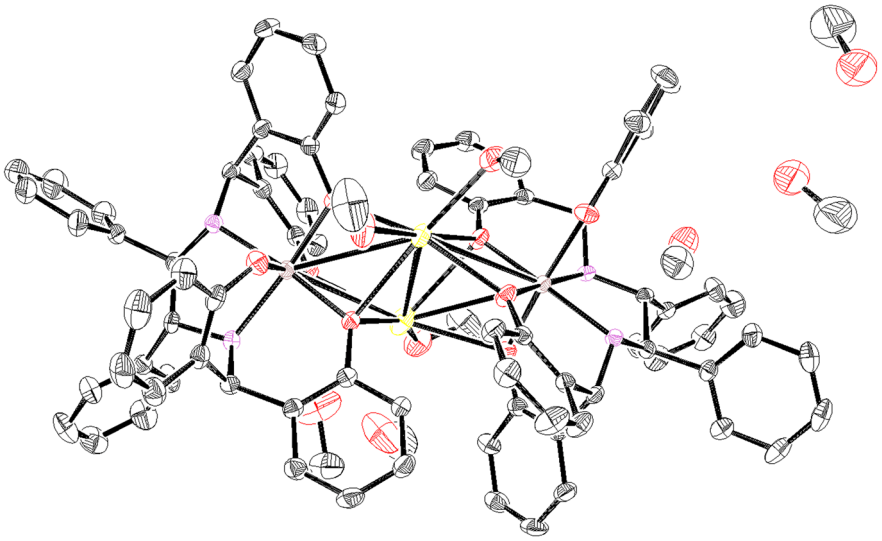

Empirical formula	$C_{88}H_{96}Ga_2N_4Na_2O_{16}$	
Formula weight	1651.10	
Temperature	223(2) K	
Wavelength	0.71073 Å	
Crystal system	Monoclinic	
Space group	$P2_1$	
Unit cell dimensions	a = 12.9954(6) Å	= 90°.
	b = 18.7634(8) Å	= 105.7467(16)°.
	c = 17.0751(8) Å	= 90°.
Volume	4007.3(3) $Å^3$	
Z	2	
Density (calculated)	1.368 Mg/m^3	
Absorption coefficient	0.754 mm^{-1}	
F(000)	1728	
Crystal size	0.220 x 0.120 x 0.090 mm^3	
Theta range for data collection	2.171 to 28.346°.	
Index ranges	-17<=h<=17, -25<=k<=24, -22<=l<=22	
Reflections collected	153202	
Independent reflections	19791 [R(int) = 0.1663]	
Completeness to theta = 25.242°	99.9 %	
Absorption correction	Semi-empirical from equivalents	
Max. and min. transmission	0.7354 and 0.6953	
Refinement method	Full-matrix least-squares on F^2	
Data / restraints / parameters	19791 / 1 / 1023	
Goodness-of-fit on F^2	1.043	
Final R indices [I>2sigma(I)]	R1 = 0.0485, wR2 = 0.0727	
R indices (all data)	R1 = 0.1005, wR2 = 0.0853	
Absolute structure parameter	0.007(4)	
Extinction coefficient	n/a	
Largest diff. peak and hole	0.384 and -0.397 $e.Å^{-3}$	

Figure S10. ORTEP representation (50% probability) of the crystal structure of [In-**L1**]Na. All hydrogens are omitted for clarity. Related to Figure 4.

X-ray quality crystals for [In-**L1**]Na were obtained by slow evaporation of its saturated solution in MeOH/THF at RT.

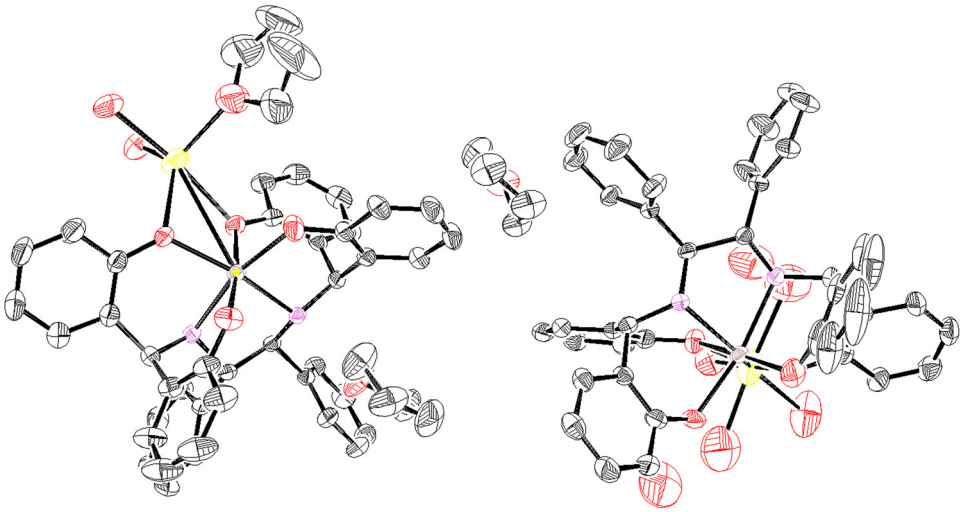

Empirical formula	C92 H106 In2 N4 Na2 O20	
Formula weight	1863.42	
Temperature	223(2) K	
Wavelength	0.71073 Å	
Crystal system	Monoclinic	
Space group	$P2_1$	
Unit cell dimensions	a = 19.3886(12) Å	= 90°.
	b = 10.5743(7) Å	= 110.065(2)°.
	c = 22.5621(14) Å	= 90°.
Volume	4344.9(5) $Å^3$	
Z	2	
Density (calculated)	1.424 Mg/m^3	
Absorption coefficient	0.614 mm^{-1}	
F(000)	1932	
Crystal size	0.260 x 0.220 x 0.140 mm^3	
Theta range for data collection	2.110 to 26.818°.	
Index ranges	-24<=h<=24, -13<=k<=13, -28<=l<=28	
Reflections collected	124427	
Independent reflections	18558 [R(int) = 0.0381]	
Completeness to theta = 25.242°	99.9 %	
Absorption correction	Semi-empirical from equivalents	
Max. and min. transmission	0.7454 and 0.7003	
Refinement method	Full-matrix least-squares on F^2	
Data / restraints / parameters	18558 / 1 / 1081	
Goodness-of-fit on F^2	1.054	
Final R indices [I>2sigma(I)]	R1 = 0.0355, wR2 = 0.0876	
R indices (all data)	R1 = 0.0441, wR2 = 0.0941	
Absolute structure parameter	-0.028(4)	
Extinction coefficient	n/a	
Largest diff. peak and hole	0.737 and -0.654 $e.Å^{-3}$	

Figure S11. The effects of ligand on enantiodiscrimination of the OH peak (C_{tot} = 20 mM, alcohol:CSA=1:1). Related to Figure 5.

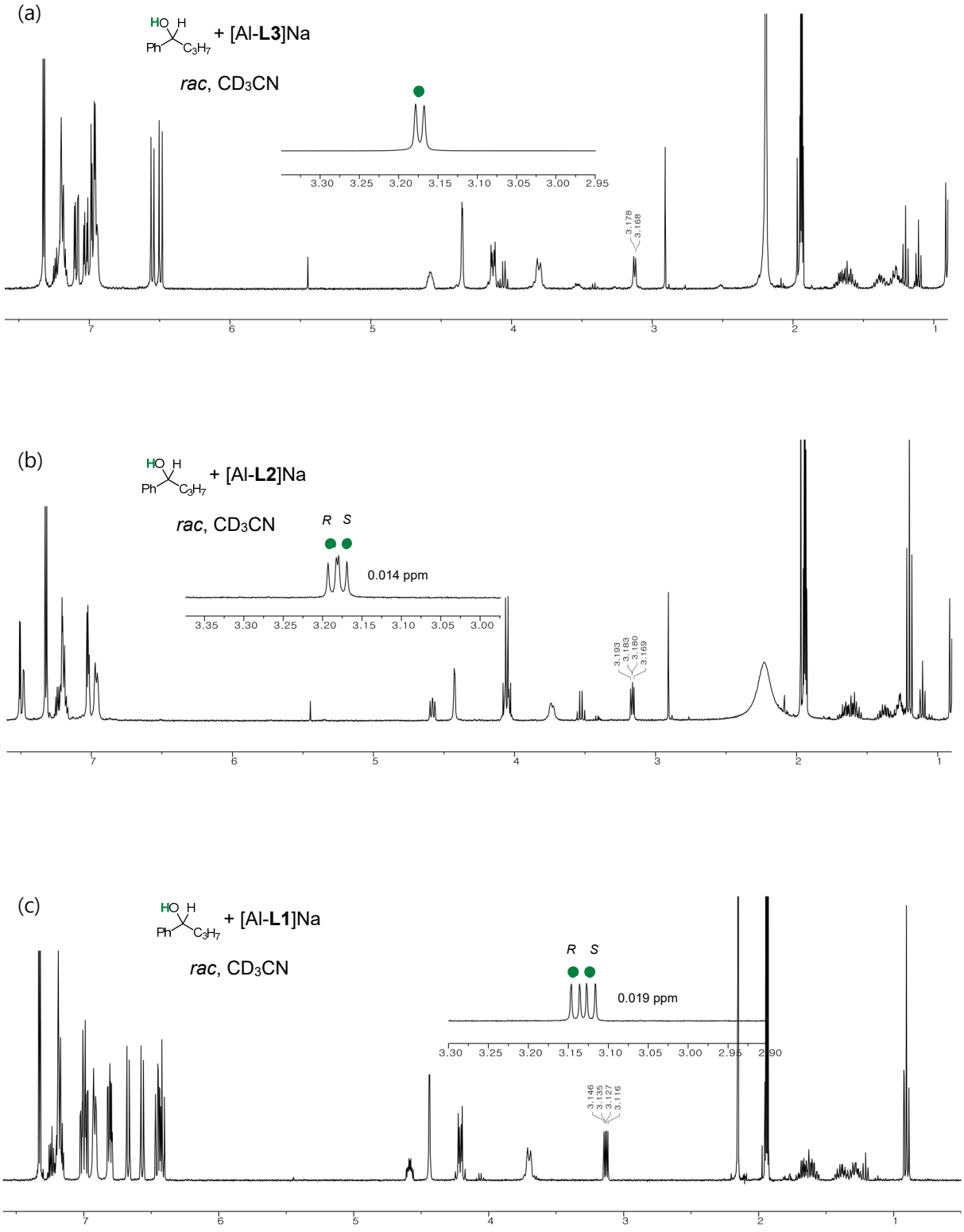

Figure S12. The effects of central metals on enantiodiscrimination of the OH peak (C_{tot} = 20 mM, alcohol:CSA=1:1). Related to Figure 5.

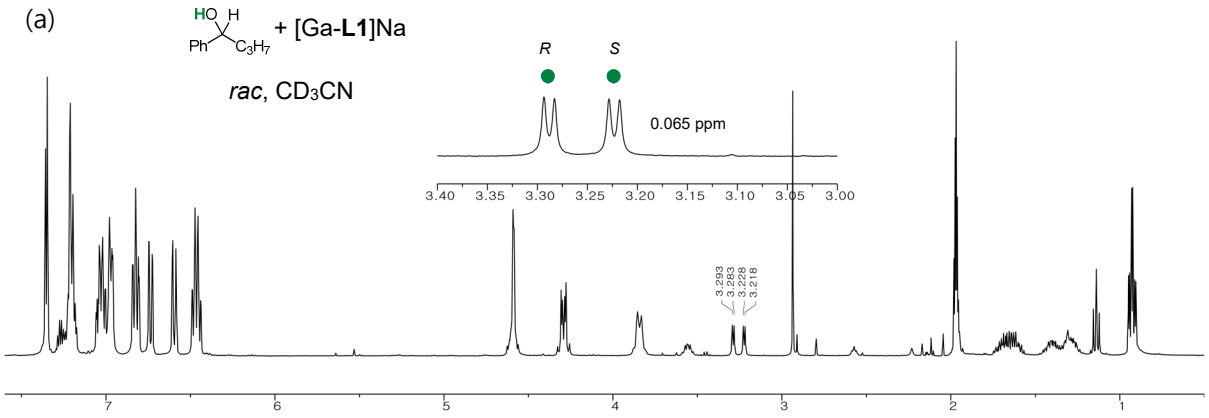

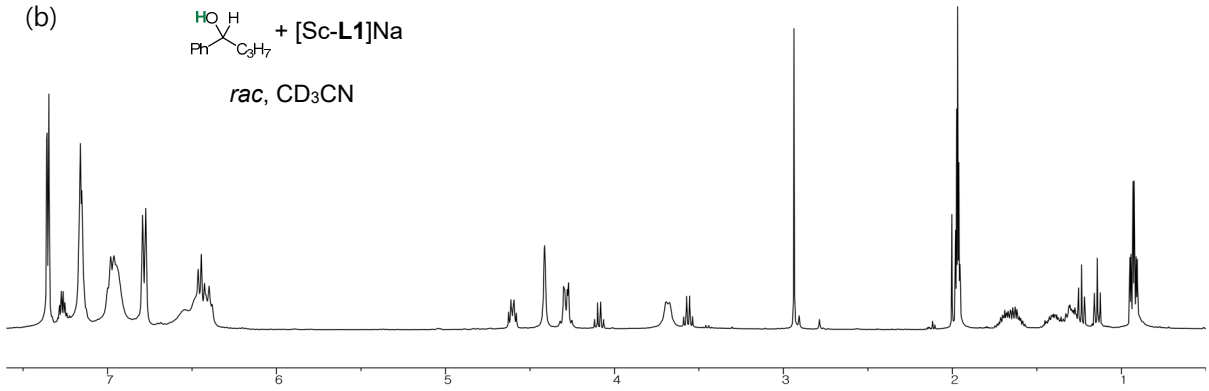

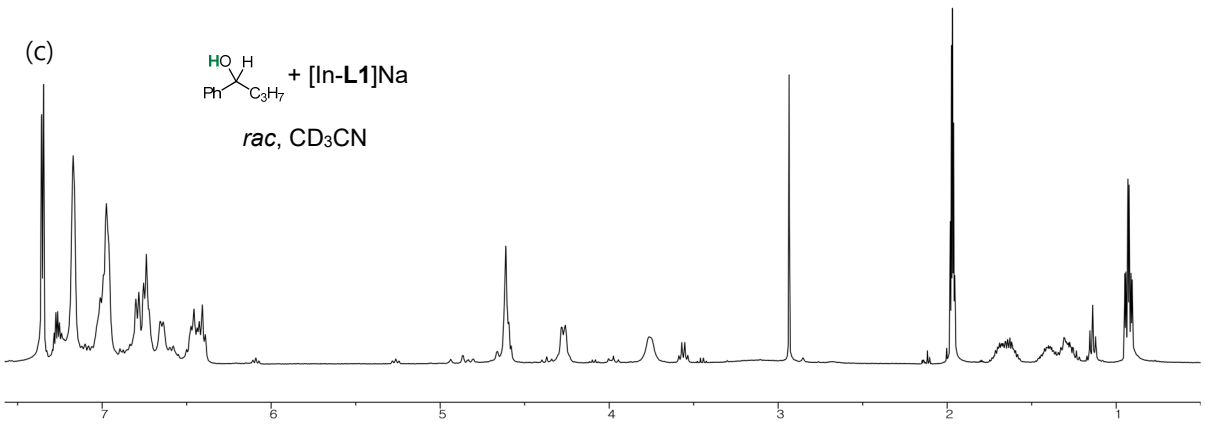

Figure S13. The effects of countercations on enantiodiscrimination of the OH peak (C_{tot} = 20 mM, alcohol:CSA=1:1). Related to Figure 5.

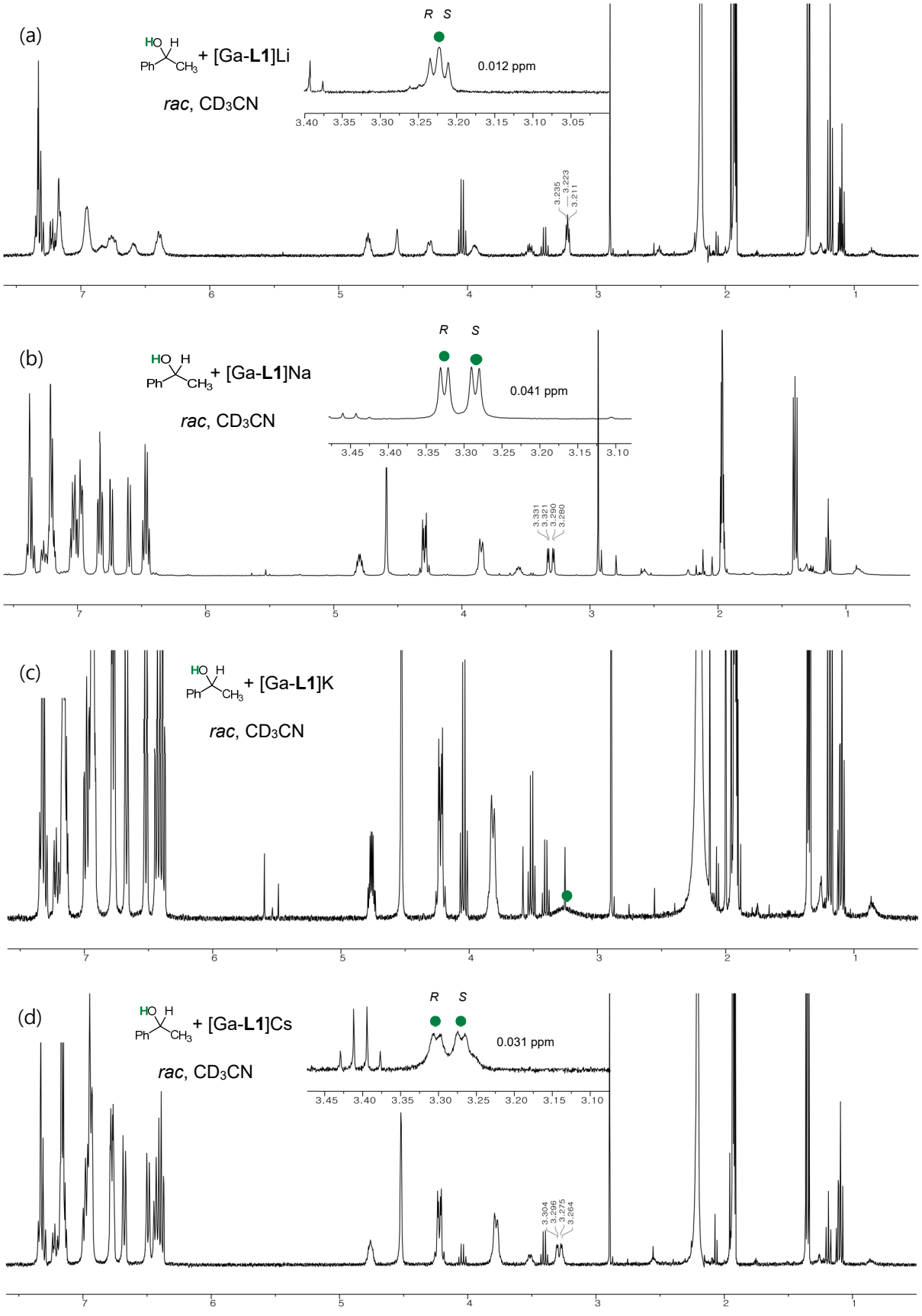

Figure S14. ^{1}H NMR spectra of a 1:1 mixture of *rac*- or enantioriched analyte (a) to (c) and [Ga-**L1**]Na (C_{tot} = 20 mM). Related to Figure 7.

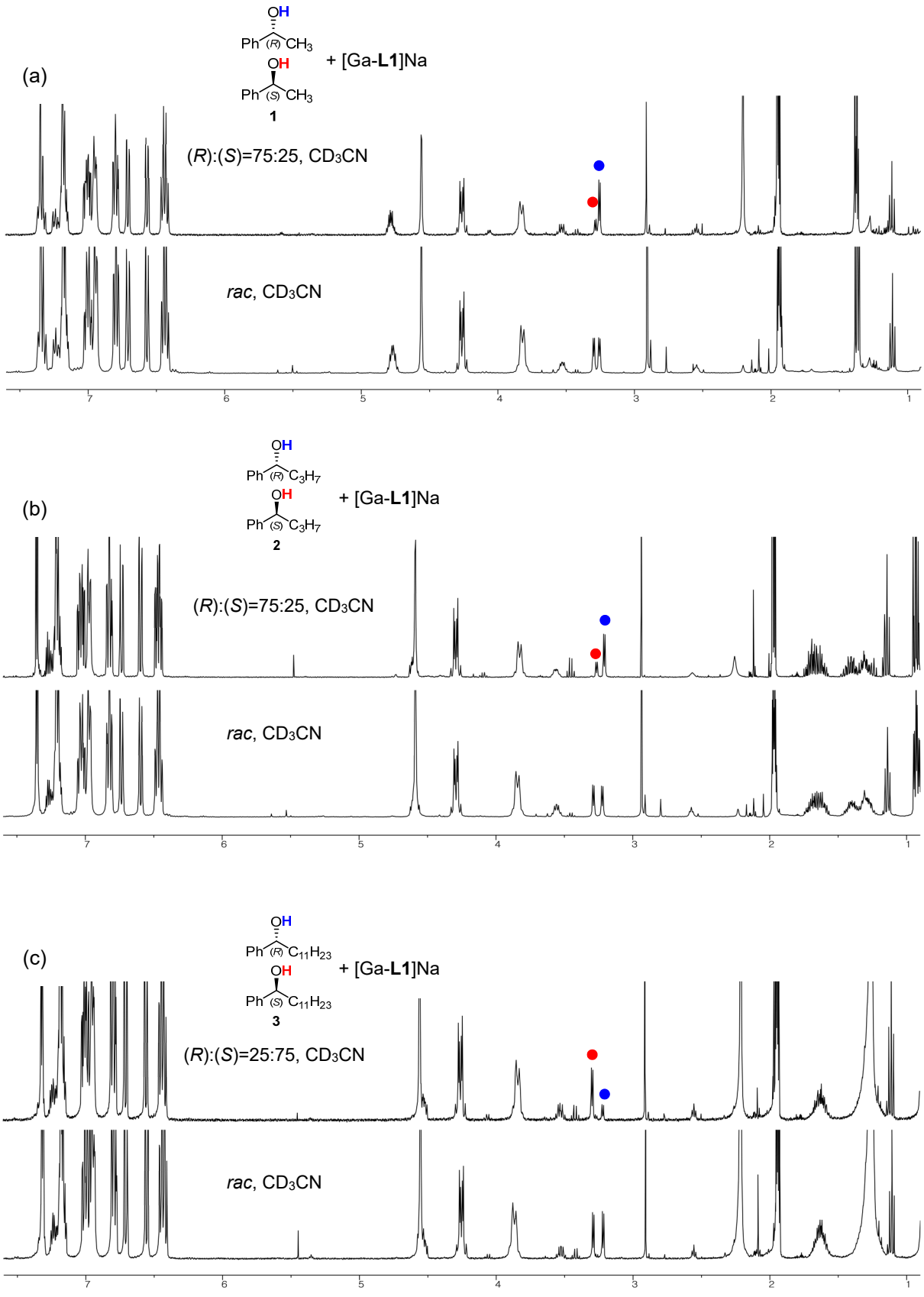

Figure S15. ^{1}H NMR spectra of a 1:1 mixture of *rac*- or enantioriched analyte (d) to (f) and [Ga-**L1**]Na (C_{tot} = 20 mM). Related to Figure 7.

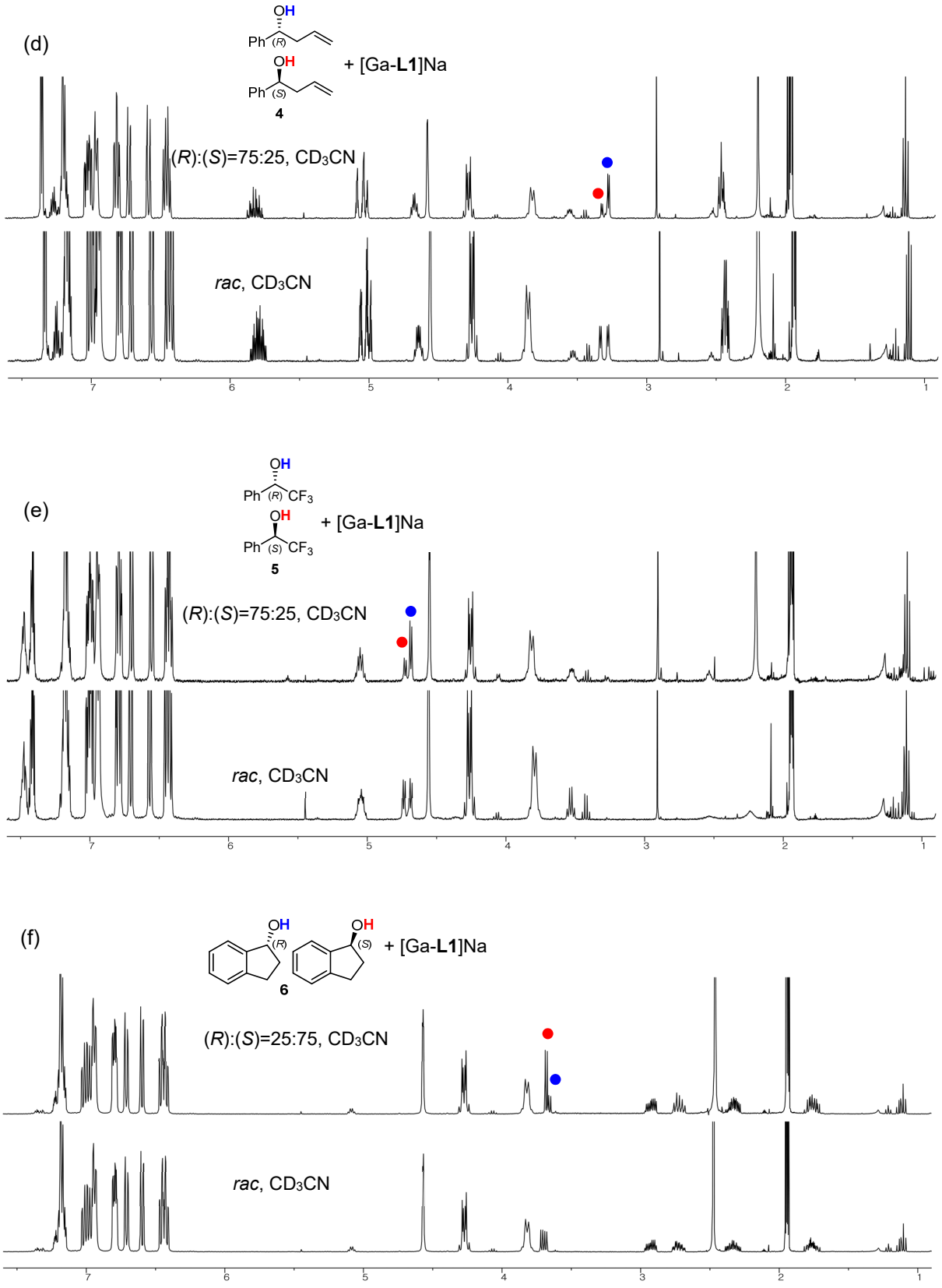

Figure S16. ^{1}H NMR spectra of a 1:1 mixture of *rac*- or enantioriched analyte (g) to (i) and [Ga-**L1**]Na (C_{tot} = 20 mM). Related to Figure 7.

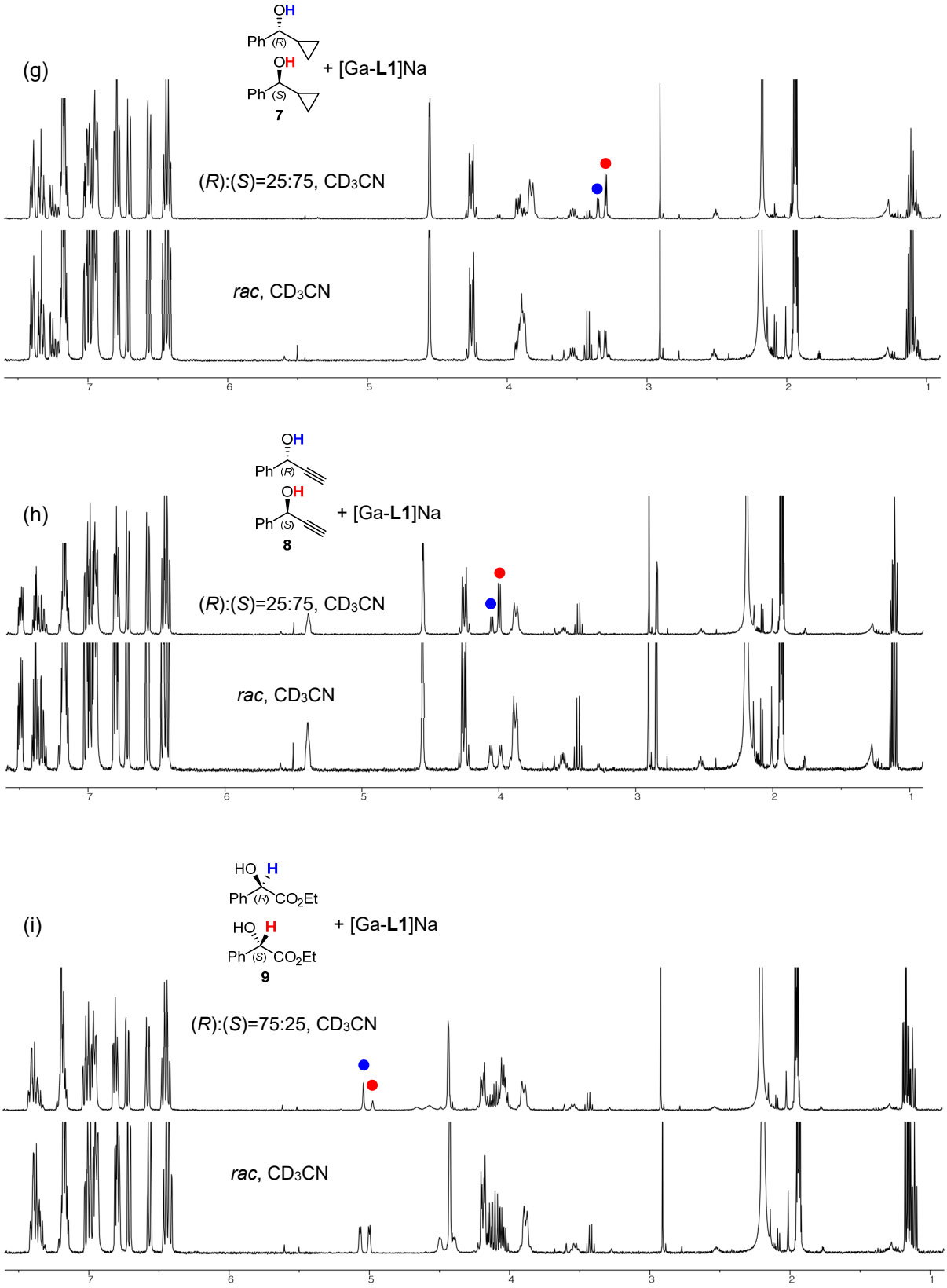

Figure S17. ^{1}H NMR spectra of a 1:1 mixture of *rac*- or enantioriched analyte (j) to (l) and [Ga-**L1**]Na (C_{tot} = 20 mM). Related to Figure 7.

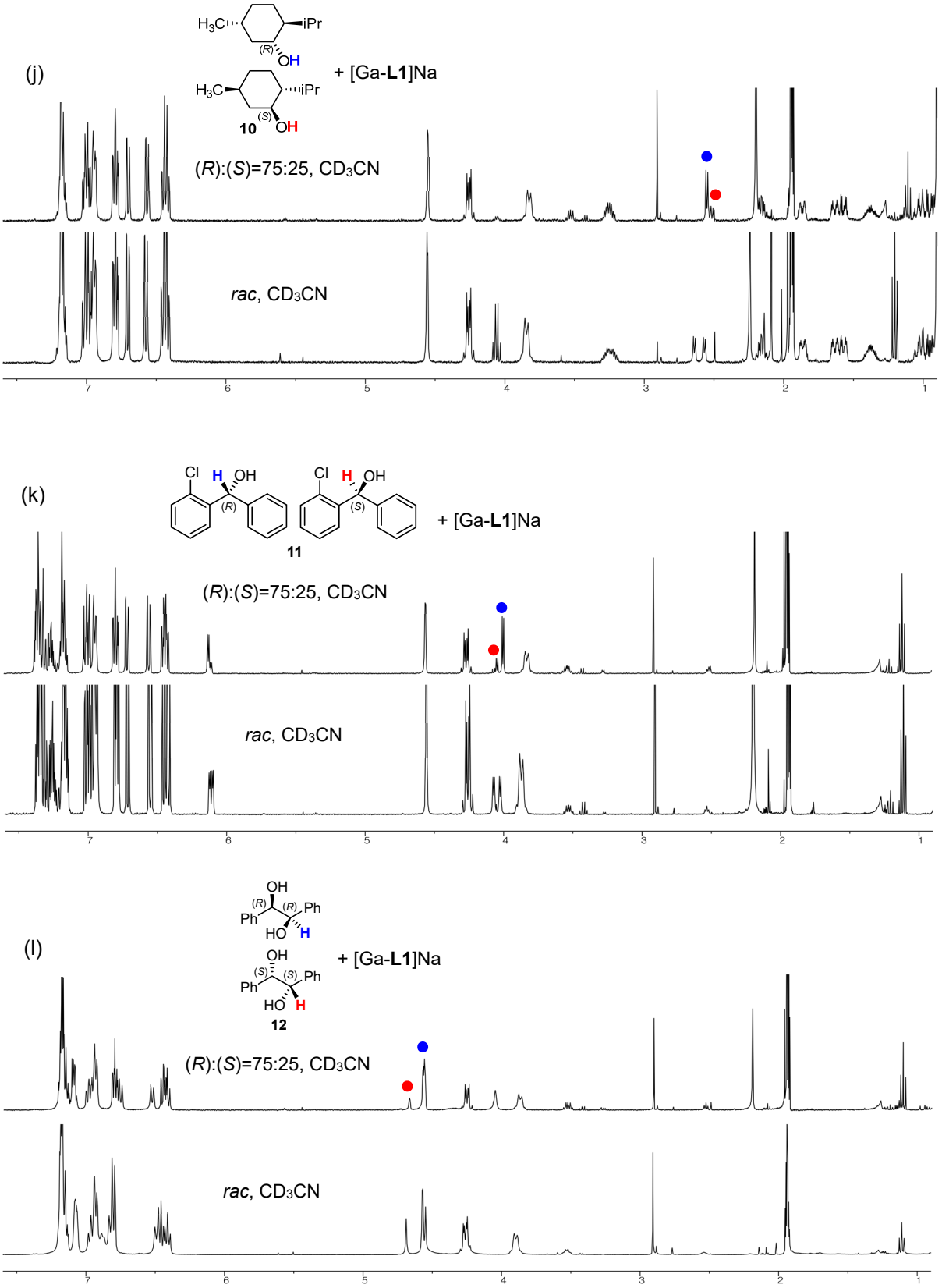

Figure S18. Partial ^{1}H NMR spectra showing chiral discrimination of hydroxyl peaks of *rac*-alcohols with [Ga-**L1**]Na and previously reported chiral solvating agents in CD_3CN (Yellow: full enantiodiscrimination, Green: partial enantiodiscrimination, C_{tot} = 20 mM, *rac*-alcohol:CSA=1:1, at room temperature). Chiral solvating agents showing no enantiodiscrimination due to broadened hydroxyl peaks are shown at the bottom of the table. Related to Figure 8.

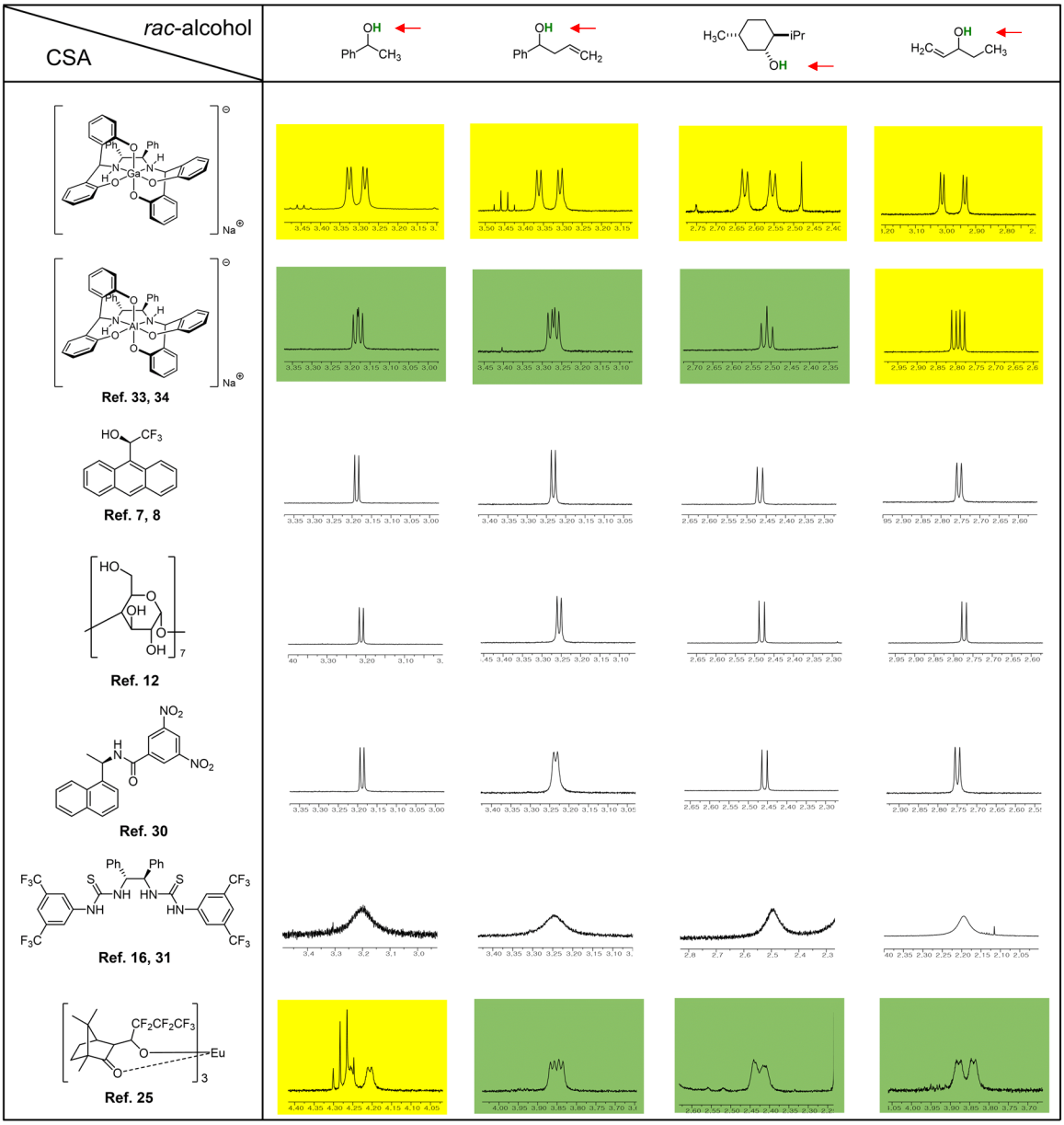

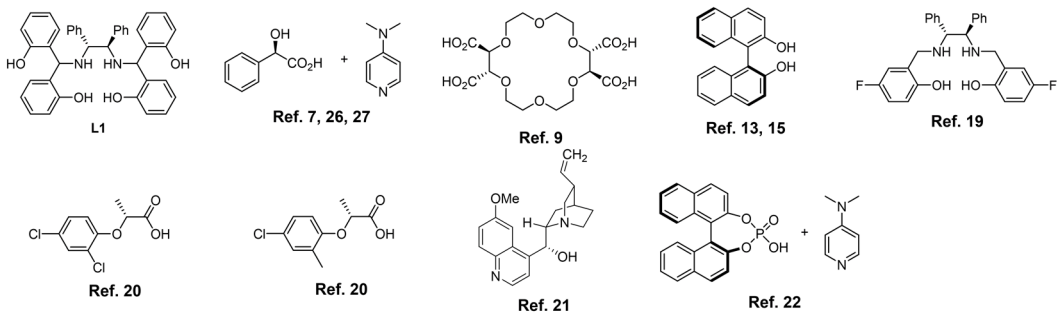

Figure S19. Partial ^{1}H NMR spectra showing chiral discrimination of C-H proton peaks with chiral solvating agents tested in Figure S16 in CD_3CN (Yellow: full enantiodiscrimination, Green: partial enantiodiscrimination, C_{tot} = 20 mM, *rac*-alcohol:CSA=1:1, at room temperature). Related to Figure 8.

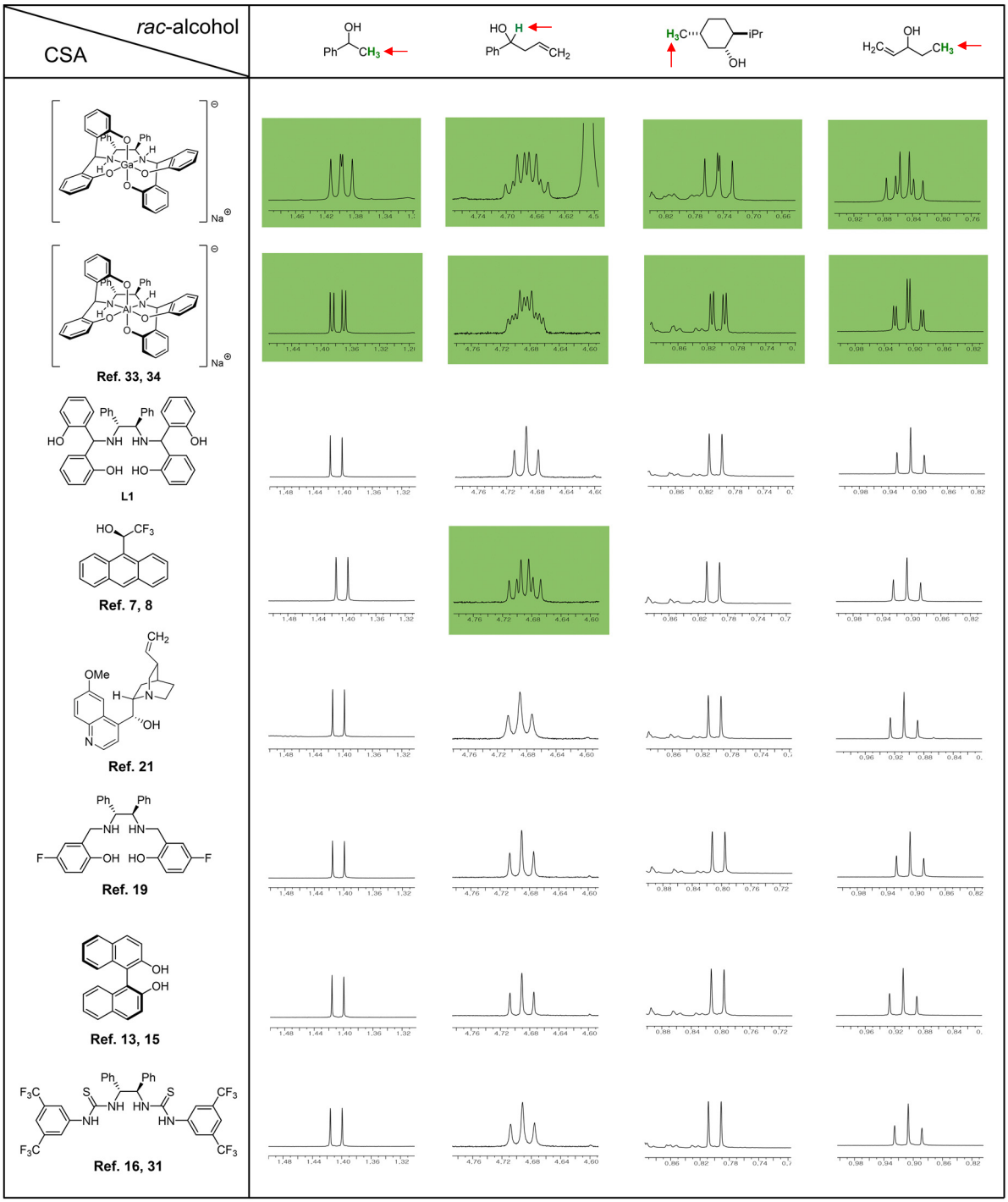

Figure S20. Partial ^{1}H NMR spectra showing chiral discrimination of C-H proton peaks with chiral solvating agents tested in Figure S16 in CD_3CN (Yellow: full enantiodiscrimination, Green: partial enantiodiscrimination, C_{tot} = 20 mM, *rac*-alcohol:CSA=1:1, at room temperature))(continued). Related to Figure 8.

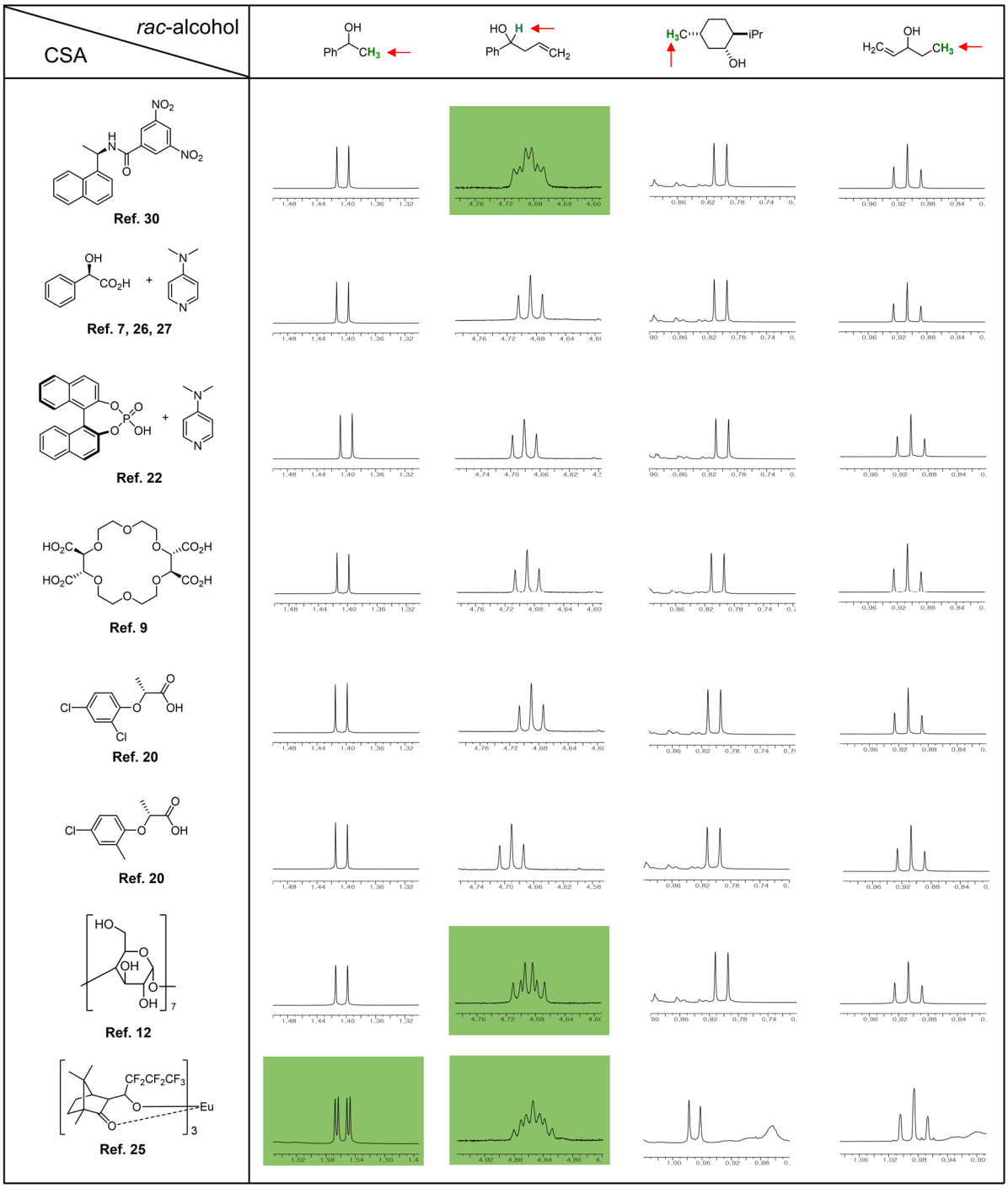

Figure S21. ^{1}H NMR spectra of a mixture of *rac*- or enantioriched 2-butanol and various equivalent of [Ga-**L1**]Na. Related to Figure 8.

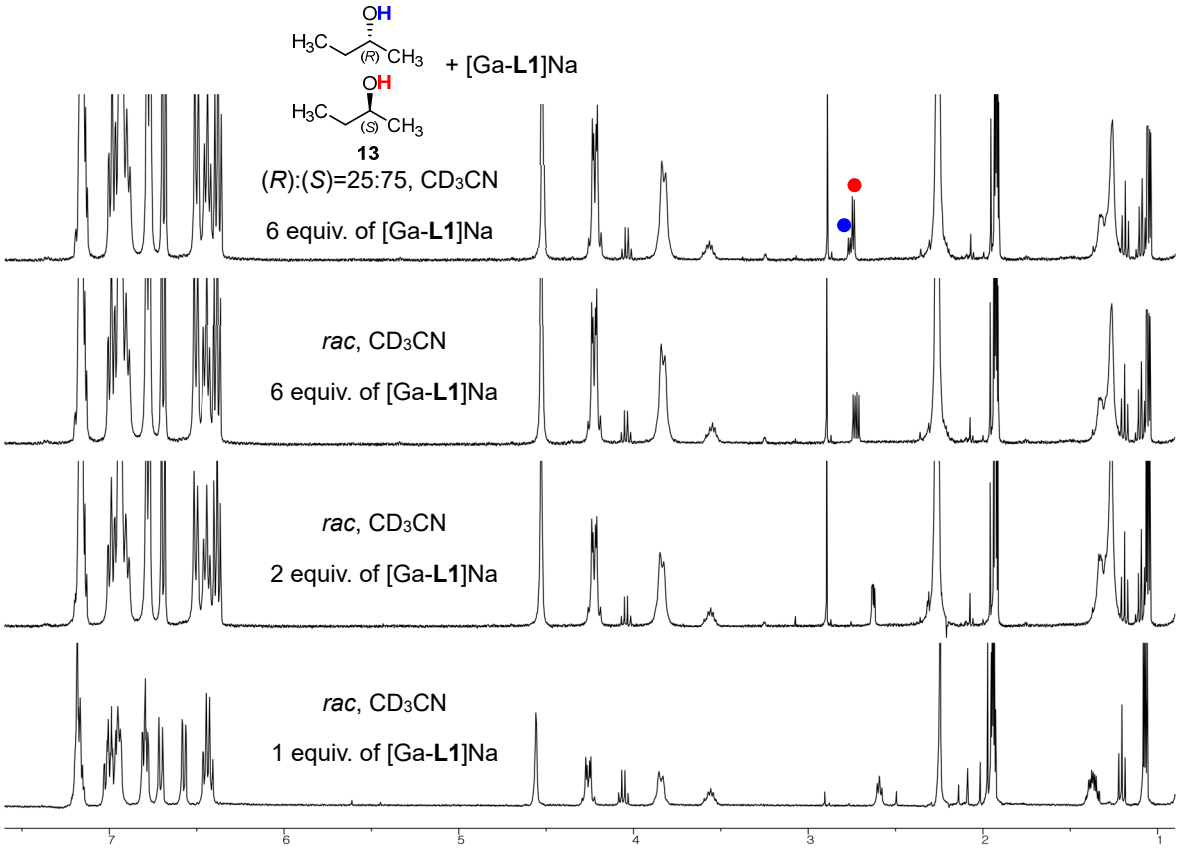

Figure S22. ^{1}H NMR spectra of a mixture of *rac*- or enantioriched mevalonolactone and various equivalent of [Ga-**L1**]Na. Related to Figure 8.

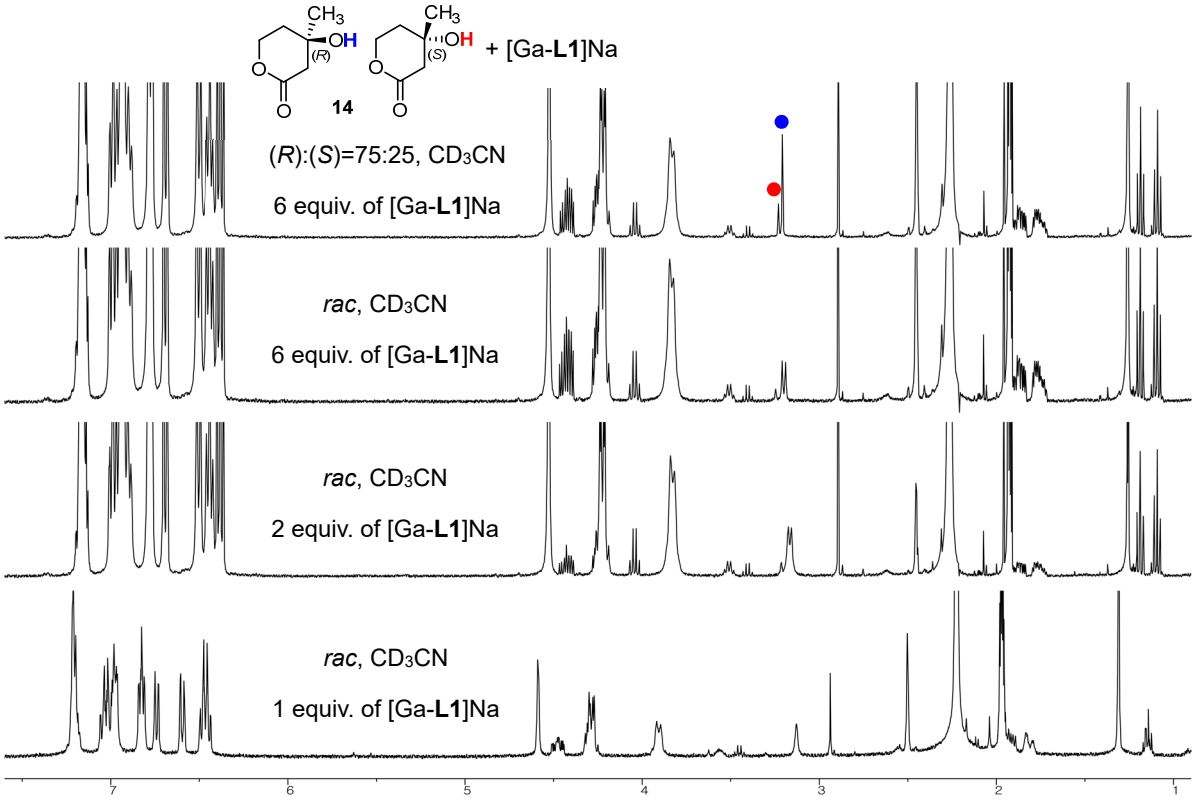

Figure S23. ^{1}H NMR spectra of a mixture of *rac*- or enantioriched 2-phenyl-1-propanol and various equivalent of [Ga-**L1**]Na. Related to Figure 8.

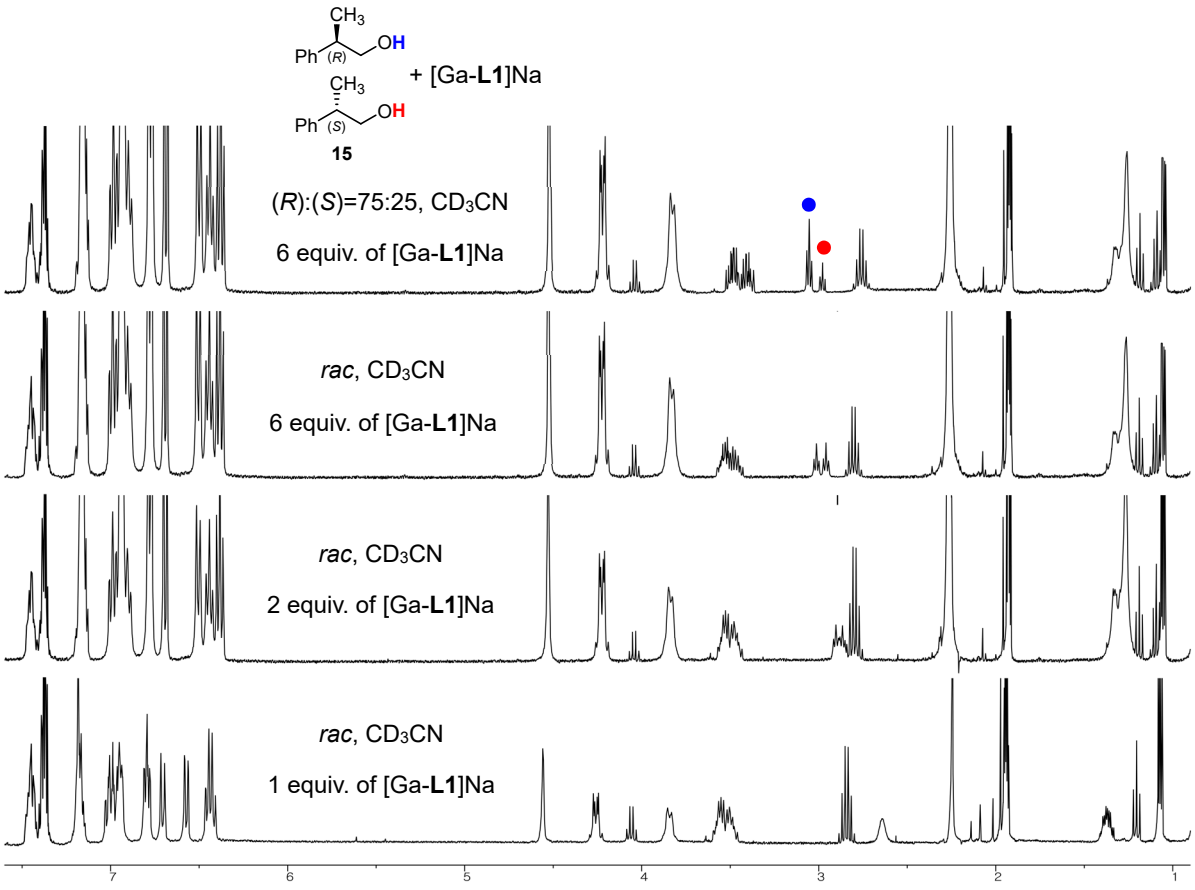

Figure S24. ^{1}H NMR spectra of Sharpless epoxidation product at (a) 3 hours (b) 7 hours (c) 14 hours with 0.04 mmol of [Ga-**L1**]Na. Related to Figure 9.

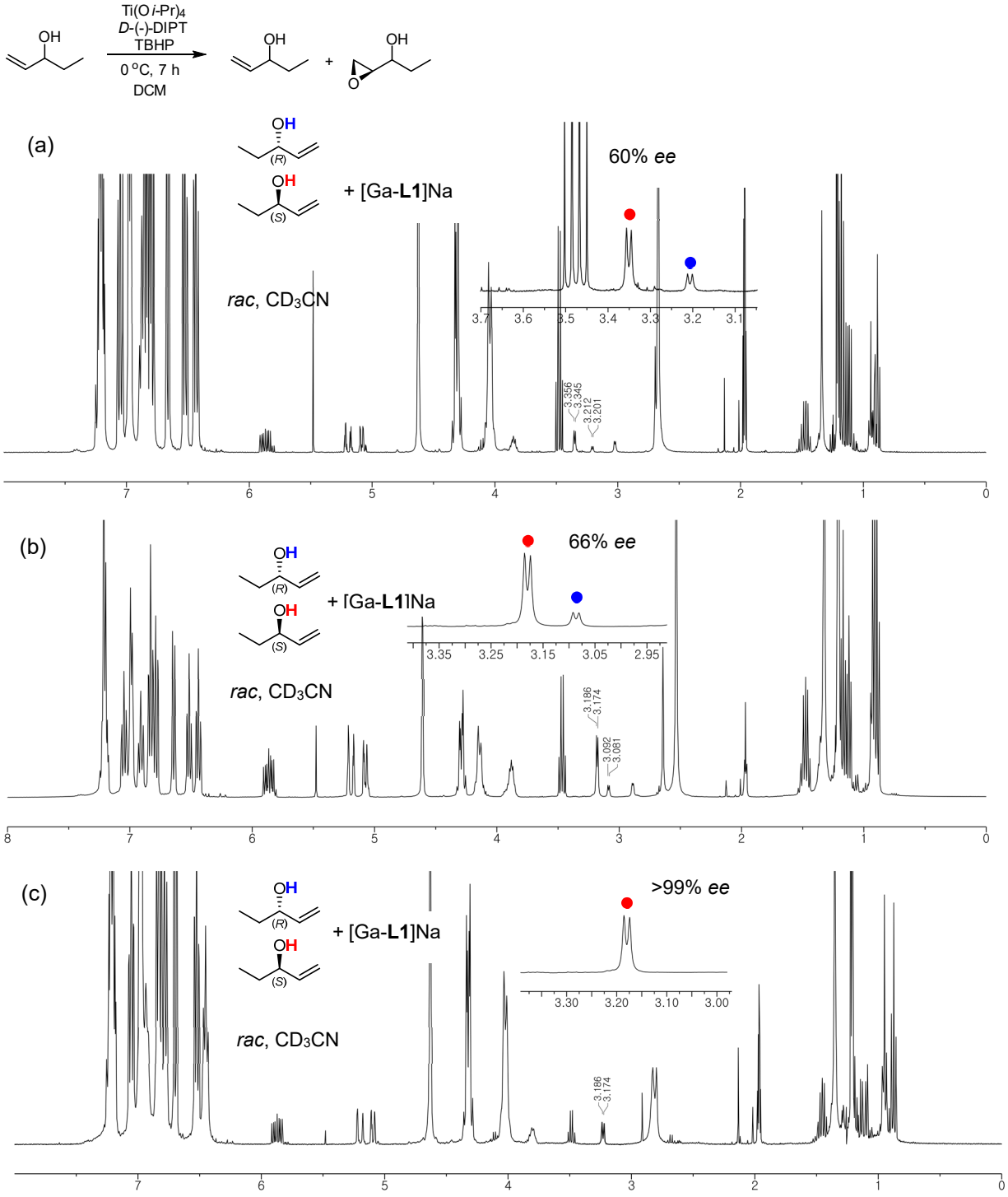

Figure S25. ^{1}H NMR spectra of a 1:2 mixture of *rac*-1-penten-3-ol and [Ga-**L1**]Na. Related to Figure 10A.

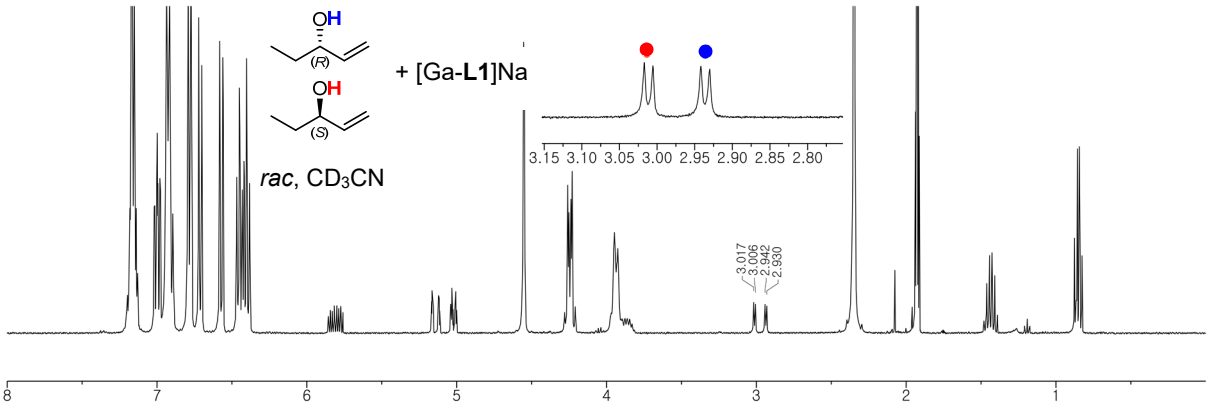

Figure S26. ^{1}H NMR spectra of a 1:1:2 mixture of *rac*-1-penten-3-ol, 1,3-pentadien-3-ol and[Ga-**L1**]Na. Related to Figure 10A.

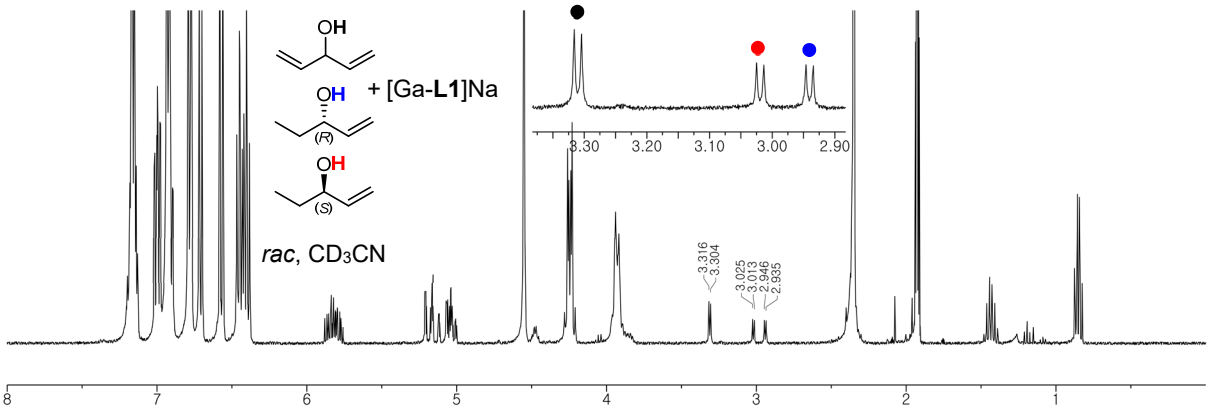

Figure S27. Partial ^{1}H NMR NMR spectra of crude reaction mixture with 0.04 mmol of [Ga-**L1**]Na for direct analysis of enantiomeric excess. Related to Figure 10C.

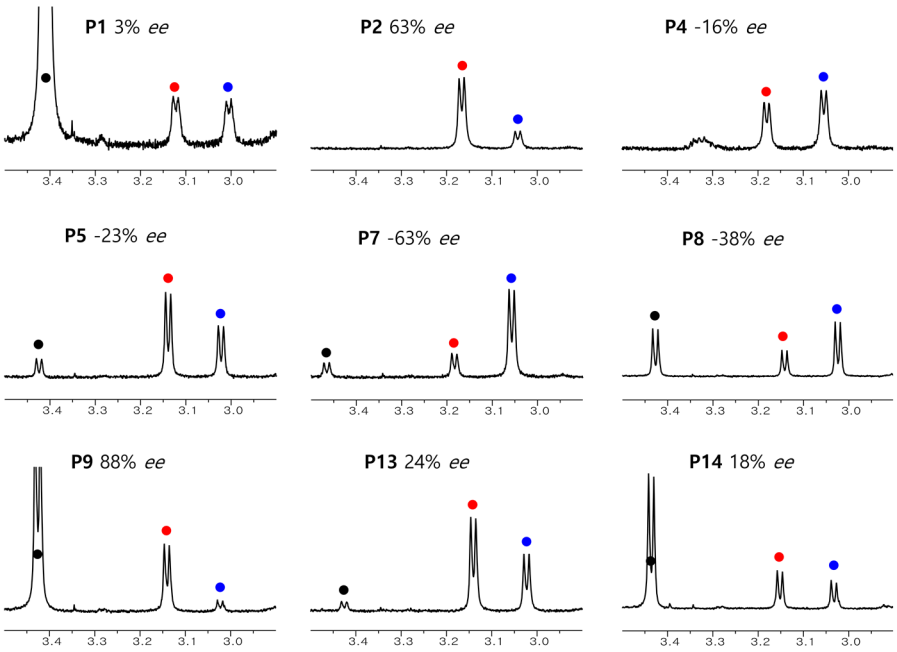

Figure S28. NMR yields and enantioselectivities of hydrogenative desymmetrization with various phosphine ligands. Related to Figure 10C.

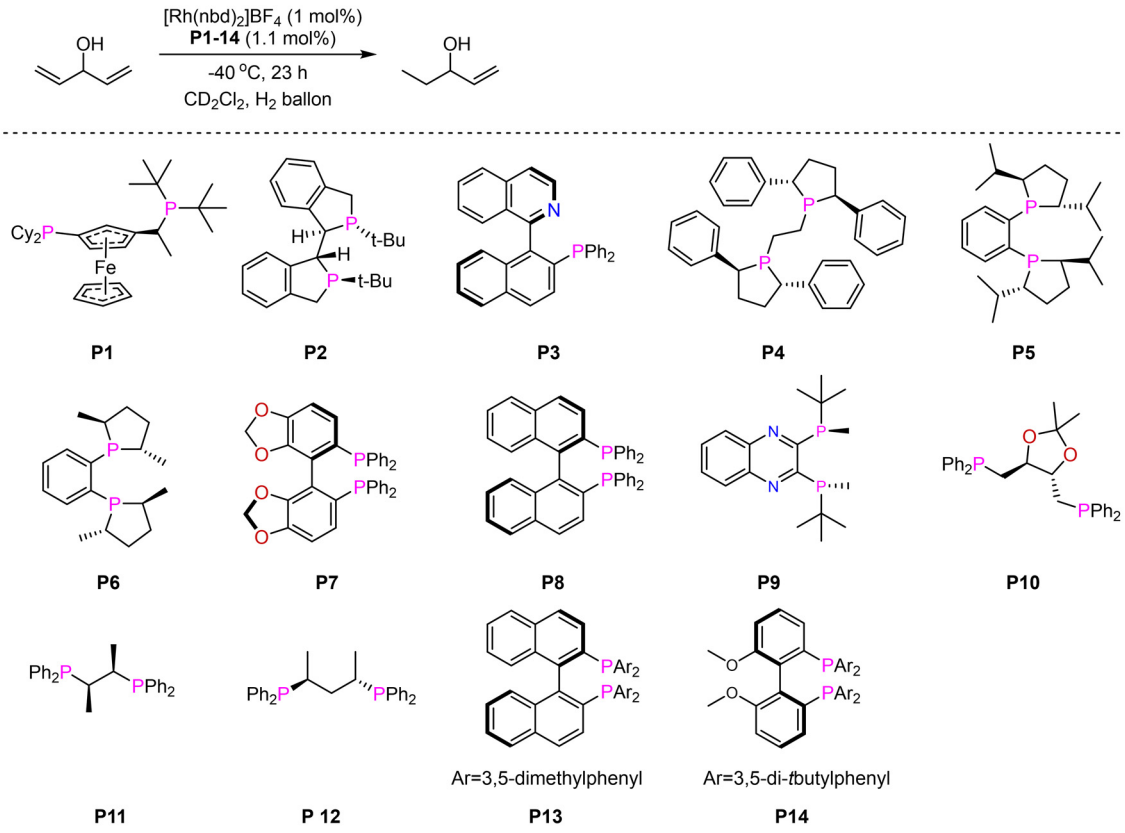

Entry	Ligand	NMR yield[a]	ee (%)[b]
1	P1	11	3
2	P2	97	63
3	P3	0	-
4	P4	95	-16
5	P5	82	23
6	P6	0	-
7	P7	78	-63
8	P8	60	-38
9	P9	25	88
10	P10	0	-
11	P11	0	-
12	P12	0	-
13	P13	91	24
14	P14	30	18

[a]Internal standard mesitylene. [b]0.04 mmol of Ga-Na in 450 ul of CD_3CN with 50 ul of reaction mixture.

Supplemental Table

Table S1. Cartesian coordinates of optimized structure of Al-**L3** for bond distance calculation. Related to Table 1.

Row	Symbol	X	Y	Z
1	Al	0.000016	-0.00043	-0.5469
2	O	-0.66448	1.76083	-0.24363
3	O	1.307539	0.514043	-1.73878
4	O	-1.30729	-0.51563	-1.7387
5	O	0.664551	-1.7615	-0.24246
6	N	-1.28604	-0.51947	1.087259
7	H	-1.20797	-1.53716	1.095475
8	N	1.285879	0.519381	1.087261
9	H	1.207641	1.537065	1.095262
10	C	-1.86866	2.173369	0.055489
11	C	-4.42021	3.204421	0.735136
12	C	-2.19871	3.5521	-0.05556
13	C	-2.89916	1.327093	0.566949
14	C	-4.15496	1.853051	0.896781
15	C	-3.44356	4.077343	0.262565
16	Br	-0.80746	4.77831	-0.67769
17	H	-4.92401	1.191613	1.284005
18	H	-3.64004	5.136304	0.148418
19	Br	-6.19448	3.915195	1.212642
20	C	-2.70767	-0.17659	0.788802
21	C	-2.45339	-1.11833	-1.57468
22	C	-4.93462	-2.44885	-1.28356
23	C	-3.03439	-1.88327	-2.6186
24	C	-3.20497	-1.03756	-0.36551
25	C	-4.4227	-1.71137	-0.22415
26	C	-4.25272	-2.54097	-2.49353
27	Br	-2.07161	-2.01553	-4.31038
28	H	-4.96797	-1.64954	0.7127
29	H	-4.65153	-3.11527	-3.3208
30	Br	-6.65193	-3.39324	-1.07176
31	C	2.707573	0.176701	0.788918
32	H	3.318617	0.440905	1.66246
33	C	3.204696	1.037573	-0.36554
34	C	4.251941	2.540815	-2.49389
35	C	2.453261	1.117511	-1.57485
36	C	4.422026	1.712094	-0.22419
37	C	4.933695	2.449499	-1.28378
38	C	3.033993	1.882384	-2.61895
39	H	4.967182	1.65088	0.712764
40	Br	6.650451	3.394913	-1.07205
41	Br	2.071412	2.013515	-4.31092
42	H	4.650567	3.115048	-3.32129
43	C	1.868962	-2.17365	0.056311
44	C	4.421019	-3.20384	0.735326
45	C	2.899378	-1.32698	0.567268
46	C	2.199347	-3.55231	-0.05454
47	C	3.444454	-4.07714	0.26328
48	C	4.155446	-1.85251	0.896774
49	Br	0.808233	-4.77904	-0.67595
50	H	3.641191	-5.13607	0.149298
51	H	4.924441	-1.19077	1.283584
52	Br	6.195661	-3.91401	1.212352
53	C	0.778599	-0.02499	2.373596
54	C	-0.77878	0.025043	2.373555
55	H	-3.31878	-0.44054	1.662372
56	H	-1.08467	1.074368	2.400894
57	H	1.084483	-1.07431	2.401082
58	C	1.371773	0.679105	3.587292
59	C	2.485869	1.973964	5.826745
60	C	1.211263	2.062268	3.768527
61	C	2.101371	-0.04166	4.541287
62	C	2.653744	0.597995	5.655203
63	C	1.763604	2.705243	4.877929
64	H	0.655413	2.6507	3.041475
65	H	2.238393	-1.11206	4.41095
66	H	3.217542	0.021075	6.383082
67	H	1.631202	3.776753	4.99903
68	H	2.916777	2.474749	6.689271
69	C	-1.37201	-0.6789	3.587305
70	C	-2.48614	-1.97351	5.826887
71	C	-2.10183	0.041932	4.541084
72	C	-1.21126	-2.062	3.768843
73	C	-1.76362	-2.70485	4.878309
74	C	-2.65423	-0.59761	5.655058
75	H	-2.23901	1.112276	4.410528
76	H	-0.65518	-2.65047	3.041993
77	H	-1.63103	-3.77631	4.999646
78	H	-3.21821	-0.02064	6.382759
79	H	-2.91706	-2.4742	6.68946

Table S2. Cartesian coordinates of optimized structure of Al-**L2** for bond distance calculation. Related to Table 1.

Row	Symbol	X	Y	Z
1	Al	0.000125	-0.00093	-1.28731
2	O	0.663367	-1.76053	-0.99343
3	O	-1.31106	-0.52643	-2.47498
4	O	1.311665	0.523689	-2.475
5	O	-0.66304	1.758902	-0.99489
6	N	1.287803	0.515696	0.367672
7	H	1.20082	1.532467	0.377574
8	N	-1.28793	-0.51669	0.367538
9	H	-1.20127	-1.53349	0.377487
10	C	1.88351	-2.16566	-0.70681
11	C	4.416133	-3.2098	-0.03717
12	C	2.202337	-3.53691	-0.88901
13	C	2.898582	-1.32042	-0.16844
14	C	4.149595	-1.8634	0.162695
15	C	3.448129	-4.0626	-0.56516
16	H	1.426585	-4.17309	-1.30524
17	H	4.915521	-1.21575	0.579904
18	H	3.659359	-5.1155	-0.72122
19	Br	6.186201	-3.93511	0.457476
20	C	2.712148	0.179257	0.069876
21	C	2.453649	1.145939	-2.29043
22	C	4.900107	2.510301	-1.9904
23	C	2.996011	1.936083	-3.33364
24	C	3.197746	1.053087	-1.07887
25	C	4.406209	1.747935	-0.93925
26	C	4.206355	2.609947	-3.19463
27	H	2.428694	2.002678	-4.25697
28	H	4.959042	1.682184	-0.00646
29	H	4.597594	3.208751	-4.01079
30	Br	6.607863	3.480316	-1.76654
31	C	-2.71215	-0.17978	0.069645
32	H	-3.32388	-0.43864	0.945049
33	C	-3.19809	-1.05344	-1.0791
34	C	-4.20767	-2.60991	-3.19473
35	C	-2.45375	-1.14737	-2.29044
36	C	-4.40728	-1.74708	-0.93966
37	C	-4.90166	-2.50924	-1.99072
38	C	-2.99663	-1.93728	-3.33357
39	H	-4.9603	-1.68055	-0.00704
40	Br	-6.61042	-3.47753	-1.76703
41	H	-2.42912	-2.00468	-4.25673
42	H	-4.59927	-3.20854	-4.01084
43	C	-1.88279	2.164658	-0.70758
44	C	-4.4145	3.210158	-0.03657
45	C	-2.89801	1.319968	-0.1686
46	C	-2.20102	3.536058	-0.8897
47	C	-3.44636	4.062405	-0.56518
48	C	-4.14854	1.863628	0.163236
49	H	-1.42517	4.171819	-1.30639
50	H	-3.65713	5.115412	-0.72119
51	H	-4.91456	1.216417	0.580959
52	Br	-6.18389	3.936428	0.459085
53	C	-0.77775	0.036872	1.646599
54	C	0.777619	-0.03803	1.64665
55	H	3.323757	0.438333	0.945305
56	H	1.068346	-1.09222	1.656819
57	H	-1.06847	1.091071	1.65686
58	C	-1.38597	-0.63814	2.869957
59	C	-2.5336	-1.88009	5.124098
60	C	-1.23028	-2.01655	3.086745
61	C	-2.12853	0.104534	3.796852
62	C	-2.6974	-0.50844	4.917557
63	C	-1.79864	-2.63357	4.202784
64	H	-0.66392	-2.62037	2.38091
65	H	-2.26455	1.17123	3.638389
66	H	-3.27157	0.08581	5.623162
67	H	-1.66858	-3.70205	4.351305
68	H	-2.97734	-2.36021	5.991948
69	C	1.385742	0.636864	2.870127
70	C	2.533229	1.878528	5.124492
71	C	2.128062	-0.10597	3.797092
72	C	1.23025	2.015292	3.086944
73	C	1.798539	2.632171	4.203094
74	C	2.696849	0.506863	4.917912
75	H	2.263945	-1.17267	3.638592
76	H	0.664114	2.619241	2.381044
77	H	1.668635	3.700668	4.351635
78	H	3.270818	-0.08751	5.623576
79	H	2.976911	2.358541	5.992432

Table S3. Cartesian coordinates of optimized structure of Al-**L1** for bond distance calculation. Related to Table 1.

Row	Symbol	X	Y	Z
1	Al	0.000024	-1.56421	-0.00035
2	O	-0.54789	-1.26241	-1.80038
3	O	1.341875	-2.75062	-0.44173
4	O	-1.3419	-2.75079	0.440378
5	O	0.547895	-1.26336	1.799821
6	N	-1.32045	0.093182	0.434273
7	H	-1.30012	0.094714	1.45451
8	N	1.32054	0.093266	-0.43433
9	H	1.300353	0.094933	-1.45457
10	C	-1.73365	-0.95904	-2.29048
11	C	-4.2064	-0.25156	-3.51841
12	C	-1.9527	-1.12116	-3.68483
13	C	-2.80331	-0.4218	-1.51313
14	C	-4.00504	-0.07785	-2.14848
15	C	-3.15911	-0.78124	-4.28567
16	H	-1.13165	-1.53526	-4.26379
17	H	-4.8089	0.337439	-1.54189
18	H	-3.28621	-0.92853	-5.35651
19	H	-5.15366	0.021027	-3.9755
20	C	-2.71942	-0.20424	-0.00151
21	C	-2.52949	-2.56869	0.974865
22	C	-5.10116	-2.27542	2.16178
23	C	-3.12882	-3.6172	1.717289
24	C	-3.26598	-1.35656	0.830206
25	C	-4.52303	-1.23187	1.433882
26	C	-4.38766	-3.47477	2.293003
27	H	-2.56119	-4.53753	1.82026
28	H	-5.06434	-0.29295	1.322785
29	H	-4.81478	-4.30245	2.856208
30	H	-6.08007	-2.15422	2.617471
31	C	2.719443	-0.20416	0.001643
32	H	3.348103	0.66909	-0.22421
33	C	3.266256	-1.35634	-0.83011
34	C	4.388571	-3.47425	-2.29291
35	C	2.529765	-2.5684	-0.97547
36	C	4.523623	-1.23159	-1.43313
37	C	5.102069	-2.27496	-2.16101
38	C	3.129434	-3.61674	-1.71787
39	H	5.064928	-0.29272	-1.32152
40	H	6.081219	-2.15369	-2.61616
41	H	2.561797	-4.53701	-1.82136
42	H	4.815931	-4.30181	-2.8561
43	C	1.733398	-0.95959	2.290255
44	C	4.205589	-0.25139	3.518908
45	C	2.803075	-0.42186	1.513253
46	C	1.952156	-1.12182	3.684645
47	C	3.158301	-0.78155	4.28583
48	C	4.004514	-0.07755	2.148953
49	H	1.131108	-1.53629	4.263339
50	H	3.285176	-0.92894	5.356679
51	H	4.808375	0.33812	1.542631
52	H	5.152638	0.021481	3.976282
53	C	0.774662	1.371146	0.080623
54	C	-0.77466	1.371122	-0.0806
55	H	-3.34808	0.668946	0.224556
56	H	-1.00801	1.387315	-1.149
57	H	1.008002	1.387282	1.149022
58	C	1.415658	2.594594	-0.56491
59	C	2.622199	4.849056	-1.75239
60	C	1.331398	2.808323	-1.95013
61	C	2.117887	3.525016	0.21197
62	C	2.715899	4.645295	-0.37367
63	C	1.928563	3.924068	-2.54001
64	H	0.798846	2.098577	-2.57938
65	H	2.199436	3.367811	1.28433
66	H	3.257234	5.353819	0.247745
67	H	1.852822	4.069702	-3.61428
68	H	3.087778	5.717315	-2.21111
69	C	-1.4157	2.594499	0.565024
70	C	-2.62234	4.848832	1.752659
71	C	-2.11799	3.524936	-0.21179
72	C	-1.33145	2.808146	1.950253
73	C	-1.92866	3.923826	2.540215
74	C	-2.71605	4.645151	0.373924
75	H	-2.19955	3.36779	-1.28416
76	H	-0.79886	2.098388	2.579462
77	H	-1.85291	4.069395	3.614493
78	H	-3.25742	5.353688	-0.24744
79	H	-3.08796	5.717041	2.211437

Table S4. Cartesian coordinates of optimized structure of Ga-**L1** for bond distance calculation. Related to Table 1.

Row	Symbol	X	Y	Z
1	Ga	0.000051	-1.50853	-0.00115
2	O	-0.55134	-1.17936	-1.83763
3	O	1.371303	-2.71068	-0.43902
4	O	-1.37155	-2.71116	0.434435
5	O	0.551204	-1.18282	1.835888
6	N	-1.32906	0.187174	0.435096
7	H	-1.30219	0.190115	1.454853
8	N	1.329334	0.187371	-0.43512
9	H	1.30303	0.190769	-1.4549
10	C	-1.75332	-0.88945	-2.30017
11	C	-4.25191	-0.21096	-3.49411
12	C	-1.99585	-1.06538	-3.68965
13	C	-2.81451	-0.35434	-1.5088
14	C	-4.02891	-0.02551	-2.12962
15	C	-3.21345	-0.73933	-4.27429
16	H	-1.18102	-1.4784	-4.27805
17	H	-4.82632	0.388029	-1.51344
18	H	-3.35645	-0.89671	-5.34168
19	H	-5.20869	0.051307	-3.9372
20	C	-2.72346	-0.1218	0.001286
21	C	-2.54643	-2.49053	0.989515
22	C	-5.09126	-2.14783	2.220401
23	C	-3.14982	-3.52328	1.750666
24	C	-3.26485	-1.26714	0.848024
25	C	-4.50912	-1.11993	1.474479
26	C	-4.39542	-3.35774	2.347823
27	H	-2.59473	-4.45159	1.850029
28	H	-5.03736	-0.17335	1.366207
29	H	-4.82502	-4.1746	2.924685
30	H	-6.0596	-2.00665	2.6926
31	C	2.723504	-0.12163	-0.00061
32	H	3.358138	0.749788	-0.21742
33	C	3.265778	-1.2665	-0.84748
34	C	4.398579	-3.35598	-2.3473
35	C	2.547309	-2.48959	-0.99146
36	C	4.511217	-1.11906	-1.47159
37	C	5.094479	-2.14636	-2.21744
38	C	3.151869	-3.52173	-1.75256
39	H	5.039498	-0.17271	-1.36148
40	H	6.063712	-2.00494	-2.68773
41	H	2.596716	-4.44981	-1.8538
42	H	4.829006	-4.1724	-2.92416
43	C	1.752334	-0.89146	2.299602
44	C	4.249011	-0.21038	3.496128
45	C	2.813591	-0.35465	1.509441
46	C	1.993849	-1.06774	3.689225
47	C	3.210514	-0.74045	4.275103
48	C	4.026993	-0.02454	2.131527
49	H	1.179008	-1.48206	4.276707
50	H	3.352743	-0.89817	5.342551
51	H	4.824414	0.390355	1.516279
52	H	5.205041	0.052915	3.940218
53	C	0.774613	1.455283	0.089534
54	C	-0.7746	1.455238	-0.08939
55	H	-3.3581	0.749427	0.218856
56	H	-0.99529	1.459385	-1.16071
57	H	0.995266	1.459293	1.160865
58	C	1.422172	2.686902	-0.53467
59	C	2.64698	4.951877	-1.68318
60	C	1.350212	2.91888	-1.91765
61	C	2.121959	3.604297	0.259705
62	C	2.728944	4.729733	-0.30657
63	C	1.956194	4.039852	-2.48825
64	H	0.820673	2.21903	-2.56034
65	H	2.194983	3.432665	1.330466
66	H	3.268266	5.427816	0.328272
67	H	1.889697	4.199664	-3.56113
68	H	3.119587	5.824166	-2.12682
69	C	-1.42225	2.686698	0.535046
70	C	-2.64721	4.95141	1.683927
71	C	-2.12214	3.604148	-0.25916
72	C	-1.35027	2.918485	1.918061
73	C	-1.95633	4.039323	2.488847
74	C	-2.7292	4.729452	0.307294
75	H	-2.1952	3.432652	-1.32995
76	H	-0.82067	2.218594	2.560647
77	H	-1.88981	4.198982	3.561746
78	H	-3.26861	5.427576	-0.32744
79	H	-3.11988	5.823596	2.127707

Table S5. Cartesian coordinates of optimized structure of In-**L1** for bond distance calculation. Related to Table 1.

Row	Symbol	X	Y	Z
1	In	-2.4E-05	-1.58264	0.000074
2	O	-0.65508	-1.15978	-1.92283
3	O	1.566265	-2.75298	-0.48896
4	O	-1.56631	-2.75286	0.489421
5	O	0.655003	-1.15938	1.922942
6	N	-1.35883	0.255575	0.443989
7	H	-1.34299	0.286693	1.463534
8	N	1.358824	0.255513	-0.44406
9	H	1.34304	0.286648	-1.4636
10	C	-1.86606	-0.83331	-2.33433
11	C	-4.39248	-0.09248	-3.43311
12	C	-2.16828	-0.99886	-3.71457
13	C	-2.88363	-0.2738	-1.49985
14	C	-4.11209	0.084425	-2.0787
15	C	-3.39802	-0.64363	-4.25357
16	H	-1.38567	-1.42921	-4.33355
17	H	-4.87702	0.515065	-1.43397
18	H	-3.5846	-0.79493	-5.31512
19	H	-5.35932	0.193933	-3.83771
20	C	-2.75969	-0.03672	0.011631
21	C	-2.72023	-2.42472	1.040492
22	C	-5.21743	-1.87041	2.295557
23	C	-3.39477	-3.39447	1.825842
24	C	-3.34519	-1.14963	0.881848
25	C	-4.56794	-0.90445	1.524147
26	C	-4.61559	-3.12771	2.435882
27	H	-2.90978	-4.36034	1.934878
28	H	-5.02624	0.076696	1.407012
29	H	-5.09766	-3.90065	3.03141
30	H	-6.16547	-1.64577	2.776429
31	C	2.759685	-0.03681	-0.01169
32	H	3.372384	0.851448	-0.22084
33	C	3.345107	-1.14982	-0.88183
34	C	4.615305	-3.12811	-2.43576
35	C	2.720116	-2.42493	-1.04024
36	C	4.56778	-0.90473	-1.5243
37	C	5.21717	-1.87079	-2.29566
38	C	3.394548	-3.39478	-1.82554
39	H	5.026104	0.076429	-1.40733
40	H	6.165154	-1.64622	-2.77668
41	H	2.909544	-4.36066	-1.9344
42	H	5.097295	-3.90112	-3.03125
43	C	1.866048	-0.83306	2.334375
44	C	4.392603	-0.09245	3.432985
45	C	2.883656	-0.27377	1.499804
46	C	2.168285	-0.99849	3.714624
47	C	3.398095	-0.64337	4.253539
48	C	4.112195	0.084347	2.078575
49	H	1.385637	-1.42867	4.333685
50	H	3.584694	-0.79458	5.315104
51	H	4.87716	0.51481	1.433762
52	H	5.359501	0.193859	3.837527
53	C	0.774924	1.502935	0.10275
54	C	-0.77489	1.502952	-0.10286
55	H	-3.37235	0.85158	0.220691
56	H	-0.97547	1.482125	-1.17807
57	H	0.97548	1.482149	1.17796
58	C	1.426026	2.754119	-0.48003
59	C	2.670123	5.044288	-1.55629
60	C	1.36764	3.023922	-1.85677
61	C	2.122782	3.646589	0.344781
62	C	2.739107	4.784393	-0.18562
63	C	1.982747	4.157377	-2.39171
64	H	0.841035	2.344331	-2.52314
65	H	2.187521	3.445011	1.410807
66	H	3.276213	5.462275	0.472554
67	H	1.926076	4.346533	-3.46037
68	H	3.150247	5.926181	-1.97197
69	C	-1.42594	2.754187	0.479869
70	C	-2.66987	5.044475	1.556079
71	C	-2.12282	3.646573	-0.34493
72	C	-1.36734	3.024146	1.856579
73	C	-1.98236	4.15766	2.39148
74	C	-2.73907	4.784432	0.185443
75	H	-2.18772	3.444883	-1.41092
76	H	-0.84061	2.344634	2.522932
77	H	-1.92552	4.346936	3.460117
78	H	-3.27627	5.462242	-0.47272
79	H	-3.14993	5.92641	1.971733

Table S6. Cartesian coordinates of optimized structure of Sc-**L1** for bond distance calculation. Related to Table 1.

Row	Symbol	X	Y	Z
1	Sc	0.000155	-1.79713	-0.00144
2	O	-0.69303	-1.31907	-1.88942
3	O	1.64396	-2.83088	-0.52782
4	O	-1.64337	-2.83179	0.524166
5	O	0.692351	-1.32094	1.887514
6	N	-1.35625	0.069872	0.423576
7	H	-1.33211	0.084539	1.443653
8	N	1.356556	0.07042	-0.42389
9	H	1.333454	0.086445	-1.44397
10	C	-1.87769	-0.95967	-2.34067
11	C	-4.37099	-0.16758	-3.47067
12	C	-2.15538	-1.10457	-3.72739
13	C	-2.89789	-0.3908	-1.5173
14	C	-4.10996	-0.00538	-2.10935
15	C	-3.37276	-0.72568	-4.28099
16	H	-1.36946	-1.53851	-4.33983
17	H	-4.87776	0.433276	-1.47346
18	H	-3.54545	-0.86256	-5.34686
19	H	-5.32686	0.136839	-3.88812
20	C	-2.76937	-0.16407	-0.00405
21	C	-2.81712	-2.52845	1.042571
22	C	-5.33144	-1.93127	2.224828
23	C	-3.51702	-3.48521	1.817224
24	C	-3.41625	-1.24691	0.858017
25	C	-4.65034	-0.97708	1.463053
26	C	-4.75101	-3.19445	2.392812
27	H	-3.04899	-4.4567	1.948811
28	H	-5.09126	0.009647	1.328597
29	H	-5.26007	-3.95448	2.982433
30	H	-6.28914	-1.69142	2.678491
31	C	2.769504	-0.16367	0.004478
32	H	3.342064	0.751845	-0.20236
33	C	3.417156	-1.2456	-0.85817
34	C	4.753476	-3.19149	-2.39372
35	C	2.81824	-2.52696	-1.04468
36	C	4.651825	-0.9751	-1.46173
37	C	5.333692	-1.92846	-2.22385
38	C	3.518925	-3.48288	-1.81965
39	H	5.092586	0.01149	-1.32579
40	H	6.291836	-1.6881	-2.67632
41	H	3.051053	-4.45425	-1.95272
42	H	5.263133	-3.95088	-2.98364
43	C	1.876651	-0.96171	2.339798
44	C	4.369024	-0.16989	3.472044
45	C	2.897164	-0.39172	1.517589
46	C	2.153604	-1.10796	3.726526
47	C	3.370533	-0.72919	4.281216
48	C	4.108737	-0.00643	2.110729
49	H	1.367484	-1.54279	4.338069
50	H	3.542657	-0.8671	5.347045
51	H	4.876765	0.433141	1.475744
52	H	5.324524	0.134477	3.890366
53	C	0.770934	1.32517	0.106265
54	C	-0.771	1.325056	-0.10578
55	H	-3.342	0.751151	0.203925
56	H	-0.96623	1.314629	-1.18209
57	H	0.966173	1.314152	1.182569
58	C	1.422686	2.575392	-0.48172
59	C	2.655901	4.867862	-1.56656
60	C	1.385371	2.826525	-1.8626
61	C	2.092348	3.488388	0.343036
62	C	2.703602	4.626981	-0.19147
63	C	1.994744	3.961109	-2.40186
64	H	0.879842	2.130757	-2.5286
65	H	2.139706	3.302074	1.412739
66	H	3.219884	5.320643	0.467006
67	H	1.954486	4.13547	-3.47383
68	H	3.131931	5.750471	-1.98551
69	C	-1.42296	2.574834	0.482943
70	C	-2.65632	4.866621	1.569057
71	C	-2.09272	3.488218	-0.3413
72	C	-1.38564	2.825205	1.863953
73	C	-1.99508	3.959457	2.403849
74	C	-2.70405	4.626475	0.193837
75	H	-2.14012	3.302463	-1.4111
76	H	-0.88008	2.129082	2.529562
77	H	-1.95481	4.133239	3.475911
78	H	-3.22041	5.32045	-0.46425
79	H	-3.13239	5.748975	1.988495

Table S7. Cartesian coordinates of Al-**L3** for NBO calculation. Related to Table 1.

Row	Symbol	X	Y	Z
1	Al	0.000113	-0.00018	-0.15898
2	O	-0.80105	1.670109	0.068535
3	O	1.250525	0.649318	-1.33638
4	O	-1.25036	-0.64974	-1.3363
5	O	0.801316	-1.67045	0.068695
6	N	-1.23049	-0.58238	1.476009
7	H	-1.04629	-1.58475	1.444747
8	N	1.230778	0.582134	1.475934
9	H	1.046537	1.584491	1.444703
10	C	-2.09362	1.895729	0.096307
11	C	-4.83898	2.541644	0.179488
12	C	-2.59034	3.150646	-0.33626
13	C	-3.04619	0.968592	0.599202
14	C	-4.40289	1.304167	0.634918
15	C	-3.93771	3.481968	-0.31504
16	Br	-1.32093	4.403055	-1.00462
17	H	-5.12266	0.587341	1.017976
18	H	-4.27494	4.445952	-0.67591
19	Br	-6.70901	2.959501	0.210965
20	C	-2.67558	-0.4306	1.102849
21	C	-2.19629	-1.52407	-1.12136
22	C	-4.27032	-3.3924	-0.68953
23	C	-2.50346	-2.53219	-2.06626
24	C	-2.97872	-1.50459	0.067472
25	C	-3.9995	-2.43158	0.280836
26	C	-3.53133	-3.44804	-1.8692
27	Br	-1.47796	-2.59412	-3.66071
28	H	-4.58349	-2.39883	1.195695
29	H	-3.74467	-4.19747	-2.6219
30	Br	-5.68374	-4.65541	-0.40215
31	C	2.675841	0.430429	1.102649
32	H	3.299911	0.635446	1.982187
33	C	2.978799	1.504484	0.067284
34	C	3.530672	3.448323	-1.86919
35	C	2.196256	1.523884	-1.12147
36	C	3.999383	2.43168	0.280638
37	C	4.26984	3.392699	-0.68963
38	C	2.50306	2.532192	-2.06628
39	H	4.583452	2.398995	1.195449
40	Br	5.68287	4.656127	-0.40219
41	Br	1.477053	2.59435	-3.6604
42	H	3.743656	4.197977	-2.62178
43	C	2.09393	-1.89594	0.09619
44	C	4.839366	-2.54161	0.178968
45	C	3.046491	-0.96872	0.598925
46	C	2.590697	-3.15082	-0.33643
47	C	3.938098	-3.48203	-0.31538
48	C	4.403235	-1.30416	0.634422
49	Br	1.321291	-4.40346	-1.00436
50	H	4.275349	-4.44601	-0.67624
51	H	5.122991	-0.58726	1.017362
52	Br	6.709424	-2.95933	0.210243
53	C	0.780624	0.124858	2.837057
54	C	0.949539	0.961869	3.522222
55	H	-0.78023	-0.12514	2.837103
56	H	-0.9491	-0.96215	3.522272
57	H	-1.56259	1.037351	3.44152
58	C	-3.00446	3.100027	4.719128
59	C	-1.3463	2.382487	3.10233
60	C	-2.50652	0.751217	4.439378
61	C	-3.22661	1.768451	5.072082
62	C	-2.06137	3.401286	3.732596
63	C	-0.64874	2.642877	2.314069
64	H	-2.67664	-0.28235	4.732259
65	H	-3.95451	1.517713	5.838658
66	H	-1.8884	4.432494	3.439084
67	H	-3.5635	3.896309	5.202303
68	H	1.563029	-1.03763	3.441405
69	C	3.005015	-3.10029	4.718921
70	C	1.346556	-2.38279	3.102411
71	C	2.507193	-0.75147	4.439045
72	C	3.22734	-1.7687	5.071694
73	C	2.061687	-3.40158	3.73263
74	C	0.64878	-2.6432	2.314356
75	H	2.677454	0.282113	4.73179
76	H	3.955425	-1.51794	5.838088
77	H	1.888561	-4.4328	3.439269
78	H	3.564088	-3.89657	5.20206
79	H	-3.29958	-0.63561	1.982434

Table S8. Cartesian coordinates of Al-**L2** for NBO calculation. Related to Table 1.

Row	Symbol	X	Y	Z
1	Al	0.000069	-0.00022	-0.97817
2	O	-0.80114	1.684061	-0.75058
3	O	1.252507	0.637545	-2.16295
4	O	-1.25227	-0.6382	-2.16294
5	O	0.801285	-1.68444	-0.75017
6	N	-1.22669	-0.5989	0.667469
7	H	-1.0406	-1.59928	0.597585
8	N	1.22668	0.598732	0.667506
9	H	1.040525	1.599087	0.597514
10	C	-2.09071	1.938036	-0.61964
11	C	-4.77679	2.688379	-0.21771
12	C	-2.56448	3.227031	-0.96624
13	C	-3.0271	1.012222	-0.07897
14	C	-4.35591	1.407286	0.114115
15	C	-3.88728	3.607229	-0.77456
16	H	-1.84545	3.921318	-1.39109
17	H	-5.06409	0.70488	0.543594
18	H	-4.22057	4.603578	-1.047
19	Br	-6.60518	3.190911	0.087562
20	C	-2.67534	-0.42156	0.322851
21	C	-2.27429	-1.43941	-1.97368
22	C	-4.47644	-3.16212	-1.6171
23	C	-2.67917	-2.33765	-2.98919
24	C	-3.02692	-1.42591	-0.76464
25	C	-4.11055	-2.29188	-0.59412
26	C	-3.76909	-3.18596	-2.81951
27	H	-2.10828	-2.34562	-3.91244
28	H	-4.67581	-2.27601	0.333513
29	H	-4.0621	-3.86548	-3.61354
30	Br	-5.97528	-4.33861	-1.36767
31	C	2.675354	0.421453	0.322958
32	H	3.286341	0.67103	1.200125
33	C	3.026878	1.425767	-0.76459
34	C	3.768886	3.185748	-2.81956
35	C	2.274349	1.439002	-1.97368
36	C	4.11033	2.291955	-0.59405
37	C	4.476135	3.162166	-1.61709
38	C	2.679139	2.337226	-2.98925
39	H	4.675529	2.276269	0.33362
40	Br	5.974771	4.338918	-1.36767
41	H	2.108318	2.344997	-3.91255
42	H	4.061831	3.865256	-3.61364
43	C	2.090906	-1.93827	-0.61935
44	C	4.777119	-2.68825	-0.21769
45	C	3.027234	-1.01232	-0.0788
46	C	2.564798	-3.22721	-0.96596
47	C	3.88767	-3.60724	-0.77441
48	C	4.356113	-1.4072	0.114149
49	H	1.845808	-3.92161	-1.39071
50	H	4.221051	-4.60355	-1.04685
51	H	5.064254	-0.70469	0.543513
52	Br	6.605618	-3.19054	0.087354
53	C	0.768884	0.183889	2.042264
54	C	0.869915	1.066043	2.681613
55	H	-0.76894	-0.18399	2.042235
56	H	-0.87001	-1.06612	2.681614
57	H	-1.62118	0.885481	2.718186
58	C	-3.24213	2.77867	4.039373
59	C	-1.47162	2.258017	2.469184
60	C	-2.57889	0.484519	3.661039
61	C	-3.38808	1.418378	4.314738
62	C	-2.2737	3.194592	3.121148
63	C	-0.75341	2.600821	1.731699
64	H	-2.69526	-0.57314	3.886261
65	H	-4.13019	1.080777	5.032894
66	H	-2.15664	4.249583	2.89186
67	H	-3.87887	3.508983	4.530584
68	H	1.621091	-0.88555	2.718315
69	C	3.241906	-2.77867	4.039759
70	C	1.471615	-2.25809	2.469297
71	C	2.578643	-0.48454	3.661309
72	C	3.387773	-1.41837	4.315132
73	C	2.273635	-3.19463	3.121388
74	C	0.753539	-2.60091	1.731697
75	H	2.694935	0.573117	3.88655
76	H	4.129763	-1.08073	5.033399
77	H	2.156653	-4.24963	2.892093
78	H	3.878595	-3.50895	4.531081
79	H	-3.28637	-0.67105	1.200015

Table S9. Cartesian coordinates of Al-**L1** for NBO calculation. Related to Table 1.

Row	Symbol	X	Y	Z
1	Al	0.000024	-1.23478	0.000623
2	O	-1.15646	-0.98759	-1.46527
3	O	1.077897	-2.41751	-0.90518
4	O	-1.07769	-2.4165	0.907982
5	O	1.156629	-0.98598	1.466235
6	N	-1.07017	0.408019	0.855599
7	H	-0.66828	0.33533	1.790133
8	N	1.070247	0.407325	-0.85605
9	H	0.668396	0.334081	-1.79054
10	C	-2.47693	-0.90683	-1.41495
11	C	-5.30757	-0.66207	-1.49999
12	C	-3.22533	-1.3052	-2.5506
13	C	-3.1887	-0.37752	-0.30222
14	C	-4.58313	-0.26719	-0.37497
15	C	-4.61011	-1.18818	-2.59546
16	H	-2.66679	-1.71394	-3.38824
17	H	-5.11554	0.144293	0.481352
18	H	-5.14921	-1.50886	-3.48475
19	H	-6.38926	-0.56235	-1.52097
20	C	-2.52352	0.056421	1.005989
21	C	-1.88349	-2.22291	1.928941
22	C	-3.62822	-1.85033	4.144396
23	C	-2.05482	-3.22938	2.909727
24	C	-2.62763	-1.01687	2.080117
25	C	-3.47233	-0.84841	3.181299
26	C	-2.91245	-3.04538	3.991166
27	H	-1.48798	-4.14774	2.788265
28	H	-4.02873	0.083278	3.278745
29	H	-3.01968	-3.83904	4.728059
30	H	-4.29225	-1.70264	4.991522
31	C	2.523543	0.055403	-1.00623
32	H	3.069121	0.934744	-1.37515
33	C	2.627359	-1.019	-2.07928
34	C	2.911564	-3.04941	-3.98843
35	C	1.883282	-2.22491	-1.92666
36	C	3.471698	-0.85164	-3.18091
37	C	3.627282	-1.85451	-4.14307
38	C	2.054291	-3.23233	-2.90652
39	H	4.028067	0.079951	-3.27946
40	H	4.291041	-1.70763	-4.99055
41	H	1.487486	-4.15058	-2.78398
42	H	3.018539	-3.84379	-4.72457
43	C	2.477116	-0.90542	1.415651
44	C	5.307802	-0.66099	1.500077
45	C	3.188818	-0.37726	0.302319
46	C	3.225617	-1.30294	2.551514
47	C	4.610428	-1.18606	2.596081
48	C	4.583272	-0.26703	0.374788
49	H	2.66715	-1.71088	3.389587
50	H	5.149597	-1.50602	3.485591
51	H	5.115608	0.143607	-0.48198
52	H	6.389516	-0.5614	1.520836
53	C	0.709686	1.77793	-0.35611
54	C	0.602451	2.412654	-1.24099
55	H	-0.70946	1.778228	0.354733
56	H	-0.60227	2.4136	1.239144
57	H	-1.76462	2.478131	-0.49621
58	C	-3.66287	3.917435	-2.00827
59	C	-1.9689	2.19017	-1.85457
60	C	-2.5242	3.503817	0.084382
61	C	-3.4687	4.218146	-0.65951
62	C	-2.90859	2.900495	-2.60161
63	C	-1.41496	1.383427	-2.3228
64	H	-2.37129	3.751889	1.132245
65	H	-4.04563	5.007185	-0.18443
66	H	-3.06364	2.643739	-3.64549
67	H	-4.39764	4.465216	-2.59217
68	H	1.764895	2.478498	0.494184
69	C	3.663119	3.919089	2.004999
70	C	1.968871	2.191992	1.852903
71	C	2.524673	3.50349	-0.08739
72	C	3.469194	4.218406	0.655891
73	C	2.908561	2.902948	2.599341
74	C	1.414689	1.385805	2.321807
75	H	2.371914	3.750491	-1.13552
76	H	4.046362	5.006844	0.180102
77	H	3.063386	2.647294	3.64353
78	H	4.397865	4.467434	2.588393
79	H	-3.06901	0.936243	1.373886

Table S10. Cartesian coordinates of Ga-**L1** for NBO calculation. Related to Table 1.

Row	Symbol	X	Y	Z
1	Ga	0.000063	-1.12212	-0.00114
2	O	-1.23474	-0.96039	-1.48491
3	O	1.022849	-2.37745	-1.01897
4	O	-1.02228	-2.37984	1.014119
5	O	1.234656	-0.96303	1.483212
6	N	-1.06343	0.514173	0.880277
7	H	-0.63343	0.446098	1.802509
8	N	1.063624	0.516058	-0.87912
9	H	0.633873	0.449792	-1.8016
10	C	-2.5478	-0.84326	-1.36373
11	C	-5.37269	-0.50953	-1.36392
12	C	-3.34492	-1.20557	-2.47838
13	C	-3.20714	-0.28547	-0.23281
14	C	-4.60088	-0.13786	-0.26372
15	C	-4.72545	-1.05235	-2.48198
16	H	-2.82317	-1.62259	-3.33545
17	H	-5.09385	0.289239	0.60822
18	H	-5.29953	-1.3517	-3.35663
19	H	-6.45104	-0.37839	-1.34883
20	C	-2.50387	0.143533	1.05853
21	C	-1.85996	-2.14527	1.996216
22	C	-3.68555	-1.77073	4.154674
23	C	-2.12501	-3.17322	2.936304
24	C	-2.59952	-0.93252	2.130731
25	C	-3.47215	-0.76204	3.211862
26	C	-3.00844	-2.98802	3.993533
27	H	-1.59383	-4.11139	2.804545
28	H	-4.0144	0.178838	3.300701
29	H	-3.17193	-3.79813	4.701649
30	H	-4.37011	-1.61605	4.983902
31	C	2.504148	0.145848	-1.05791
32	H	3.045969	1.02406	-1.43584
33	C	2.599881	-0.92768	-2.1326
34	C	3.008242	-2.97877	-4.00031
35	C	1.860224	-2.14067	-2.00081
36	C	3.472344	-0.75469	-3.21346
37	C	3.68545	-1.76117	-4.1587
38	C	2.124991	-3.16642	-2.94336
39	H	4.014653	0.186346	-3.30015
40	H	4.369875	-1.60462	-4.98768
41	H	1.593771	-4.10487	-2.81373
42	H	3.171539	-3.78722	-4.71038
43	C	2.547765	-0.84618	1.362266
44	C	5.37273	-0.51322	1.363144
45	C	3.207252	-0.2862	0.232523
46	C	3.344773	-1.21104	2.476163
47	C	4.725353	-1.05817	2.480083
48	C	4.60103	-0.13907	0.263703
49	H	2.822913	-1.62968	3.332372
50	H	5.299348	-1.35946	3.354116
51	H	5.094115	0.289713	-0.60734
52	H	6.451123	-0.38236	1.348308
53	C	0.722489	1.862833	-0.32594
54	C	0.660213	2.54886	-1.17649
55	H	-0.72249	1.862082	0.329694
56	H	-0.66033	2.546447	1.181595
57	H	-1.74818	2.490981	-0.60596
58	C	-3.52341	3.867837	-2.31179
59	C	-1.88871	2.114738	-1.95048
60	C	-2.50643	3.573074	-0.13845
61	C	-3.39282	4.255438	-0.97788
62	C	-2.76838	2.793239	-2.79229
63	C	-1.33954	1.259049	-2.32728
64	H	-2.39965	3.891675	0.895921
65	H	-3.97215	5.088627	-0.58898
66	H	-2.87564	2.468602	-3.82316
67	H	-4.2109	4.391369	-2.97067
68	H	1.748079	2.490017	0.610947
69	C	3.52295	3.863697	2.319674
70	C	1.888968	2.11072	1.954563
71	C	2.505768	3.573523	0.145805
72	C	3.391978	4.254337	0.986682
73	C	2.768458	2.787671	2.797818
74	C	1.340202	1.253919	2.329401
75	H	2.39866	3.894465	-0.88781
76	H	3.970858	5.088694	0.599629
77	H	2.876022	2.460716	3.827927
78	H	4.210305	4.386019	2.979647
79	H	-3.04564	1.020826	1.438681

Table S11. Cartesian coordinates of Sc-**L1** for NBO calculation. Related to Table 1.

Row	Symbol	X	Y	Z
1	Sc	0.000026	0.000165	-1.47974
2	O	-1.36085	1.51113	-1.16997
3	O	1.338293	1.173349	-2.43819
4	O	-1.33883	-1.17143	-2.43938
5	O	1.361781	-1.5101	-1.17211
6	N	-1.13998	-0.77261	0.441302
7	H	-0.75624	-1.71751	0.408553
8	N	1.139842	0.772052	0.441679
9	H	0.755504	1.716697	0.408613
10	C	-2.67064	1.42546	-1.00063
11	C	-5.48919	1.43439	-0.61794
12	C	-3.48447	2.497388	-1.44907
13	C	-3.31158	0.332843	-0.34711
14	C	-4.70178	0.373734	-0.16979
15	C	-4.86263	2.50496	-1.26822
16	H	-2.97786	3.319576	-1.94728
17	H	-5.1829	-0.46261	0.335166
18	H	-5.44998	3.346166	-1.63114
19	H	-6.56449	1.424847	-0.46278
20	C	-2.60636	-0.93478	0.158922
21	C	-2.15258	-2.13731	-2.06338
22	C	-3.8723	-4.25857	-1.27585
23	C	-2.41049	-3.23502	-2.91882
24	C	-2.79464	-2.11726	-0.78862
25	C	-3.62852	-3.17917	-0.42089
26	C	-3.25632	-4.27184	-2.53318
27	H	-1.91876	-3.24008	-3.88727
28	H	-4.10677	-3.1542	0.557416
29	H	-3.43208	-5.10081	-3.21585
30	H	-4.52803	-5.06791	-0.96725
31	C	2.6062	0.934785	0.159765
32	H	3.108124	1.212993	1.097803
33	C	2.794642	2.117757	-0.78714
34	C	3.257144	4.272914	-2.53079
35	C	2.152534	2.138641	-2.06187
36	C	3.628909	3.179198	-0.41896
37	C	3.873088	4.258883	-1.27345
38	C	2.410905	3.236595	-2.91686
39	H	4.107165	3.153629	0.559332
40	H	4.529113	5.067846	-0.96448
41	H	1.919167	3.242262	-3.8853
42	H	3.433244	5.102099	-3.21311
43	C	2.671437	-1.42454	-1.00169
44	C	5.489682	-1.43375	-0.61687
45	C	3.311848	-0.33245	-0.34675
46	C	3.485609	-2.49608	-1.45042
47	C	4.863637	-2.50378	-1.26854
48	C	4.70191	-0.37349	-0.16841
49	H	2.979384	-3.31786	-1.94968
50	H	5.451269	-3.34467	-1.63171
51	H	5.182633	0.46242	0.337633
52	H	6.564856	-1.42433	-0.46086
53	C	0.755554	0.23273	1.787275
54	C	0.808761	1.066087	2.498335
55	H	-0.75587	-0.23352	1.787154
56	H	-0.809	-1.06716	2.49786
57	H	-1.66748	0.836508	2.383131
58	C	-3.245	2.771952	3.701385
59	C	-1.73364	2.155405	1.906554
60	C	-2.40456	0.511576	3.531828
61	C	-3.19022	1.46492	4.186741
62	C	-2.514	3.110393	2.558688
63	C	-1.2138	2.427046	0.993994
64	H	-2.35999	-0.50205	3.923485
65	H	-3.75456	1.183517	5.071935
66	H	-2.56444	4.118595	2.157641
67	H	-3.8562	3.518405	4.201548
68	H	1.666886	-0.83778	2.382795
69	C	3.243576	-2.77452	3.700123
70	C	1.733568	-2.15614	1.904779
71	C	2.403046	-0.51403	3.532408
72	C	3.18828	-1.46804	4.186889
73	C	2.513534	-3.11176	2.556456
74	C	1.214458	-2.42682	0.991514
75	H	2.358085	0.499162	3.925128
76	H	3.751903	-1.18755	5.072828
77	H	2.564421	-4.1195	2.154311
78	H	3.854471	-3.52146	4.199929
79	H	-3.10857	-1.2134	1.096683

Transparent Methods

General information

Commercially available compounds were used without further purification or drying. The ^{1}H and ^{13}C NMR spectra were recorded on a Bruker Ascend 400 spectrometer (400 MHz for ^{1}H and 100 MHz for ^{13}C) and are reported in ppm, relative to residual protonated solvent peak. The high-resolution mass spectra (HRMS) were obtained on a Bruker Daltonik microTOF-QII spectrometer at the KAIST Analysis Center for Research Advancement (KARA). All calculations were performed using Gaussian 09.

Experimental procedures

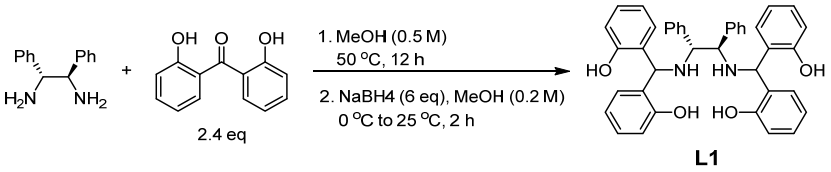

The ligand **L1** was prepared by a reported procedure and confirmed by ^{1}H and ^{13}C NMR spectra.

^{1}H NMR (400 MHz, DMSO-d_6) δ 10.07 (br, 4H), 7.16–7.08 (m, 8H), 7.01–6.92 (m, 8H), 6.77 (dd, *J*=8.1, 1.0 Hz, 2H), 6.75–6.71 (m, 4H), 6.69 (dd, *J*=8.0, 1.1 Hz, 2H), 6.60 (td, *J*=7.5, 1.2 Hz, 2H), 4.94 (s, 2H), 3.79 (s, 2H); ^{13}C NMR (100 MHz, DMSO-d_6) δ 155.9, 155.8, 139.6, 128.9, 128.2, 128.1, 128.0, 128.0, 128.0, 127.8, 127.7, 127.0, 125.8, 118.9, 118.4, 115.6, 115.5, 65.2, 55.5.

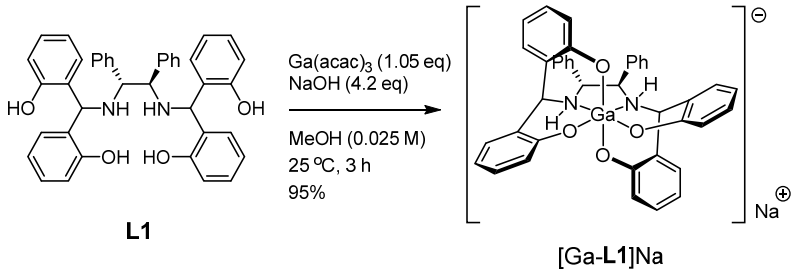

To a solution of **L1** (609 mg, 1 mmol) in MeOH (40.0 mL) were added NaOH (120 mg, 3.00 mmol) and $Ga(acac)_3$ (385 mg, 1.05 mmol). After the resulting solution was stirred for 2 h at 25 °C, NaOH (48 mg, 1.2 mmol) was added to the reaction mixture and it was stirred for 1 h at 25 °C. The reaction mixture was concentrated under reduced pressure. The crude mixture was dissolved in EtOAc, and the resulting organic phase was washed with brine, dried over anhydrous sodium sulfate and concentrated under reduced pressure to afford the [Ga-**L1**]Na (663 mg, 95%) as an off-white solid.

^{1}H NMR (400 MHz, DMSO-d_6) δ 7.18-7.14 (m, 6H), 6.96-6.88 (m, 8H), 6.75-6.73 (m, 4H), 6.60 (d, *J* = 8.0 Hz, 2H), 6.53 (d, *J* = 8.0 Hz, 2H), 6.34 (m, 4H), 4.46 (s, 2H), 4.27 (m, 2H), 4.17 (m, 2H).^{13}C NMR (100 MHz, DMSO-d_6) δ 163.3, 163.0, 135.9, 129.8, 128.9, 128.58, 128.6, 128.2, 128.1, 128.0, 127.9, 123.2, 120.9, 120.8, 113.8, 113.6, 66.26, 61.8. HRMS (ESI/Q-TOF) m/z: [M + Na]+ Calcd for $C_{40}H_{32}GaNaN_2O_4Na^+$ 719.1408; Found 719.1410; $[\alpha]_D^{22}$ +72 (*c* 1.0, MeCN).

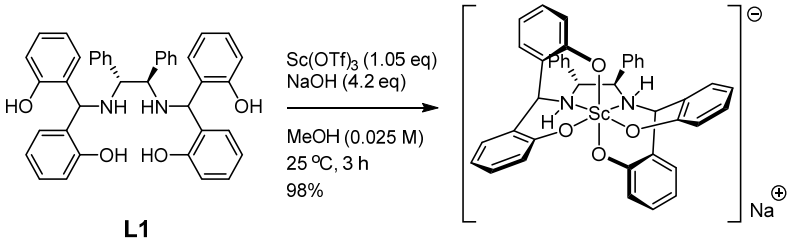

L1 [Sc-**L1**]Na

To a solution of **L1** (609 mg, 1 mmol) in MeOH (40.0 mL) were added NaOH (120 mg, 3.00 mmol) and $Sc(OTf)_3$ (517 mg, 1.05 mmol). After the resulting solution was stirred for 2 h at 25 °C, NaOH (48 mg, 1.2 mmol) was added to the reaction mixture and it was stirred for 1 h at 25 °C. The reaction mixture was concentrated under reduced pressure. The crude mixture was dissolved in EtOAc, and the resulting organic phase was washed with brine, dried anhydrous sodium sulfate and concentrated under reduced pressure to afford the [Sc-**L1**]Na (659 mg, 98%) as an off-white solid.

^{1}H NMR (400 MHz, DMSO-*d*$_6$) δ 7.13–7.05 (m, 6H), 6.93–6.81 (m, 8H), 6.68 (d, *J*=7.04 Hz, 2H), 6.63 (d, *J*=7.16 Hz, 2H), 6.41 (d, *J*=7.78 Hz, 2H), 6.35 (d, *J*=8.09 Hz, 2H), 6.30–6.21 (m, 4H), 4.24 (s, 2H), 4.21–4.14 (m, 2H), 3.91–3.83 (m, 2H); ^{13}C NMR (100 MHz, DMSO-*d*$_6$) δ 163.7, 163.4, 137.8, 131.2, 129.9, 129.3, 128.5, 128.2, 128.2, 127.9, 127.6, 126.7, 119.4, 118.7, 113.9, 113.6, 66.3, 65.3; HRMS (ESI/Q-TOF) m/z: [M + Na]+ Calcd for $C_{40}H_{32}ScNaN_2O_4Na^+$ 695.1711; Found 695.1720; $[\alpha]_D^{22}$ +57 (*c* 1.0, MeCN).

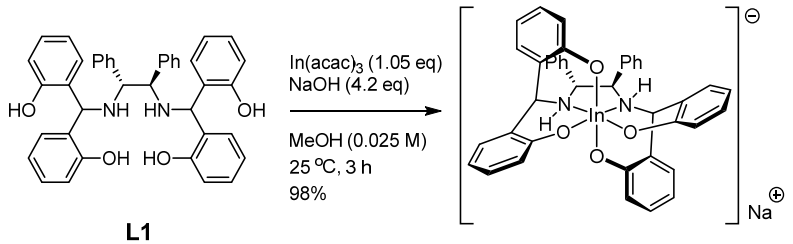

L1 [In-**L1**]Na

To a solution of **L1** (609 mg, 1 mmol) in MeOH (40.0 mL) were added NaOH (120 mg, 3.00 mmol) and $In(acac)_3$ (433 mg, 1.05 mmol). After the resulting solution was stirred for 2 h at 25 °C, NaOH (48 mg, 1.2 mmol) was added to the reaction mixture and it was stirred for 1 h at 25 °C. The reaction mixture was concentrated under reduced pressure. The crude mixture was dissolved in EtOAc, and the resulting organic phase was washed with brine, dried over anhydrous sodium sulfate and concentrated under reduced pressure to afford the [In-**L1**]Na (728 mg, 98%) as an off-white solid.

^{1}H NMR (400 MHz, DMSO-*d*$_6$) δ 7.12 – 7.06 (m, 6H), 6.99 (ps, 3H), 6.88 (m, 4H), 6.77 – 6.42 (m, 8H), 6.29 (q, *J* = 6.4 Hz, 4H), 4.86 (s, 2H), 4.45 (s, 2H), 4.21 (s, 2H). ^{13}C NMR (100 MHz, DMSO-*d*$_6$) δ 165.18, 164.56, 136.66, 130.51, 130.43, 128.94, 128.94, 128.59, 128.53, 128.02, 127.76, 127.63, 121.85, 113.58, 113.27, 68.57, 62.53, 59.79. HRMS (ESI/Q-TOF) m/z: [M + Na]+ Calcd for $C_{40}H_{32}InNaN_2O_4Na^+$ 765.1191; Found 765.1199; $[\alpha]_D^{22}$ +20 (*c* 1.0, MeCN).

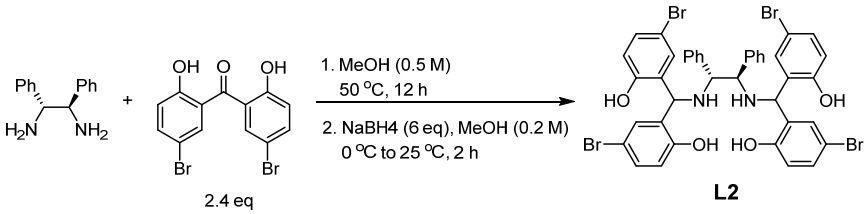

The ligand **L2** was prepared by a modified procedure.[1]

^{1}H NMR (400 MHz, DMSO-d_6) δ 10.11 (s, 3H), 7.22 (m, 2H), 7.14 (m, 10H), 7.05 (m, 6H), 6.71 (d, *J* = 8.6 Hz, 2H), 6.64 (d, *J* = 8.6 Hz, 2H), 4.93 (s, 2H), 3.77 (s, 2H). ^{13}C NMR (100 MHz, DMSO-d_6) δ 154.93, 154.72, 139.93, 130.86, 130.70, 130.57, 130.28, 129.04, 128.07, 127.82, 127.04, 117.67, 117.59, 110.18, 109.75, 65.56, 54.30; HRMS (ESI/Q-TOF) m/z: [M + H]+ Calcd for $C_{40}H_{33}Br_4N_2O_4^+$ 924.9127; Found 924.9142; $[\alpha]_D^{22}$ +9 (*c* 1.0, MeCN).

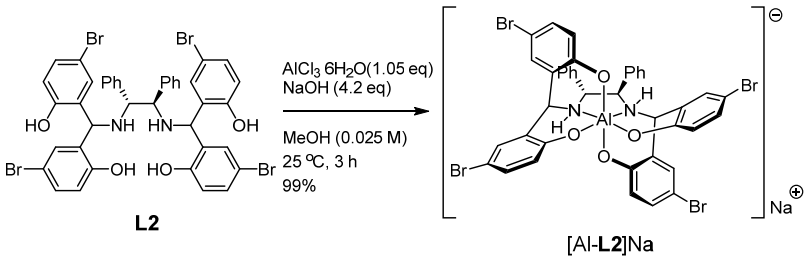

To a solution of **L2** (924 mg, 1 mmol) in MeOH (40.0 mL) were added NaOH (120 mg, 3.00 mmol) and $AlCl_3$•$6H_2O$ (254 mg, 1.05 mmol). After the resulting solution was stirred for 2 h at 25 °C, NaOH (48 mg, 1.2 mmol) was added to the reaction mixture and it was stirred for 1 h at 25 °C. The reaction mixture was concentrated under reduced pressure. The crude mixture was dissolved in EtOAc, and the resulting organic phase was washed with brine, dried over anhydrous sodium sulfate and concentrated under reduced pressure to afford the Na[Al-**L2**] (960 mg, 99%) as an off-white solid.

^{1}H NMR (400 MHz, DMSO-d_6) δ 7.18–7.11 (m, 6H), 7.06–6.96 (m, 8H), 6.93–6.86 (m, 4H), 6.55 (d, *J*=8.94 Hz, 2H), 6.43 (d, *J*=8.70 Hz, 2H), 4.29 (s, 2H), 4.11–4.03 (m, 2H), 4.03–3.95 (m, 2H); ^{13}C NMR (100 MHz, DMSO-d_6) δ 161.5, 160.8, 135.6, 131.3, 131.1, 130.8, 130.6, 130.2, 128.6, 128.2, 127.9, 126.1, 122.7, 122.1, 104.0, 103.9, 63.0, 62.8; HRMS (ESI/Q-TOF) m/z: [M + Na]+ Calcd for $C_{40}H_{28}AlNaBr_4N_2O_4Na^+$ 992.8347; Found 992.8339; $[\alpha]_D^{22}$ +53 (*c* 1.0, MeCN).

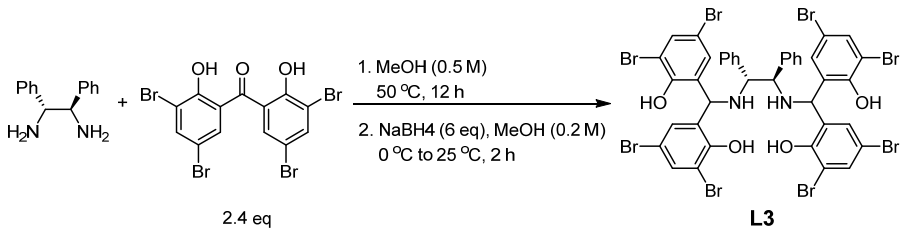

The ligand **L3** was prepared by a procedure.[1]

^{1}H NMR (400 MHz, DMSO-d_6) δ 8.66 (s, 4H), 7.64 (s, 2H), 7.54 (s, 2H), 7.26 – 7.15 (m, 4H), 7.09 (m, 6H), 6.99 (d, *J* = 6.8 Hz, 4H), 5.07 (s, 2H), 3.89 (s, 2H). ^{13}C NMR (101 MHz, DMSO) δ 152.43, 151.67, 138.51, 133.54, 133.19, 131.58, 130.48, 129.76, 129.62, 128.20, 127.92, 127.29, 112.11,

111.92, 110.80, 110.68, 65.37, 56.07; HRMS (ESI/Q-TOF) m/z: [M + H]+ Calcd for $C_{40}H_{29}Br_8N_2O_4^+$ 1240.5594; Found 1240.5615; $[\alpha]_D^{22}$ +24 (*c* 1.0, MeCN).

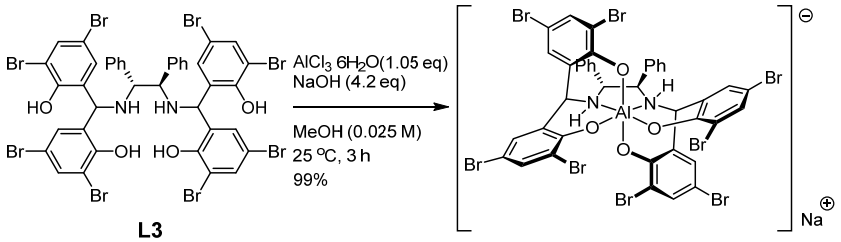

L3 [Al-**L3**]Na

To a solution of **L3** (1.24 g, 1 mmol) in MeOH (40.0 mL) were added NaOH (120 mg, 3.00 mmol) and $AlCl_3$•$6H_2O$ (254 mg, 1.05 mmol). After the resulting solution was stirred for 2 h at 25 °C, NaOH (48 mg, 1.2 mmol) was added to the reaction mixture and it was stirred for 1 h at 25 °C. The reaction mixture was concentrated under reduced pressure. The crude mixture was dissolved in EtOAc, and the resulting organic phase was washed with brine, dried over Na_2SO_4 and concentrated under reduced pressure to afford the Na[Al-**L3**] (1.05 g, 99%) as an off-white solid.

^{1}H NMR (400 MHz, DMSO-d_6) δ 7.42 (d, *J*=2.56 Hz, 2H), 7.41 (d, *J*=2.59 Hz, 2H), 7.23–7.15 (m, 10H), 6.90–6.84 (m, 4H), 4.46 (s, 2H), 3.93–3.86 (m, 2H), 3.72–3.64 (m, 2H); ^{13}C NMR (100 MHz, DMSO-d_6) δ 158.1, 156.8, 135.3, 133.3, 132.9, 131.5, 131.0, 129.8, 128.9, 128.5, 127.6, 125.7, 116.1, 115.2, 103.8, 103.6, 62.8, 62.4; HRMS (ESI/Q-TOF) m/z: [M + Na]+ Calcd for $C_{40}H_{24}AlNaBr_8N_2O_4Na^+$ 1306.4747; Found 1306.4765; $[\alpha]_D^{22}$ +69 (*c* 1.0, MeCN).

Hydrogenative desymmetrization

General procedure for catalytic hydrogenative desymmetrizations was performed following a method reported in the literature (Fernandez-Perez et al., 2016).

Sharpless expoxidation

General procedure for Sharpless expoxidation was performed following a method reported in the literature (Ryan et al., 2006).

DFT calculation

Gaussian 09 was used for all calculations. All geometry optimizations and frequency calculations for equilibrium geometries were performed at the B3LYP/GENECP level. All geometry optimizations and frequency calculations for NBO charges were performed at the B3LYP/6-31G+(d,p).

Measurement of pK_a values

The acidity of metal complexes were determined by acid-base titration using UV-Vis spectroscopy and 2,4-dinitrophenol as indicator.

The acid-base equilibrium between indicator (**HIn**) and the Brønsted acid (**HA**)

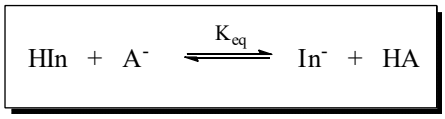

The equilibrium constant is

$$K_{eq} = \frac{[HA]}{[A^-]} \times \frac{[In^-]}{[HIn]} \qquad \textbf{eq 1}$$

The logarithm of **eq 1** is

$$pK_a(HA) = \log K_{eq} + pK_a(HIn) \qquad \textbf{eq 2}$$

When Abs_{max} is absorbance of HIn, Abs_{min} is absorbance of **In**$^-$ at λ_{max} and *Abs* is absorbance of Indicator solution containing the Brønsted (**HA**) and conjugated base (**A**$^-$), **eq 1** could be transformed to

eq 3

The absorbance of 2,4-dinitrophenol, its conjugated base were measured.

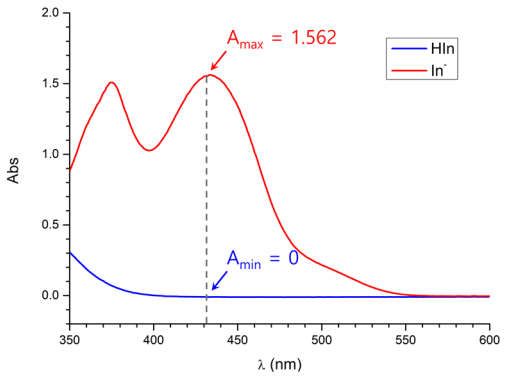

The absorbance of solution containing 2,4-dinitrophenol (0.1 mM), [Al-**L1**]H and [Al-**L1**]Na in DMSO were measured. The initial concentration of [Al-**L1**]H was 10 mM and [Al-**L1**]Na was formed by adding varying amounts of a sodium hydroxide solution (5 M in H_2O).

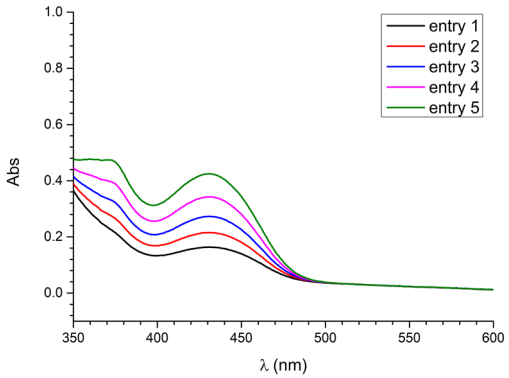

UV-vis data and calculated pK_a value.

Entry	[Al-**L1**]H (mM)	[Al-**L1**]Na (mM)[a]	Abs[b]	K_{eq}[c]	pK_a [HA][d]
1	9	1	0.16314	1.458256	5.283834
2	8	2	0.21487	0.899857	5.074173
3	7	3	0.27239	0.708077	4.97008
4	6	4	0.34188	0.619258	4.911872
5	5	5	0.4244	0.569206	4.875269

(a) [Al-**L1**]Na was generated in-situ by addition of 5 M NaOH (aq), (b) λ_{max}=430 nm, path length=1 cm at 25 °C. (c) Calculated from **eq 3**. (d) Calculated from **eq 2**.

The average pK_a value for [Al-**L1**] is =5.02 ± 0.26

The absorbance of solution containing 2,4-dinitrophenol (0.1 mM), [Al-**L2**]H and [Al-**L2**]Na in DMSO were measured. The initial concentration of [Al-**L2**]H was 10 mM and [Al-**L2**]Na was formed by adding varying amounts of a sodium hydroxide solution (5 M in H_2O).

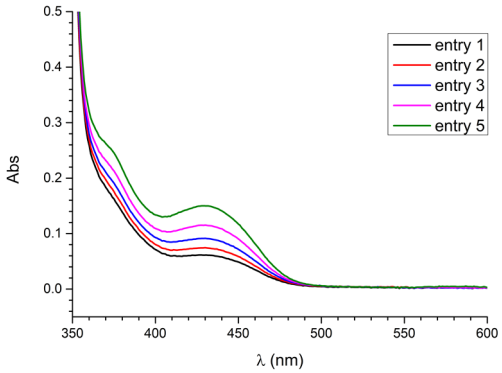

Entry	[Al-**L2**]H (mM)	[Al-**L2**]Na (mM)[a]	Abs[b]	Keq[c]	pKa [HA][d]
1	9	1	0.06093	0.494441	4.814115
2	8	2	0.07376	0.269138	4.549975
3	7	3	0.09083	0.196389	4.413116
4	6	4	0.11436	0.162499	4.33085
5	5	5	0.14979	0.146823	4.286793

(a) [Al-**L2**]Na was generated in-situ by addition of 5 M NaOH (aq), (b) λ_{max}=430 nm, path length=1 cm at 25 °C. (c) Calculated from **eq 3**. (d) Calculated from **eq 2**.

The average pK_a value for [Al-**L2**]H is =4.48 ± 0.33

The absorbance of solution containing 2,4-dinitrophenol (0.1 mM), [Al-**L3**]H and [Al-**L3**]Na in DMSO were measured. The initial concentration of [Al-**L3**]Na was 10 mM and [Al-**L3**]H was formed by adding varying amounts of a concentrated HCl.

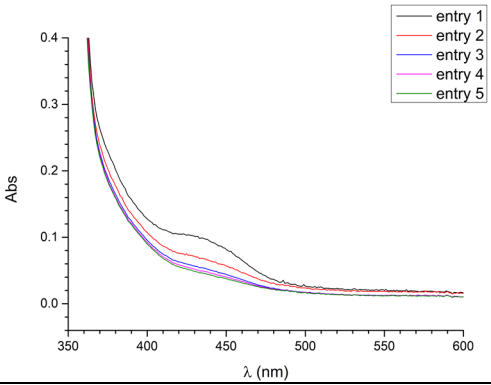

Entry	[Al-**L3**]H (mM)	[Al-**L3**]Na (mM)[a]	Abs[b]	Keq[c]	pKa [HA][d]
1	1	9	0.04739	0.032401	3.630558
2	2	8	0.05084	0.23228	3.486011
3	3	7	0.05563	0.016393	3.334657
4	4	6	0.07026	0.0122	3.206364
5	5	5	0.1013	0.00799	3.022548

(a) [Al-**L3**]H was generated in-situ by addition of conc. HCl (aq), (b) λ_{max}=430 nm, path length=1 cm at 25 °C. (c) Calculated from **eq 3**. (d) Calculated from **eq 2**.

The average pK_a value for [Al-**L3**]H is =3.33 ± 0.31

The absorbance of solution containing 2,4-dinitrophenol (0.1 mM), [Ga-**L1**]H and [Ga-**L1**]Na in DMSO were measured. The initial concentration of [Ga-**L1**]H was 10 mM and [Ga-**L1**]Na was formed by adding varying amounts of a sodium hydroxide solution (5 M in H_2O).

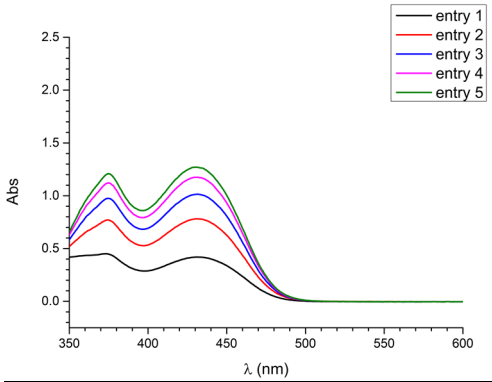

Entry	[Ga-**L1**]H (mM)	[Ga-**L1**]Na (mM)[a]	Abs[b]	Keq[c]	pKa [HA][d]
1	9	1	0.41813	3.288449	5.636991
2	8	2	0.77896	3.97667	5.71952
3	7	3	1.01229	4.293003	5.752761
4	6	4	1.17024	4.475105	5.770803
5	5	5	1.26499	4.252067	5.7486

(a) [Ga-**L1**]Na was generated in-situ by addition of 5 M NaOH (aq), (b) λ_{max}=430 nm, path length=1 cm at 25 °C. (c) Calculated from **eq 3**. (d) Calculated from **eq 2**.

The average pK_a value for [Ga-**L1**]H is =5.73 ± 0.09

The absorbance of solution containing 2,4-dinitrophenol (0.1 mM), [Sc-**L1**]H and [Sc-**L1**]Na in DMSO were measured. The initial concentration of [Sc-**L1**]H was 10 mM and [Sc-**L1**]Na was formed by adding varying amounts of a sodium hydroxide solution (5 M in H_2O).

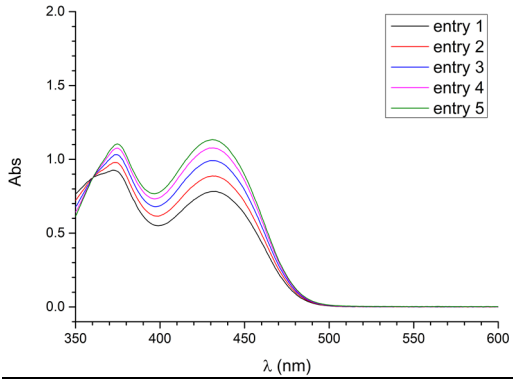

Entry	[Sc-**L1**]H (mM)	[Sc-**L1**]Na (mM)[a]	Abs[b]	Keq[c]	pKa [HA][d]
1	9	1	0.78157	18.10913	6.377898
2	8	2	0.8867	12.51959	6.21759
3	7	3	0.99162	12.97107	6.232976
4	6	4	1.07677	17.32441	6.358659
5	5	5	1.13143	29.33446	6.587378

(a) [Sc-**L1**]Na was generated in-situ by addition of 5 M NaOH (aq), (b) λ_{max}=430 nm, path length=1 cm at 25 °C. (c) Calculated from **eq 3**. (d) Calculated from **eq 2**.

The average pK_a value for [Sc-**L1**]H is =6.35 ± 0.24

The absorbance of solution containing 2,4-dinitrophenol (0.1 mM), [In-**L1**]H and [In-**L1**]Na in DMSO were measured. The initial concentration of [In-**L1**]H was 10 mM and [In-**L1**]Na was formed by adding varying amounts of a sodium hydroxide solution (5 M in H_2O).

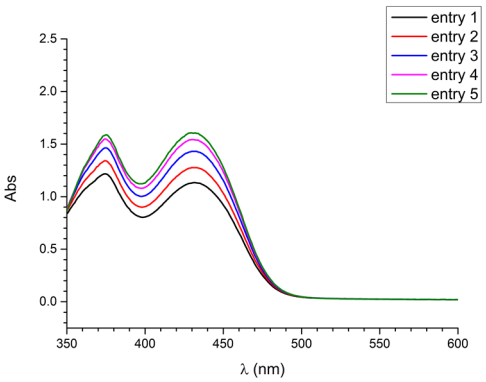

Entry	[In-**L1**]H (mM)	[In-**L1**]Na (mM)[a]	Abs[b]	Keq[c]	pKa [HA][d]
1	9	1	1.13065	23.70059	6.494759
2	8	2	1.27605	17.9757	6.374686
3	7	3	1.43055	25.78563	6.531378
4	6	4	1.53757	102.8246	7.132097
5	5	5	1.59	159	7.321397

(a) [In-**L1**]Na was generated in-situ by addition of 5 M NaOH (aq), (b) λ_{max}=430 nm, path length=1 cm at 25 °C. (c) Calculated from **eq 3**. (d) Calculated from **eq 2**.

The average pK_a value for [In-**L1**]H is =6.77 ± 0.55

Measurement of binding constants

$$H + G \rightleftharpoons HG \qquad K_a = \frac{[HG]}{[H][G]}$$

(δ_H) (δ_{HG})

$[H]_0 = [H] + [HG]$ and $[G]_0 = [G] + [HG]$

$\Delta\delta = \delta_{exp} - \delta_H \qquad \Delta\delta_{HG} = \delta_{HG} - \delta_H$

$$K_a = \frac{[HG]}{[H][G]} = \frac{[HG]}{([H]_0-[HG])([G]_0-[HG])}$$

$$\Delta\delta = \Delta\delta_{HG}\frac{[HG]}{[H]_0}$$

$$[HG]^2 - ([G]_0 + [H]_0 + K_a^{-1})[HG] + [H]_0[G]_0 = 0$$

$$[HG] = \frac{1}{2}\left\{([G]_0 + [H]_0 + K_a^{-1}) - \sqrt{([G]_0 + [H]_0 + K_a^{-1})^2 - 4[H]_0[G]_0}\right\}$$

Nonlinear square fitting

$$y = \frac{\Delta\delta_{HG}}{2[H]_0}\left\{(x + [H]_0 + K_a^{-1}) - \sqrt{(x + [H]_0 + K_a^{-1})^2 - 4[H]_0x}\right\}$$

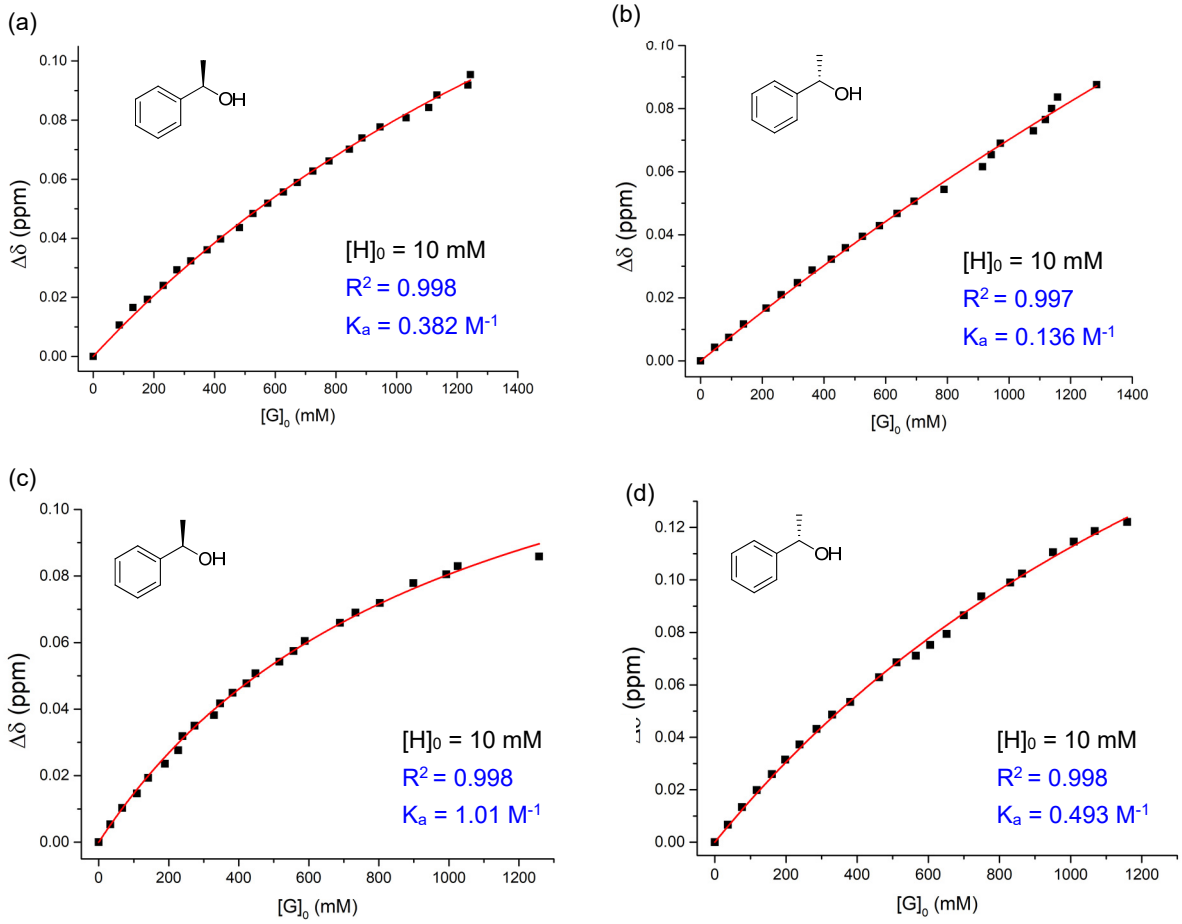

Plots of the complexation-induced shift for [Al-**L1**]Na as a function of (a) (*R*)-1-phenylethanol, (b) (*S*)-1-phenylethanol and plots of the complexation-induced shift for [Ga-**L1**]Na as a function of (c) (*R*)-1-phenylethanol, (d) (*S*)-1-phenylethanol.

Supplemental References

Fernandez-Perez, H., Lao, J. R., Vidal-Feran, A. (2016). Stereoselective Rh-Catalyzed Hydrogenative Desymmetrization of Achiral Substituted 1,4-Dienes. Org. Lett. *18,* 2836-2839.

Ryan, M. M., Jaimison, T. F. (2006). Mechanistic Implications of Nickel-Catalyzed Reductive Coupling of Aldehydes and Chiral 1,6-Enynes. Org. Lett, *8,* 455-458.